The influence of CO_2 on the steam gasification rate of a typical South African coal

Gillis J.D. Du Toit
20094485
B.Eng (Chem) (North-West University)

Dissertation submitted in fulfilment of the requirements for the degree *Magister Scientiae* in *Chemical Engineering* at the Potchefstroom campus of the North-West University, South Africa.

Supervisor: Prof. H.W.J.P. Neomagus (North-West University)

Co-Supervisors: Prof. R.C. Everson (North-West University)
Prof. J.R. Bunt (Sasol / North-West University)
Mr. L. Koen (Sasol Technology)

September 2013

Declaration

I, Gillis Johannes De Korte Du Toit, hereby declare that the dissertation entitled: "The influence of CO_2 on the steam gasification rate of a typical South African coal", submitted in fulfilment of the requirements for the degree M.Eng is my own work, except where acknowledged in the text, and has not been submitted at any other tertiary institution in whole or in part.

Signed at Potchefstroom

_____ _____

Gillis J.D. Du Toit Date

Acknowledgements

"Rise and Rise again, until Lambs become Lions"

I would like to express my sincere gratitude and appreciation to all the persons and institutions that contributed to the completion of this research project. The following persons and institutions deserve special recognition:

- To my lovely wife Wanja, for her continual support and understanding through the entirety of the study.
- Our Heavenly Father whom granted me the opportunity and ability to study.
- Professor Hein Neomagus, Professor John Bunt, Professor Raymond Everson and Mr Louis Koen, for their brilliant leadership, guidance and extra effort.
- Mr Adrian Brock, Mr Johan Broodryk, Oom Jan Kroeze and Mr Ted Paarlberg, for their technical support in building the apparatus and his willingness to help during the commissioning of the equipment.
- The coal research group at the North-West University for the valuable discussions and critique.
- Sasol for their financial support.

Abstract

It is recognised that the reactions with steam and CO_2 are the rate limiting step during coal gasification, and a vast number of studies has been dedicated to the kinetics of these reactions. Most studies were carried out by using a single reactant (CO_2 or H_2O), either pure or diluted with an inert gas. Research using gas mixtures of CO_2 and steam and their effects on gasification kinetics have been undertaken but are limited.

The objective of this study is to determine the effects of CO_2 on the steam gasification rate of a typical Highveld seam 4 coal.

The South African medium ranked high volatile bituminous coal was charred at 950 °C. 2.0 g samples of ± 1 mm particles were analysed in a modified large particle thermo gravimetric analyser under various reactant gas concentrations. Experiments were conducted at atmospheric pressure (87.5 kPa) and temperatures from 775 to 900 °C, such that the conversion rate was controlled by chemical reaction. Reagent mixtures of steam-N_2, steam-CO_2 and CO_2-N_2 at concentrations of 25-75 mol%, 50-50 mol%, 75-25 mol% and 100 mol% were investigated.

Arrhenius plots for steam and CO_2 gasification produced activation energy values of 225 ± 23 kJ/mol and 243 ± 32 kJ/mol respectively. The calculated reaction orders with respect to reagent partial pressure were 0.44 ± 0.08 and 0.56 ± 0.07 for steam and CO_2 respectively.

Comparisons of the experimental data showed a higher reaction rate for the steam-CO_2 mixtures compared to steam-N_2 experiments. The semi empirical Wen model (m = 0.85) with an additive Langmuir-Hinshelwood styled rate equation predicted the mixed reagent gasification accurately. Reaction constants that were determined from the pure reactant experiments could directly be applied to predict the results for the experiments with mixtures of steam and CO_2. The conclusion was made that under the investigated conditions steam and CO_2 reacts simultaneously on different active sites on the char surface.

Keywords:
Coal, Steam – CO_2 Gasification, Kinetics, Char Reactivity

Opsomming

Dit word algemeen aanvaar dat die reaksies met stoom en CO_2 die tempo beherende stappe is tydens steenkool vergassings. „n Groot verskeidenheid studies is al onderneem om die kinetika van die reaksies te beskryf. Die meeste van die studies maak gebruik van „n enkele reagens (CO_2 of H_2O) hetsy suiwer of verdun met „n inerte gas. Studies wat die kinetika van vergassing met mengsels van stoom en CO_2 ondersoek is seldsaam beskikbaar.

Die doel van hierdie studie is om vas te stel wat die uiterking van CO_2 is op die stoom vergassings tempo van „n tipiese Hoëveld soom 4 steenkool.

Die Suid Afrikaanse medium rang hoë vlugtige stof inhoud bituminous steenkool is gepiroliseer by 950 °C. 2.0 g van ± 1 mm partikels is in „n self gemodifiseerde groot partikel termo gravimetriese analiseerder geanaliseer met verskillende gas konsentrasies. Die eksperimentele werk is by atmosferiese druk (87.5 kPa) en temperature van 775 tot 900 °C ondersoek, sodanig dat die omsettings tempo deur die chemiese reaksie beheerd is. Reagens mengsels van stoom-N_2, stoom-CO_2 en CO_2-N_2 is ondersoek by gas konsentrasies van 25-75 mol%, 50-50 mol%, 75-25 mol% en 100 mol%.

Aktiverings energie waardes van 225 ± 23 kJ/mol en 243 ± 32 kJ/mol is onderskeidelik bereken vanaf Arrhenius plots vir stoom en CO_2 vergassing. Die reaksie ordes m.b.t. die reagens konsentrasies is bereken as 0.44 ± 0.08 en 0.56 ± 0.07 vir stoom en CO_2 onderskeidelik.

„n Vergelyking van die eksperimentele data het „n hoër reaksie tempo getoon vir die stoom-CO_2 mengsel as vir die stoom-N_2 eksperimente. Die semi empiriese Wen Model (m = 0.85) met „n sommerende Langmuir-Hinshelwood tempo vergelyking het die experimentele data die beste voorspel. Reaksie konstantes is bereken vanuit die suiwer reagens data en kon direk gebruik word om die uitslag van die eksperimente met mengsels van stoom en CO_2 te bepaal. Die gevolgtrekking is gemaak dat binne die perke van die studie, stoom en CO_2 gelyktydig reageer op afsonderlike aktiewe punte op die steenkool oppervlak.

Sleutel woorde:
Steenkool, Stoom – CO_2 Vergassing, Kinetika, Reaktiwiteit

Index

List of symbols

Symbol	Description	Units
b	Solid stoichiometric constant	-
C_{Ag}	Gas concentration	mol/l
CV	Calorific value	MJ/kg
D_e	Diffusion constant	m^2/s
d_p	Particle diameter	mm
dX/dt	Conversion rate	1/min
E_a	Activation energy	kJ/mol
ε_o	Porosity	%
f(X)	Structural model	-
ΔH	Adsorption enthalpy	kJ/mol
$\Delta h°_{rxn}$	Enthalpy of reaction	kJ/mol
K_A	Adsorption constant	1/Pa
K_i	Inhibitor adsorption constant	1/Pa
K_{H_2O}	H_2O adsorption constant	1/Pa
K_{CO_2}	CO_2 adsorption constant	1/Pa
K_{H_2}	H_2 adsorption constant	1/Pa
K_{CO}	CO adsorption constant	1/Pa
k`s	Surface reaction rate constant	m/Pa
$k`_{H_2O}$	Steam rate constant	m/Pa
$k`_{CO_2}$	Carbon dioxide rate constant	m/Pa
k_o	Pre-Exponential Factor	1/(s Pa)
$k_{p,coal}$	Thermal conductivity of coal	W/(m K)
L_o	Pore length per unit volume	m/m^3
M_i	Mass value at point *i*	g
M_o	Initial mass	g
M_f	Final Mass value	g
m	Solid reaction order	-
n	Power rate law Reaction order	-
N	Number of experimental points	-
n_i	Normalised mass value	-
P	Total pressure	Pa
p_A	Partial pressure of component A	Pa
p_i	Partial pressure of inhibitor	Pa
p_{H_2O}	H_2O partial pressure	Pa
p_{CO_2}	CO_2 partial pressure	Pa
p_{H_2}	H_2 partial pressure	Pa
p_{CO}	CO partial pressure	Pa
Ψ	RPM Structural parameter	-
R	Universal gas constant	J/(mol K)
R_s	Specific reaction rate	g / (g s)
R_{50}	Reactivity index	1/min
r_A'''	Reaction rate	$mol/(m^3 s)$
r_s	Reaction rate constant	1/min
S_o	Initial surface area	m^2
T	Temperature	K
t_i	time value *i*	min

t_o	Initial time value	min
t_{50}	Time at 50 % conversion	min
t_{90}	Time at 90 % conversion	min
t_f	RPM time factor	1/min
τ	SUCM time constant	$(mol^2\ K)/(min\ m^4)$
X_i	Conversion	-
X_o	Initial conversion	-
x_i	Arbitrary experimental conversion	-
x_{calc}	Modelled conversion	-
x_{exp}	Experimental conversion	-
y_A	Gas molar fraction	-

Abbreviations

a.d.	Air dried	-
ASTM	American Society for Testing and Materials	-
BET	Brunauer, Emmett, Teller	-
CTL	Coal to Liquids	-
d.a.f.	Dry ash free	-
d.v.m.f.	Dry + volatile matter free	-
a.d.b.	Air dried basis	-
D-R	Dubinin-Radushkevich	-
FBG	Fixed Bed Gasifier	-
HM	Homogeneous Model	-
ISO	International Standards Organisation	-
L-H	Langmuir-Hinshelwood	-
m.m.f.b.	Mineral matter free basis	-
PDTF	Pressurised Drop Tube Furnace	-
RPM	Random Pore Model	-
SABS	South-African Bureau of Standards	-
SUCM	Shrinking Un-reacted Core Model	-
TGA	Thermo Gravimetric Analyser	-
v.m.f.	Volatile matter free	-

List of Figures

List of Tables

Chapter 1: General Introduction

1.1 Overview

In this chapter the common uses and applications of coal are discussed and the motivation of this study is presented. In Section 1.2 an overview of where coal gasification fits into the global energy perspective is given. In Section 1.3 relevant studies from literature are briefly reviewed and the problem statement for this study is formulated. In Section 1.4 the objectives of this study are given and in Section 1.5 the scope is presented. In Section 1.6 an overview of the chapters to follow is given.

1.2 Background and motivation

In a fossil fuel dependent world, the efficient utilisation of the available natural resources is of utmost importance. Under current consumption rates, the global fossil fuel reserves are estimated to last 47 years for oil, 59 years for natural gas and 118 years for coal (BP, 2011), (WCA, 2012). In 2010, coal constituted for 30 % of the total global energy market, which is the highest it has been since 1970. Coal showed the largest increase in consumption (7.6 %) in 2010 compared to oil (2 %) and natural gas (7.4 %) (BP, 2011). The five largest coal users in the world are: China, USA, Japan, Russia and India. These countries consumed 82 % of the global coal produced in 2010 (WCA, 2012).

In light of these figures it is important for countries such as South Africa, with no crude oil reserves, limited natural gas, but substantial coal reserves (DOE SA, 2012), to re-evaluate how to most effectively utilise its limited resources.

In 2010 South Africa had a proven coal reserve of 30 billion tons that was projected to last for 118 years. From these reserves South Africa produced 143 million tons oil equivalent of coal and consumed 88.7 million tons oil equivalent in 2010 (BP, 2011). Coal is used to produce 41% of the global electricity demand and South Africa relies on coal for 93% of their electricity production (WCA, 2012).

The true value of coal not only lies in its use to produce electricity, but also as a feedstock for the production of valuable chemical and petroleum products, the firing of cement kilns, and its use as coke in the steel industry (Higman and Van der Burgt, 2008).

Chemical products derived from coal include: polymers, olefins, solvents, surfactants and waxes (WCA, 2011). South Africa produces 36% of its annual fuel demand from coal and

natural gas (DOE SA, 2012). Coal can be converted into a liquid fuel by means of CTL technologies, by either direct- or indirect liquefaction (Higman and Van der Burgt, 2008). The direct process involves dissolving the coal in a solvent at high pressure and moderate temperature; although this method is efficient, the product requires further processing before it can be used. In the indirect method the coal is gasified with steam to produce a gas mixture containing carbon monoxide and hydrogen, also called synthesis gas. This gas can be used for ammonia and methanol synthesis, or the Fischer-Tropsch process can be applied to produce high quality petroleum products (Liu *et al*., 2010). A whole range of products can be made with this process including ultra-clean petrol and diesel, synthetic waxes, lubricants and aromatic chemicals (Miura, 2000), (Higman and Van der Burgt, 2008), (WCA, 2011).

In South Africa, the indirect liquefaction route is used, because of the low quality of the coal locally available and the fact that indirect liquefaction methods work effectively with a wide variety of coals (Liu *et al*., 2010). The design and make of an industrial gasifier may vary greatly but the chemistry can be summed into three primary gas-solid reactions (Higman and Van der Burgt, 2008), (Liu *et al*., 2010), (Xu *et al*., 2011_b):

$C(s) + O_2(g) \rightarrow CO_2(g)$ $\Delta h°_{rxn}$ = -394 kJ/mol [1.1]

$C(s) + CO_2(g) \rightarrow 2CO(g)$ $\Delta h°_{rxn}$ = +172 kJ/mol [1.2]

$C(s) + H_2O(g) \rightarrow H_2(g) + CO(g)$ $\Delta h°_{rxn}$ = +131 kJ/mol [1.3]

A fourth gas phase reaction (Reaction 1.4), the water gas shift reaction, is an equilibrium gas phase reaction. This reaction is crucial to the CTL process because it allows for the manipulation of the hydrogen to carbon monoxide ratio in synthesis gas (Higman and Van der Burgt, 2008), (Liu *et al*., 2010).

$CO(g) + H_2O(g) \leftrightarrow H_2(g) + CO_2(g)$ $\Delta h°_{rxn}$ = -41 kJ/mol [1.4]

A large variety of industrial gasification processes have been developed in the past and more are still being developed. In general, all of these processes can be divided into three categories namely; moving/fixed bed gasification, fluidised-bed gasification, and entrained flow gasification (Liu *et al*., 2010), (Bell *et al*., 2011).

A moving bed design uses lump coal particles and has a residence time in the order of hours. This design has a slow heating rate and more modest operating temperatures (Higman and Van der Burgt, 2008), (Liu *et al*., 2010), (Bell *et al*., 2011). For fluidised bed reactors particles in the order of millimetres are used with residence times of a couple of minutes (Liu *et al*., 2010), (Bell *et al*., 2011). The entrained flow process uses fine coal which is gasified in the order of seconds (Higman and Van der Burgt, 2008), (Liu *et al*., 2010). Both of these processes are operated at high temperatures and short residence times.

Because of the heterogeneous nature of coal and the large variety of coal conversion technologies available, it is essential to know how a coal will react under specified reaction conditions. Therefore the modelling of the coal gasification process is of cardinal value to effective coal utilisation (Mühlen *et al*., 1984) and accurate chemical reaction kinetic data forms an essential part of the modelling of industrial gasification processes such as fluidised beds and moving bed gasifiers.

1.3 Problem statement

In either of the processes mentioned in Section 1.2, the coal particle undergoing gasification will come into contact with a variety of gases during the gasification process. The primary gasification agents are steam and CO_2, but as the process progresses the CO and H_2 concentrations also increase and may participate in secondary gasification reactions (Everson *et al*., 2006_a), (Huang *et al*., 2010).

The kinetic behaviour of char with steam and CO_2 has been extensively studied and compared *i.e.* (Ye *et al*., 1997), (Molina and Mandragon, 1998), (Kajitani *et al*., 2002), (Irfan *et al*., 2011). Both H_2 and CO have been found to act as inhibitors during steam and CO_2 gasification respectively *i.e.* (Everson *et al*., 2006_a), (Espinal *et al*., 2009), (Lussier *et al*., 1998).

Kinetic data for gasification with both the primary gasification reagents (steam and CO_2) present is limited in literature (Everson *et al*., 2006_a), (Mühlen *et al*., 1984), (Huang *et al*., 2010), (Roberts and Harris, 2007). Most of the studies involving mixtures of gasification reagents either focussed on the inhibiting effects of CO and H_2, or used equilibrium mixtures of (H_2, CO, H_2O and CO_2) as gasification reagent. A limited number of studies have investigated how the presence of CO_2 influences the steam-char reaction (Roberts and Harris, 2007) and to our knowledge none on South African coals.

The South African coal that is generally available to the domestic coal conversion industry has a high ash and inertinite content. Various authors have shown that the presence of inorganic matter can influence the gasification reactivity of coal-char significantly (Everson *et al*., 2011), (Everson *et* al., 2006_a), (Hattingh *et al*., 2011), (Matsuoka *et al*., 2009).
Therefore this study will focus on the steam-CO_2 interactions during the gasification of a typical South African conversion coal (Highveld seam 4) over a broad temperature range, with reagent concentrations ranging from pure to 25%. This study will also focus on the evaluation of various kinetic models and the implementation of such a model to accurately predict the kinetics of steam-CO_2 gasification.

1.4 Objectives of the investigation

This investigation will focus on the influence of CO_2 on the reaction kinetics of steam gasification. To achieve this goal the following primary objective is defined:

- Determine how the addition of CO_2 influences the steam gasification rate of a typical South African Highveld coal.

The following sub-objectives are set:

- Determine the chemically controlled char gasification kinetics for steam, CO_2, and mixtures of the two over a temperature range.
- Compare the single reagent kinetic data to the corresponding mixtures of steam and CO_2.
- Propose an appropriate kinetic model and its parameters to predict gasification rates for different partial pressures of steam and CO_2.

1.5 Scope of the study

In order to achieve the objectives of this study a scope was developed to guide the research process. The scope is summarised in the following points:

- An in-house designed and built TGA apparatus will be used for the gasification experiments. Preliminary experiments will be carried out to ensure chemically controlled reaction kinetics
- Experiments will be conducted at different temperatures and different reagent partial pressures. A comparison will be done of experiments with Steam-N_2, Steam-CO_2 and CO_2-N_2 mixtures.
- A selection of structural and kinetic models will be evaluated to determine an appropriate model to be used to model steam-CO_2 gasification kinetics.

1.6 Study outline

A schematic outline of the study is presented in Figure 1-1. In Chapter 1 an overview of the current global energy utilisation and where gasification fits into the bigger picture was discussed as well as the problem statement, the objectives of this study and the scope were given. In Chapter 2 a literature survey is presented to provide insight into the nature of coal and its applications, the survey focuses predominantly on coal gasification and factors influencing the gasification rate. A review is also given of commonly used gasification models. In Chapter 3 the coal and char characterisation is presented as well as the procedures followed for characterisation. The experimental equipment developed for this study, the experimental reaction conditions and the procedures followed are presented in Chapter 4. In Chapter 5 the experimental results are reported and discussed, as well as the procedures followed in selecting a kinetic gasification model to be used to predict the mixed reagent experimental behaviour. Final conclusions and recommendations for future study are presented in Chapter 6.

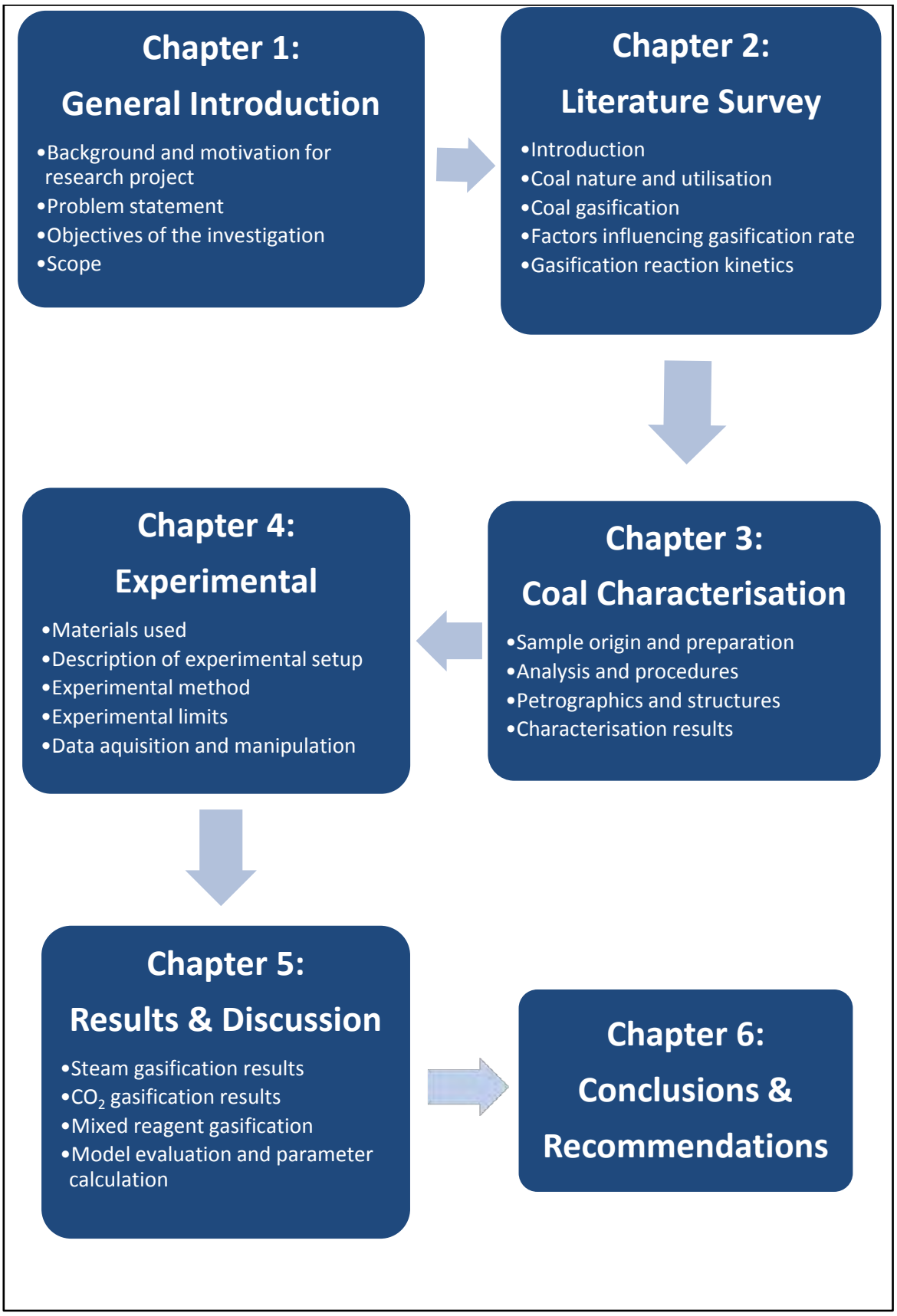

Figure 1-1: Schematic representation of the scope

Chapter 2: Literature survey

2.1 Introduction

Chapter 2 contains the literature survey, which will provide background information to form a basis for this study. In Section 2.2 the nature of coal is discussed. In Section 2.3 a broad overview of coal gasification is presented and the main factors influencing gasification rate are discussed in Section 2.4. In Section 2.5 gasification kinetics and the associated models are presented as well as a discussion of steam-, CO_2- and mixed reagent gasification. In Section 2.6 a brief summary of the literature discussed in this chapter is presented.

2.2 Coal nature

Coal is a combustible sedimentary rock that consists mainly of organic components containing carbon, oxygen, hydrogen and minerals (Speight, 2005). Coal was formed from masses of vegetation that has collected during the Carboniferous Period and was buried beneath the earth‟s surface. As this organic material is exposed to increasing temperatures and pressure in the absence of oxygen, it is turned into coal by a process called coalification. During coalification oxygen and hydrogen are released from the organic material in the form of water, methane and CO_2 (Speight, 2005).

Depending on the extent of coalification, coal can be classified into different ranks. The lowest rank is brown coal, which forms from peat. Brown coal can have a moisture content of 50-70 % and has a very aliphatic carbon structure (Ye *et al*., 1997). As coalification progresses brown coal is transformed into bituminous coal. These coals have a more aromatic carbon structure and a typical volatile matter content of 30-40 % (Molina and Mandragon, 1998), (Kajitani *et al*., 2002). The highest ranking coals are called anthracite. Anthracite has a very high carbon content (> 80 %, d.a.f) which is arranged in a highly aromatic, graphitic structure (Miura *et al*., 1986).

Various inorganic- matter was deposited with the vegetation and trapped in the carbon structure. The grade of coal is determined by the degree of mineral matter contamination of the coal (Suàrez-Ruiz and Crelling, 2008).

Coal type is reflected by the various fossilised plant components present in coal, which are known as macerals and form the basis for petrography studies (Du Cann, 2007). Macerals are

divided into three main types, vitrinite, liptinite (exinite) and inertinite. These macerals are identified by their visual appearance and relate directly to the original plant matter that the coal was formed from. Vitrinite forms from wood and bark, liptinite from algae, spores, resin or pollen, and inertinite forms from carbonised wood and cell protoplasm (Suàrez-Ruiz and Crelling, 2008).

By characterising a coal according to rank, chemical and petrographic content, valid assumptions can be made of how the coal will behave during utilisation (Hattingh *et al*., 2011), (Irfan *et al*., 2011).

2.3 Coal gasification

2.3.1 Introduction

In a broad sense gasification can be defined as any process that converts a carbonaceous fuel into a gaseous product with a useable heating value. Earlier technology relied heavily on de-volatilisation, where a feedstock is heated in the absence of oxygen (Higman and Van der Burgt, 2008). Nowadays, the primary technology is the gasification of coal, biomass and/or residual oils to produce synthesis gas (Liu *et al*., 2010).

Synthesis gas production plays a vital role in the future of energy utilisation and addresses three major challenges in the modern energy sector; (1) The supply of clean gaseous or liquid fuels to meet increasing demands, (2) to maximise the utilisation of current energy resources, and (3) the elimination of pollutants and minimisation of greenhouse gas emissions in energy production (Liu *et al*., 2010).

Synthesis gas is most useful and can be used in any of three ways:

- Combustion to produce electricity, such as in an integrated gasification combined cycle gasifier (IGCC).
- As a raw material for chemical synthesis of products such as ammonia, Fischer-Tropsch liquid fuels or methanol.
- Methanation for producing synthetic natural gas.

2.3.2 Char Gasification

Char gasification is slow when compared to the other gasification steps such as de-volatilisation and oxidation (Everson *et al*., 2006_a). This results in the gasification step most often being the rate controlling step in a gasifier (Irfan *et al*., 2011). When developing gasification mechanisms and rate equations, the molecular structure is normally ignored, and it is assumed that the coal-char is pure carbon reacting with gaseous reactants in the gasifier (Liu *et al*., 2010), (Bell *et al*., 2011). The main heterogeneous gas-solid reactions are shown in Reactions 2.1-2.7. The primary reaction in steam gasification is the reaction of steam with solid carbon, presented in its basic form in Reaction 2.1. Reaction 2.2 is a combination of Reaction 2.1 and the gas phase water gas shift reaction (Higman and Van der Burgt, 2008):

$C(s) + H_2O(g) \leftrightarrow CO(g) + H_2\,(g)$ $\quad \Delta h°_{rxn}$ = +131 kJ/mol [2.1]

$C(s) + 2H_2O(g) \leftrightarrow CO_2(g) + 2H_2\,(g)$ $\quad \Delta h°_{rxn}$ = +90 kJ/mol [2.2]

Reactions 2.1 and 2.2 are endothermic reactions and require thermal input to remain sustainable (Liu *et al*., 2010). To maintain these endothermic reactions, the reactor is either heated externally or the char is combusted and gasified simultaneously (Higman and Van der Burgt, 2008). Air or oxygen is fed with the steam to the reactor oxidising some of the carbon and producing energy to drive the endothermic gasification reactions. Once a thermal equilibrium is attained between these exothermic and endothermic reactions the process can run continuously. By combusting and gasifying simultaneously in the same reactor the heat transfer efficiency is increased substantially (Liu *et al*., 2010).

If oxygen is fed to the gasifier, the following reactions can occur:

$C(s) + \frac{1}{2}O_2(g) \rightarrow CO(g)$ $\quad \Delta h°_{rxn}$ = -111 kJ/mol [2.3]

$CO(g) + \frac{1}{2}O_2(g) \rightarrow CO_2(g)$ $\quad \Delta h°_{rxn}$ = -283 kJ/mol [2.4]

$C(s) + O_2(g) \rightarrow CO_2(g)$ $\quad \Delta h°_{rxn}$ = -394 kJ/mol [2.5]

$H_2(g) + \frac{1}{2}O_2(g) \rightarrow H_2O(g)$ $\quad \Delta h°_{rxn}$ = -242 kJ/mol [2.6]

The formation of CO_2 during the combustion processes allows for secondary gasification reactions such as the reverse Boudouard reaction (Reaction 2.7) to occur:

$$C(s) + CO_2(g) \leftrightarrow 2CO(g) \qquad \Delta h°_{rxn} = +172 \text{ kJ/mol} \qquad [2.7]$$

The endothermic Boudouard reaction is slower than the water gas reaction (Reaction 2.1) and much slower than the combustion reactions *i.e.* (Messenbock *et al*., 1999), (Everson *et al*., 2006_a), (Irfan *et al*., 2011).

2.4 Factors influencing gasification rate

The rate of gasification is dependent on a wide variety of factors. These influencing factors can be divided into, mainly, coal properties and reaction conditions. This study focuses on the influence of reaction conditions on the gasification rate, and therefore the influence of coal properties will only be summarised briefly in Section 2.4.1.

2.4.1 Effect of coal properties

The coal rank and type play a definite role in determining the reaction rate of the char. It has been found that generally higher ranking coal-chars have lower reactivities than low ranking coals (Takarada and Tomita, 1985), (Miura *et al*., 1986), (Irfan *et al*., 2011).

The presence of alkali and alkaline earth metals such as Ca, Mg, Na or K has been found to catalyse the gasification reaction *i.e.* (Huttinger and Nattermann, 1994), (Ye *et al*., 1997), (Seth *et al*., 2003).

The coal properties and de-volatilisation conditions are closely related (Wu *et al*., 2006). More severe de-volatilisation conditions may lead to a more ordered graphitic structure which ultimately lowers char reactivity (Miura *et al*., 1986). Rapid de-volatilisation has also been observed to cause heat fracturing which leads to a higher surface area and therefore a higher reaction rate (Sangtong-Ngam and Narasingha, 2009).

Knowing the petrographic composition of the coal gives a good indication of how it will react during utilisation (Hattingh *et al*., 2011), (Irfan *et al*., 2011). Generally the order of reactivity is observed to be vitrinite > liptinite > inertinite (Sun *et al*., 2004). Maceral reflectance has

been used to indicate the coal rank and reactivity (Cloke and Lester, 1994). Maceral reflectance can also be used as an indication of the calorific value of the coal (Speight, 2005).

2.4.2 Effect of temperature

Temperature plays a very important role in coal gasification, *i.e.* with increasing temperature the carbon conversion rate and gasification efficiency increases *i.e.* (Seth *et al*., 2003), (Liu *et al*., 2010), (Irfan *et al*., 2011). For a low rank lignite char Liu *et al*. (2000) found that from 827 to 1727 °C, that the intrinsic reaction rate increases by four orders of magnitude. However, when comparing coal conversion profiles it has been found that at high temperatures (1150-1200 ºC) that the conversion profiles of various coals may overlap. This phenomenon is believed to be due to the low ash fusion temperatures of certain coals studied (Irfan *et al*., 2011). This means that if a char is heated beyond its ash fusion temperature, the ash melts and blocks char reactive surface from further reaction. Ye *et al*. (1997) found that for Bowman‟s coal, that the steam-char reactivity was equal to the CO_2-char reactivity at a reaction temperature of 633 ºC, and double the CO_2-char reaction rate at 765 ºC. The Arrhenius equation which is discussed in Section 2.5.3 provides a direct relation of the reaction rate to temperature.

2.4.3 Effect of pressure

During coal de-volatilisation an increased pressure physically suppresses the de-volatilisation process. This decreases volatile matter and tar yields, but increases the total gas yield (Megaritis *et al*., 1999), (Wall *et al*., 2002). Methane and CO_2 production has been found to increase with an increase in pressure as well (Molina and Mandragon, 1998). The increase in methane and CO_2 production decreases synthesis gas yield.

An increase in pressure during char gasification has been found to increase the reaction rate *i.e.* (Liu *et al*., 2000), (Everson *et al*., 2008_a). This phenomenon would be due to the increased partial pressure of the reactant gases at the char surface, therefore increasing the amount of reactant available for gasification. It has been observed that the effect of pressure on reaction rate is significant at lower pressures, but tends to saturate at higher pressures *i.e.* (Liu *et al*., 2000), (Irfan *et al*., 2011), (Huttinger and Nattermann, 1994), (Roberts and Harris, 2006).

Gasifying under pressure also has considerable other advantages, and most modern processes are operated between 10 and 100 bar (Liu *et al*., 2010). The benefit of not needing to

compress the product gas is energetically far superior to the product losses experienced due to CO_2 and methane formation (Higman and Van der Burgt, 2008). Both the power rate law and the L-H equations which are discussed in Section 2.5.3 provide a relation of reaction rate to partial and total pressure.

2.5 Gasification kinetics

A good understanding of coal gasification reactivity and the governing kinetics is essential for optimisation of the gasification process. Coal gasification has been extensively researched, however the specifics of the mechanism of coal-char gasification remains unclear (Liu *et al*., 2010). Gasification kinetic modelling and the kinetics of steam and CO_2 gasification are discussed in this section.

2.5.1 Heterogeneous reaction modelling

Gasification involves the heterogeneous reaction of a gaseous reactant with coal-char, to produce a desired product (synthesis gas). A general representation of a gas-solid reaction would be Reaction 2.8 (Levenspiel, 1999):

$$aA(g) + bB(s) \leftrightarrow Products \qquad [2.8]$$

Models that describe these types of reactions are functions of the physical structure of the coal-char and the mechanisms of the gas solid reactions.

Yagi and Kunii (1955) developed a model for gas-solid reactions, they described the physical interactions between the gaseous reactant and the solid surface by adding the adsorption and desorption of reactants and products from and to the solid surface (Liu *et al*., 2010). A thin gas film is said to develop around a reacting solid particle and is described as an area where drastic velocity changes are observed.

The interaction of the reactant gas with the solid surface is summarised in the following steps:

- First, the reagent diffuses through a gas film from the bulk gas onto the particle surface.
- The reactant diffuses through the pore structure or the ash layer of the particle to the un-reacted solid.
- Reactant gas adsorbs onto the solid surface
- Chemical reaction of the gas and the solid takes place on the reaction surface.
- Desorption of products from the solid surface
- The products then diffuse through the pore structure or the ash layer to the outside of the particle.
- Lastly, the products diffuse through the gas film into the bulk gas.

The individual resistances that these steps contribute to the overall reaction rate usually vary greatly. It is considered that the step that gives the most resistance will be the rate controlling step. Following this analogy, there are three principles that govern gas-solid reaction rate, (1) external mass transfer, (2) internal diffusion and (3) chemical reaction control (Levenspiel, 1999).

At low temperatures the chemical reaction dominates the reaction rate. In this regime the reaction rate is strongly dependent on the reaction temperature. As the reaction temperature increases, the chemical reaction rate increases and gas diffusion inside the particle becomes the rate controlling step. In this regime particle size will start to play a role. In the third regime (very high temperatures), the reactant diffusion rate from the bulk gas to the particle surface will determine the reaction rate. The reaction rate will be more dependent on the gas flow rate in this regime.

Reactivity index as defined in Equation 2.1 is a parameter that has been widely used for the comparison of different gasification reactivities *i.e.* (Miura *et al*., 1986), (Molina and Mandragon, 1998), (Ye *et al*., 1997).

$$R_{50} = \frac{0.5}{t_{50}} \qquad (2.1)$$

To accurately describe the gasification process an equation is required that relates the physical changes to the experimental variables. A general kinetic model that relates temperature, composition and conversion to gasification rate is shown in Equation 2.2.

$$\frac{dX}{dt} = g(T)h(p_A)f(X) \tag{2.2}$$

Here g(T) is a function relating reaction rate to temperature, function h(p_A) relates reagent partial pressure to reaction kinetics, and f(X) being the structural model, describes the physical changes of the particle during the gasification process. f(X) usually incorporates some of the particle characteristics such as surface area, porosity and conversion. Equation 2.2 is generally simplified to the following:

$$\frac{dX}{dt} = r_s(T, p_A)f(X) \tag{2.3}$$

This form simplifies the kinetic rate equation into two parts, an intrinsic rate equation that is a function of temperature and partial pressure, and the structural model which is a function of particle conversion.

2.5.2 Structural models

Description of the reaction will be strongly dependent on the nature of the solid and the reaction conditions. A porous solid particle with high concentrations of impurities will remain almost unchanged during reaction, while a dense "ashy" solid may react from the outer surface inward and leave an ash layer on the outer surface (Levenspiel, 1999). In this section a selection of commonly used structural models are discussed and their equations presented.

Homogeneous model

The homogeneous model or progressive conversion model is a very simplistic fundamental model. This model is independent of particle shape and size and was developed under the assumption that the gaseous reactants can penetrate and react throughout the char particle (Fermoso *et al*., 2010), (Zang *et al*., 2010). This model is generally valid for very porous

particles and for low conversion rates, such as when the reaction rate is chemically controlled (Levenspiel, 1999). The homogeneous model, structural model is given by:

$$f(X) = (1 - X) \tag{2.4}$$

The homogeneous model kinetic equation can be differentiated and rewritten with respect to time to give:

$$t = -\frac{1}{r_s}\ln(1 - X) \tag{2.5}$$

Equation 2.5 gives a direct relation between time and conversion and can be used to evaluate the applicability of the homogeneous model when compared to experimental data.

Shrinking Un-reacted Core Model

The Shrinking Un-reacted Core Model (SUCM) was developed by Yagi & Kunii (1961) under the assumption that the gas-solid reaction takes place on the outer surface of the solid particle or grain. As the reaction progresses an ash layer will form on the outer surface of the particle (Levenspiel, 1999), (Zang *et al*., 2010). This leads to three variations of the SCM. The particle conversion rate can be controlled by the chemical reaction on the reactive surface, the diffusion rate of the gas through the formed ash layer, or the gas diffusion through the gas film boundary. If the chemical reaction controls the conversion rate, the structural model is given by:

$$f(X) = S_o \frac{(1-X)^{2/3}}{(1-\varepsilon_o)} \tag{2.6}$$

The reaction models for different controlling mechanisms are described by the equations in Table 2.1 (Levenspiel, 1999).

Table 2-1: SUCM equations

Rate controlling step	Equation		
Chemical reaction	$\tau = \frac{br_s C_{Ag}}{\rho_b R}$	$t = \frac{1}{\tau}\left[1-(1-X)^{1/3}\right]$	(2.7)
Ash diffusion	$\tau = \frac{6bD_e C_{Ag}}{\rho_b R^2}$	$t = \frac{1}{\tau}\left[1-3(1-X)^{2/3}+2(1-X)\right]$	(2.8)
External mass transfer	$\tau = \frac{3bk_g C_{Ag}}{\rho_b R^2}$	$t = \frac{1}{\tau}X$	(2.9)

The constants for each equation are lumped together into one parameter τ. Because τ includes the rate constant (r_s), τ can be used as an indication of the reaction rate.

To ease the use of these equations Everson *et al*. (2006_a) and (Njapha, 2003) proposed normalising these equations with respect to time. Normalising the equations eliminate the τ parameter and simplifies the equations. These equations normalised to the time at 90 % conversion is presented in Table 2-2.

Table 2-2: Normalised SUCM equations

Rate controlling step	Equation	
Chemical reaction	$\frac{t}{t_{90}} = \left[\frac{1-(1-X)^{1/3}}{1-(1-0.9)^{1/3}}\right]$	(2.10)
Ash diffusion	$\frac{t}{t_{90}} = \frac{\left[1-3(1-X)^{2/3}+2(1-X)\right]}{\left[1-3(1-0.9)^{2/3}+2(1-0.9)\right]}$	(2.11)
External mass transfer	$\frac{t}{t_{90}} = \frac{X}{0.9}$	(2.12)

In practice, the conversion of a particle is controlled by a combination of these three steps, depending on the reaction conditions and the particle characteristics. The SUCM can incorporate multiple rate controlling steps by summing Equations 2.7, 2.8 and/or 2.9.

Random Pore Model

Another fundamental model that has been widely used is the chemical reaction controlled random pore model (RPM). Developed by Bhatia & Perlutter (1980) and Gavalas (1980), this model takes into account how the internal pore structure of the char changes with conversion (Fermoso *et al*., 2010). The model assumes that a reacting solid consists of a network of long cylindrical pores, intersecting at random angles (Zang *et al*., 2010). This makes the chemically controlled RPM independent of particle size since it regards only the internal pore structure. This model contains two parameters, the reaction rate constant and a structural parameter (Ψ), which is defined as a function of the physical properties of the parent coal/char (Equation 2.13).

$$\Psi = \frac{4\pi L_o(1-\varepsilon_o)}{S_o^2} \tag{2.13}$$

The equation for the RPM is as follow:

$$f(X) = \frac{S_o(1-X)}{(1-\varepsilon_o)}\sqrt{1-\Psi \ln(1-X)} \tag{2.14}$$

After inserting Equation 2.14 into Equation 2.3 and integration, the RPM can be rewritten in terms of time as shown in Equation 2.15:

$$t = \frac{2(1-\varepsilon_o)}{r_s S_o \Psi}\left(\sqrt{1-\Psi \ln(1-X)} - 1\right) \tag{2.15}$$

The model can be simplified by defining a time factor as (Feng and Bhaita, 2003):

$$t_f = \frac{r_s S_o}{(1-\varepsilon_o)} \tag{2.16}$$

Because the initial surface area and the initial porosity are constant values, the time factor can be used as an indication of the reactivity constant.

The structural parameter as defined in Equation 2.13 is dependent on the physical structure of the reacting char. The physical structure of char is difficult to determine accurately and therefore Ψ is often obtained from regression of the conversion graphs

(Everson *et al*., 2011). By normalising the RPM kinetic equation to 90 % conversion, the structural values are eliminated from the equation and the structural parameter can be determined from the regression of Equation 2.17 (Everson *et al*., 2011), (Kaitano, 2007).

$$\frac{t}{t_{90}} = \frac{\sqrt{1-\Psi \ln(1-X)}-1}{\sqrt{1-\Psi \ln(1-0.9)}-1} \quad (2.17)$$

Equation 2.17 shows the RPM normalised to 90 % conversion. The RPM can be modified to incorporate different coal/char properties or experimental conditions (Irfan *et al*., 2011), (Zang *et al*., 2010).

Wen model

Numerous other models can be found in literature with different structural models and approaches. One such model is the semi-empirical Wen model which was developed to predict a wide variety of carbon conversion shapes (Wen, 1968). The proposed structural model is shown in Equation 2.18.

$$f(X) = (1-X)^m \quad (2.18)$$

This semi empirical model uses the power of the structural model as a fitting parameter. Therefore if m = 1 we have the homogeneous model, and with m = 2/3 the SUCM with chemical reaction controlled kinetics. With the additional solid reaction fitting parameter the Wen model is very robust. After integration of the kinetic Wen model and rearranging the terms Equation 2.18 was obtained:

$$t = -\frac{1}{r_s}\left[\frac{(1-X)^{1-m}}{1-m} - \frac{1}{1-m}\right] \quad (2.19)$$

Equation 2.19 relates time directly with conversion by means of the Wen structural model and the solid reaction order (m).

2.5.3 Kinetic rate models

For the description of gasification intrinsic kinetic reaction rate, one of two main models is normally implemented (Huttinger and Merdes, 1992). The power rate law (*n*-th order) and the Langmuir-Hinshelwood (L-H) rate equations, which are respectively given in Equation 2.20 and 2.21.

$$r_s = k'_s p_A^n \tag{2.20}$$

$$r_s = \frac{k'_s K_A p_A}{1+K_A p_A} \tag{2.21}$$

Partial pressure is calculated by multiplying the gaseous molar fraction with the total pressure, as shown in Equation 2.22.

$$p_A = y_A P \tag{2.22}$$

The power rate law is an empirical kinetic rate model and has been used widely *i.e.* (Roberts and Harris, 2000), (Kajitani *et al*., 2002), (Everson *et al*., 2008_a). The rate constant normally follows an Arrhenius temperature dependency. Equation 2.20 can be rewritten to the form:

$$r_s = k_o e^{-\frac{E_a}{RT}} p_A^n \tag{2.23}$$

Although the power rate law is widely used and easy to implement, the experimental conditions for its application should be scrutinised (Roberts and Harris, 2006), (Liu *et al*., 2000).

The advantage of using the more complex L-H model is that it incorporates the heterogeneous gas-solid surface reactions and has been proven to be accurate over wide temperature and pressure ranges *i.e.* (Fushimi *et al*., 2011), (Roberts and Harris, 2000). The L-H model is also easily adapted to incorporate gas reagent mixtures and is used predominantly with multiple gaseous reactants when inhibition is present. Equation 2.21 can be modified to incorporate product inhibition by adding a term to the de-nominator (Everson *et al*., 2006_a).

$$r_s = \left[\frac{k_s' K_A p_A}{1+K_A p_A + K_i p_i}\right] \quad (2.24)$$

The kinetic rate constants are related to temperature dependence with the Arrhenius Equation (2.25) and the adsorption constants with the van't Hoff Equation (2.26).

$$k_s' = k_o e^{-\frac{E_a}{RT}} \quad (2.25)$$

$$K_A = K_o e^{-\frac{\Delta H}{RT}} \quad (2.26)$$

If more than one gaseous reagent is present such as with steam and CO_2 gasification, one of two surface mechanisms are proposed. Either the steam / H_2-char reactions and the CO_2 / CO-char reactions occur on separate active sites (Equation 2.27) and do not compete for reactive surface, or the reactions occur on the same active sites (Equation 2.28) and compete for the same reactive surface area (Mühlen *et al*., 1984), (Everson *et al*., 2006_a), (Huang *et al*., 2010). The Langmuir Hinshelwood equations for these two scenarios are as follow:

Additive model:

$$r_s = \left[\frac{k'_{CO_2} K_{CO_2} p_{CO_2}}{1+K_{CO_2} p_{CO_2} + K_{CO} p_{CO}} + \frac{k'_{H_2O} K_{H_2O} p_{H_2O}}{1+K_{H_2O} p_{H_2O} + K_{H_2} p_{H_2}}\right] \quad (2.27)$$

Competitive model:

$$r_s = \left[\frac{k'_{H_2O} K_{H_2O} p_{H_2O} + k'_{CO_2} K_{CO_2} p_{CO_2}}{1+K_{H_2O} p_{H_2O} + K_{H_2} p_{H_2} + K_{CO_2} p_{CO_2} + K_{CO} p_{CO}}\right] \quad (2.28)$$

Various different forms of the L-H equations have been derived (Blackwood and Ingeme, 1960), (Mühlen *et al*., 1984), (Roberts and Harris, 2007). The work by Mühlen *et al*. (1984) reported L-H equations that incorporated various mixed and squared terms. Although these extra terms do increase the model accuracy and can incorporate methane formation, the large amount of terms make this model complex to solve.

2.5.4 Boudouard reaction kinetics and mechanism

The CO_2-char reaction is commonly used to investigate different gasification parameters. The surface reaction mechanism of CO_2 and solid carbon is generally reported to be (Mühlen *et al*., 1984), (Chen *et al*., 1993), (Irfan *et al*., 2011):

$$CO_2(g) + C_f(s) \rightarrow CO(g) + C(O) \quad [2.9]$$

$$C(O) + C_i \rightarrow CO(g) + C_f \quad [2.10]$$

Gasification relies on the ability of the free carbon atoms to detach oxygen from the CO_2 molecule colliding with the char surface (Kapteijn *et al*., 1992), (Chen *et al*., 1993). The rate of gasification is dependent on the de-sorption rate of the adsorbed C(O) species as shown in Reaction 2.10 (Chen *et al*., 1993). If the formed CO re-adsorbs onto free carbon sites (C_f) it prevents further reaction on that site until the C(CO) has desorbed (Roberts and Harris, 2006). By this mechanism CO inhibits the CO_2-char reaction (Ergun, 1961).

Adánez *et al*., (1985) gasified a Spanish lignite char at 1000 °C and clearly showed how an increase in carbon monoxide partial pressure inhibits the char CO_2 reaction.

Liu *et al*. (2000) reviewed literature on coal-char gasification with CO_2, and developed a model to extrapolate moderate temperature, high pressure data to high temperature, high pressure systems. They found that the L-H expression was superior to the *n*-th order rate equation. The apparent CO_2 gasification rate was observed to increase with CO_2 partial pressure. An average activation energy of 212 kJ/mol was calculated for the CO_2 gasification of bituminous coal-chars. The Authors found that from 1123 to 1727 °C the reaction shifted from chemical reaction controlled to diffusion controlled.

Sun *et al*. (2004) studied the CO_2 gasification kinetics of a Shenmu coal with and without the addition of catalysts. They found that the gasification rate increased 2.3 times with temperature (850-900 °C) and 6 times with pressure (0.1-3 MPa) increase. The gasification kinetics were analysed by DAEM and the activation energy for Chinese Shenmu coal-chars ranged from 200 to 300 kJ/mol.

Kajitani *et al*. (2006) studied the CO_2 reactivity of four coal-chars in a pressurised drop tube furnace (PDTF) and TGA at high temperatures and pressures. Chars from an Australian coal, an American coal and two Chinese coals were prepared at 1400 °C and an average particle

diameter of 40 μm was used. The RPM was successfully implemented to model the char conversion curves, with structural parameter (Ψ) values ranging from 1 to 26. A definite decrease in reaction rate was observed with an increase in carbon monoxide partial pressure, for all temperatures and chars. Both the *n*-th order and the L-H rate equations were evaluated. Although both equations were relevant below 0.2 MPa, only the L-H equation was able to predict carbon monoxide inhibition accurately. Power rate law reaction orders ranged from 0.43 to 0.53 and Langmuir activation energy ranged from 212 to 251 kJ/mol.

Everson *et al*. (2008_a & b) investigated the CO_2 gasification of a high ash (33.8 %wt), inertinite-rich South African coal under fluidised bed gasification conditions (850-900 °C and 287.5 kPa). A 200 mg sample of 1 mm particles was used in a TGA apparatus. It was found that the RPM with a power rate law (*n*-th order) fitted the experimental data well. A structural parameter (Ψ) of 1.0 ± 0.3 was calculated by regression of the experimental data. The activation energy increased from 192 kJ/mol to 247 kJ/mol for 20 % and 100 % CO_2 respectively. An average reaction order of 0.50 ± 0.04 was determined.

2.5.5 Steam gasification kinetics and mechanism

The reaction mechanism of the steam-hydrogen-carbon reaction can be described by the following equations (Molina and Mandragon, 1998), (Roberts and Harris, 2006):

$$H_2O(g) + C_f \leftrightarrow C(O) + H_2(g) \qquad [2.11]$$

$$C(O) + C_i \rightarrow CO(g) + C_f \qquad [2.12]$$

Reaction 2.11 shows the oxygen dissociation step, forming a carbon oxygen bond on the char surface and releasing H_2 (Srivastava *et al*., 2007). The second step (Reaction 2.12) involves the CO release from the char surface and the forming of a new active site (C_f), Reaction 2.13 is identical to reaction 2.10 for CO_2 gasification.

Matsuoka *et al*. (2009) investigated steam gasification in a pressurised fluidised bed. Two coals were studied, an Indonesian sub-bituminous coal and an Australian lignite. About 2 g of 0.5-1 mm sample was loaded into the reactor. Experiments were conducted at 773 and 841 °C with pressures ranging from 0.2 to 0.5 MPa. A homogeneous kinetic model showed good linearity over all the conditions. The *n*-th order rate equation was implemented and predicted

the rate data well, but was only valid over a narrow pressure range. To predict the reactivity data over a broader pressure range, the L-H equation was implemented which fitted the reactivity data well. Reaction orders for the two coals were 0.4 and 0.5 respectively. The calculated activation energies were reported as 250 and 230 kJ/mol. They concluded that an increase in steam partial pressure directly increases the gasification rate.

Wu *et al*. (2006) investigated the steam gasification kinetics for chars prepared at high pyrolysis temperatures. Four chars (3-6 mm) were prepared from a Yanzhou coal each at a different temperature ranging from 950 to 1400 °C. Experiments were conducted in a fixed bed-reactor with sample sizes of 7 g and temperatures ranging from 900 to 1200 °C. They found that reactivity decreased with increasing pyrolysis temperature. The influence of gasification temperature was much more pronounced than the influence of heating rate. It was also found that nitrogen-BET surface area increased gradually with steam gasification at 1100 °C, and then declined above 70 % conversion. Because of the high gasification temperatures, the reaction diffusion model based on the SUCM was implemented. Calculated activation energies ranged from 124 to 197 kJ/mol.

Fermoso *et al*. (2010) investigated the non-isothermal kinetic behaviour of a Spanish bituminous coal and its blends with biomass. The analyses were conducted in a TGA apparatus with heating rates of 5, 10 and 15 K/min up to 1100 °C. *n*-th order rate kinetics was applied to, the volumetric (homogeneous) model, the grain (SUCM) model and the RPM. The calculated activation energies for the respective models were 304, 237, and 259 kJ/mol. The RPM was found to describe the coal-char reactivity best with a structural parameter (Ψ) of 0.9.

2.5.6 Multi component gasification kinetics

As the primary reactions progress during gasification, reaction products such as CO_2, CO, H_2 and CH_4 are produced. As the concentrations of these gases increase, they may retard the primary gasification reactions or participate in secondary gasification reactions. Many authors have done comparative studies of these reactions or investigated how these product gases influence the primary gasification kinetics (Mühlen *et al*., 1984), (Everson *et al*., 2006_a), (Roberts and Harris, 2007), (Ahmed and Gupta, 2011).

Ergun (1961) investigated steam and CO_2 gasification of a metallurgical coke in a fluidised bed reactor with a temperature range of 900-1000 °C and atmospheric pressure. He found that

steam reacts on 60 % more of the char surface than CO_2 does. He also postulated that gasification rates of steam and CO_2 mixtures could be predicted from pure gas rates.

Mühlen *et al*. (1984) gasified a German bituminous char at high pressures in pure H_2, steam and CO_2 and investigated the inhibition of H_2 and carbon monoxide on the steam-char reaction and the CO_2-char reaction respectively. The experimental ranges investigated for temperature and pressure were 800-1000 °C and 1-70 bar. While evaluating multiple forms of the L-H equation Mühlen *et al*. (1984) developed a model that incorporates H_2, methane and carbon monoxide inhibition with a SUCM structural model. Activation energies of 153 and 154 kJ/mol were calculated for CO_2 and steam gasification respectively. The authors successfully modelled a pressurised fluidised bed reactor with their derived equation.

In an attempt to elucidate how steam and CO_2 reacts with char Czechowski and Kidawa (1991) investigated the physical changes of a bituminous coal-char at 50 % conversion. The coal and samples of its macerals were gasified in a TGA apparatus at 900 °C and then subjected to optical microscopy, scanning electron microscopy (SEM), CO_2 adsorption analysis and elemental analysis. The conclusion was that the steam gasification reaction proceeds preferentially on the internal pore structure and the CO_2 reaction proceeds preferentially on the outer pore structure.

Roberts and Harris (2000) measured the intrinsic reaction rates of two Australian coal chars in a fixed bed reactor and a pressurised TGA. Experiments were conducted below 940 °C for CO_2 and 900 °C for steam to ensure chemical reaction controlled reaction rates. A pressure range from 1 to 30 bar was investigated using a particle size of 1.0 ± 0.6 mm. They found that the increase in reactivity (due to pressure increase) diminished significantly above 10 bar. To keep the model simple for practical application and to validate its effectiveness for high pressure extrapolation, they opted for a global rate model with an *n*-th order kinetic equation. The calculated reaction orders for steam and CO_2 gasification were 0.4-0.5 and 0.5-0.7 respectively. Activation energies were found to increase with a pressure increase of 1-10 bar. The calculated values ranged from 209-250 kJ/mol for CO_2 and 227-235 kJ/mol for steam gasification.

The high temperature and pressure gasification kinetics of two bituminous coals were investigated by Kajitani *et al*. (2002). A pressurised drop tube furnace at temperatures of 1100-1500 °C and pressures of 0.2-2.0 MPa was used. They found that the effect of pressure during pyrolysis was insignificant. After some evaluation it was found that the RPM with *n*-th order rate kinetics predicted the experimental data well. A structural parameter of 3 was

determined, as well as reaction orders of 0.54-0.73 for CO_2 gasification and 0.86 for steam gasification. Activation energies for steam gasification were found to be constant at 214 kJ/mol. CO_2 gasification activation energies were 261-283kJ/mol for low temperatures (<1200 °C) and 163 kJ/mol for high temperatures (>1200 °C).

Roberts and Harris (2006) investigated the application of the L-H rate equation in chemical reaction controlled systems over a wide range of reactant partial pressures. The authors concluded that the *n*-th order rate equation would not be able to describe char gasification rates at high pressures because *n* was not constant with pressure. Experiments were conducted on three Australian bituminous coals similar to previous studies (Roberts and Harris, 2000). It was found that a general L-H equation with surface area incorporated was suitable to describe systems with reactant partial pressures of up to 3.0 MPa. In determining how to model mixed gas reactivity by using pure gas rate data Roberts and Harris (2007) compared rate data for steam, CO_2 and mixtures of steam and CO_2. Using an adapted L-H rate equation they concluded that the data could be modelled under the assumption that the steam reaction is inhibited by the slower CO_2 reaction.

Chen *et al*. 2013 implemented the shrinking core model to predict the gasification rates of two lignite chars. The chars were gasified with steam, CO_2 and their mixtures in a TGA system. They found that the gasification rate of the mixtures of steam and CO_2 were slower than the sum of the two individual rates but definitely faster than the independent rates. They concluded that the char-steam reaction proceeded independent of the presence of CO_2, but the char-CO_2 reaction was inhibited by the char-steam reaction.

Everson *et al*. (2006) investigated the gasification of two inertinite rich South African high-ash coals over a temperature range of 800-950 °C. Both the effects of H_2 inhibition and CO inhibition were evaluated. They found that the SUCM with L-H kinetic equations predicted the experimental data well (under the assumption that the reactions proceed on separate active sites). Activation energies for steam gasification were 201-212 kJ/mol and 109-137 kJ/mol for CO_2. An experiment with an equilibrium concentration of steam, CO_2, CO and H_2 confirmed the applicability of the developed model.

Research done by Huang *et al*. (2010) on a lignite coal delivered similar results. The coal-char was gasified in reactant mixtures of steam-H_2 and CO_2-carbon monoxide respectively. The rate constants for these reactions were used to predict the gasification rate of an equilibrium mixture of steam, H_2, CO and CO_2. Calculated activation energies were 216

kJ/mol for steam and 143 kJ/mol for carbon-dioxide gasification. It was found that the homogeneous model with additive L-H kinetics fitted the experimental data best.

Guizani *et al*. (2013) researched the gasification reactivity of high and low heating rate beech wood chars. The chars were gasified in a macro (large particle) TGA apparatus at temperatures of 850 to 950 °C and atmospheric pressures. Steam, CO_2 and its mixtures were used as gasification reagents with concentrations ranging from 10% to 30%. They concluded that steam and CO_2 react on separate active sites and that CO does not affect the char structure to influence the steam-char surface reaction.

In a study considering the sharing of coal char active sites, Umemoto *et al*. (2013) gasified three bituminous coal chars in the presence of steam and CO_2. The experiments were conducted at atmospheric pressure and temperatures of 900 to 1100 °C in both a PDTF and a TGA apparatus. They found that the additive L-H model over predicted their experimental results while the competitive model made under predictions, thus they developed an L-H model that assumes steam and CO_2 share some of the active char surface but not all.

2.6 Summary

Gasification studies obtained from literature are summarised in Table 2-3. It is observed that the majority of gasification reactivity studies were conducted in a TGA apparatus. Particle sizes investigated ranged from 0.075 to 6 mm. Most studies were conducted at low temperatures (< 1000 °C). A variety of structural models have been applied either with the *n*-th order or L-H kinetic rate equations. Activation energies ranging from 91 to 280 kJ/mol were observed, with no clear trend between steam and CO_2 gasification values.

The primary focus of this study and its uniqueness lies in the mathematical modelling of the chemical reaction controlled gasification kinetics of a South African Highveld coal in the presence of both steam and CO_2 concentrations ranging from 25 mol% to 100 mol%. This information is valuable for both the South African and Global gasification industry.

Table 2-3: Summary of kinetic gasification literature

Reference	Analysis technique	Coal rank and/or %C d.a.f.	Particle size [mm]	Temperature [°C]	Pressure [bar]	Reagent	Model	Ea [kJ/mol] H_2O	Ea [kJ/mol] CO_2	Order H_2O	Order CO_2
(Everson *et al.*, 2006_a)	TGA	Inertinite rich 80	1	800-950	Atmospheric	H_2O,H_2, CO_2,CO	SUCM, L-H	212,204	109,137		
(Everson et al., 2008_a)	TGA	Inertinite-Rich	1	850-900	1-3	CO_2	RPM, *n*-th		192-247		0.46-0.54
(Feng and Bhaita, 2003)	Tube furnace	Semianthracite 93	0.09-0.18	800	Atmospheric	CO_2	RPM				
(Fermoso *et al.*, 2010)	TGA	Spanish Bituminous	< 0.15	Non-Isothermal	Atmospheric	H_2O	HM, SCM, RPM	304, 237, 259			
(Hattingh et al., 2009)	TGA	Bituminous 71,72,66	0.15-0.25	900-1000	1-10	CO_2	RPM				
(Huang *et al.*, 2010)	TGA	Lignite 68	0.2	850-950	0.05-0.3	H_2O,H_2, CO_2,CO	L-H, HM	216	143		
(Kajitani *et al.*,2002)	PDTF, TGA	2 x Bituminous 83,98		1100-1500	2-20	H_2O, CO_2	RPM, *n*-th	214	163,261, 283	0.86	0.49,0.54 0.73
(Kajitani et al., 2006)	PDTF, TGA	4 x Bituminous 83,78,81,78	0.04	1400	7	CO_2	RPM, L-H, *n*-th		240-280		0.43-0.56
(Lee and Kim, 1995)	TGA	Australian subbituminous	0.3-0.7	700-850	Atmospheric	H_2O	HM, SCM	211		0.43-0.67	
(Matsuoka *et al.*, 2009)	PFB	2 x Sub-bituminous 70,61	0.5-1	700-900	1-5	H_2O	L-H,HM	230,250		0.4-0.5	
(Mühlen *et al.*, 1984)	TGA	German Bituminous		800-1000	1-70	H_2O,H_2, CO_2,CO	L-H	154	153		
(Roberts and Harris, 2000,2006,2007)	TGA	3 x Bituminous 83,91	0.6-1.0	850-900	1-30	H_2O, CO_2	L-H, *n*-th	221-235	209-250	0.4-0.5	0.5-0.7
(Wu *et al.*, 2006)	Fixed bed	Yanzhou 67	3-6	900-1200	Atmospheric	H_2O	SUCM	127-197			
(Xu *et al.*, 2011_1&2)	Bench reactor	Lignite 81,92	6x10 Pellet	850-950	Atmospheric	H_2O	RPM	176	248		
(Umemoto *et al.*, 2013)	TGA, PDTF	Bituminous 97, 81, 78	0.04	900-1100	Atmospheric	H_2O, CO_2	RPM, L-H				

Chapter 3: Coal characterisation

3.1 Introduction

In this chapter the origin, preparation and characterisation of the coal used in this study and its resulting char are discussed. In Section 3.2 and 3.3 the coal origin and its preparation prior to experimentation are presented. In Section 3.4 the coal characterisation analyses are discussed. The analyses conducted include: conventional analysis, pore structure analysis and petrographic analysis. In Section 3.5 the results from the characterisation analyses are presented and discussed. In Section 3.6 a summary of the properties of the coal and its char is presented.

3.2 Sample origin

The coal selected for this study originates from the South African Highveld coal-fields (seam 4). This coal seam is mainly utilised for local power generation and as a feedstock for the petrochemical industry (Hattingh *et al*., 2011).

3.3 Sample preparation

A run-of-mine coal sample was collected by SGS Laboratories (Pty) Ltd. Further coal preparation was done at the North-West University. The coal particle size was reduced in a hammer mill (Usborn Coal equip Engineering (PTY) Ltd., Speed: 425 rpm, Size: 4x6 macro crusher, Model no.: 46-126) to a top size maximum of 7 mm. The coal was then screened, and the particles in a size range of - 1.2 mm + 0.8 mm were kept for experimentation.

To ensure a uniform starting material for all experiments, the coal was charred beforehand (Molina and Mandragon, 1998). Approximately 2 kg of the screened coal was charred for the intended gasification experiments. Batches of 100 g coal were charred in a 2.2 kW vertical furnace supplied by Ultra-Furn SA (Pty) Ltd. The coal was kept under constant nitrogen flow during the charring process. A heating rate of 25 °C/min was implemented up to a final temperature of 950 °C. Once the final temperature had been reached, the char was kept at a temperature of 950 °C for 1 hour before allowing the reactor to cool to ambient temperature.

To ensure that the de-volatilisation was complete, one char sample was placed in a TGA and left for 48 hours at 950 °C, no further mass loss was detected.

The char was stored in the laboratory in a re-sealable Nampak bag to keep moisture and oxygen exposure to a minimum. The bags are lined with aluminium foil to reduce gas diffusion into the bag. Prior to experiments char samples were weighed and kept in polytop sample holders.

3.4 Experimental

Because of the heterogeneous nature of coal, the coal and the prepared char were characterised on a structural, petrographic and chemical basis. The different characterisation analyses conducted in this study are summarised in Table 3-1.

Table 3-1: Coal analysis summary

Analysis	Property	Laboratory
Chemical	Proximate	ACT
	Ultimate	ACT
	Total Sulphur	ACT
	Calorific value	ACT
Petrographic	Maceral composition	ACT
	Vitrinite reflectance	ACT
Structural	CO_2 adsorption	NWU
	Mercury porosimetry	NWU

The proximate, ultimate, calorific value and petrographic analyses were outsourced to Advanced Coal Technologies (Pty) Ltd (ACT). The structural analyses were done at the North-West University (NWU).

The standards used for the various analyses are shown in Table 3-2.

Table 3-2: Chemical analysis methods

Procedure	Standard used
Proximate analysis	
Sample preparation	ISO 13909-4 :2001
Moisture content (%)	SANS 5925: 2007
Ash content (%)	SABS ISO 1171: 1997
Volatile Matter content (%)	SABS ISO 562: 1998
Ultimate analysis	
Ultimate analysis	ISO 29541 : 2010
Total sulphur via IR spectroscopy	ISO 19579 : 2006
Calorific value	
Calorific value (MJ/kg)	SABS ISO 1928 : 1995
Petrographic analysis	
Bituminous coal and anthracite	SABS ISO 7404: 1994 Part 1-5

3.4.1 Petrographic analysis

Coal samples with a particle size of -7 mm (analysis requirement) were sent to ACT for petrographic analyses. For the petrographic analyses, a petrographic block was prepared and polished according to the ISO Standard 7404-2. 100 Vitrinite random reflectance measurements were taken from the coal sample according to the ISO Standard 7404-5 to determine the coal rank. To determine the group maceral composition the 500 point count technique was implemented according to ISO Standard 7404-3.

3.4.2 Gas adsorption analysis

CO_2 gas adsorption analysis was used to investigate the micro pore (4-12 Å) structures of the coal and its char. A Micrometrics ASAP 2010 analyser was used for the analysis. Pulverised coal samples (< 100 µm) of 2 g were loaded into the degassing tubes and connected to the degassing ports of the apparatus. The samples were degassed at 25 °C and at a pressure of < 4 µm Hg for 48 hours. The low temperature of the degassing process ensures that only the moisture is driven off from the coal / char pore structure. After the degassing was completed, the samples were connected to the analysis port and analysed overnight in an ice bath to keep the sample temperature at 0 °C. Micrometrics ASAP 2010 software was used to report the

pore diameter and surface area using the Langmuir and Dubinin-Radushkevich gas adsorption models.

3.4.3 Mercury porosimetry analysis

Mercury porosimetry is applied to investigate pores between 500 µm and 3.5 nm (Giesche, 2006), *i.e.* the meso pore range. The density and pore area was determined using a Micrometrics AutoPore IV 9500 VI.05 analyser. Coal particles of 2-3 mm in size were used for this analysis. A micrometrics penetrometer with a stem volume of 0.392 cm^3 was used. The samples were first loaded to obtain a used stem volume of 60-90 % and then degassed at 50 µmHg for 5 minutes. The bulk density was determined at a pressure of 3.59 kPa, while the skeletal density, porosity and total pore area was determined at pressures ranging from 0.96 kPa to 413.7 MPa.

3.5 Results and discussion

All characterisation experiments were done twice, *i.e.* once before experimentation started and again six months after the initial analyses. In the results, the average of the 2 analysis values is reported, and between brackets half of the difference between the values is given as an indication of the error. So, if a value of 4 and 6 is measured, the result will be given as 5 (±1).

The CO_2 adsorption analysis was only done once and an error was estimated from previous research (Hattingh *et al*., 2011). The results obtained from the different analyses are presented and evaluated.

3.5.1 Proximate analysis

In Table 3-3 the proximate analysis results for both the char and the parent coal is shown.

Table 3-3: Proximate analysis comparison

Variable [wt%]	Coal (a.d)	Coal (d.b.)	Char (a.d.)	Char (d.b.)
Moisture content	5.6 ± 0.1		3.0 ± 1.2	
Volatile matter content	23.8 ± 0.1	25.2 ± 0.1	1.9 ± 0.1	2.0 ± 0.1
Fixed carbon content[1]	49.1 ± 0.3	52.0 ± 0.3	70.4 ± 1.3	72.5 ± 1.3
Ash Content	21.6 ± 0.3	22.9 ± 0.3	24.8 ± 0.3	25.5 ± 0.3
Fuel ratio	2.1		37	

[1] Obtained by difference

The charring process was accompanied by a strong decrease in volatile matter content which caused an increase in the fixed carbon and ash content of the char. Similar volatile matter loss trends have been observed by other gasification studies *i.e.* (Wu *et al*., 2006), (Kajitani *et al*., 2002), (Huang *et al*., 2010), (Roberts and Harris, 2006). Okolo (2010) investigated four high inertinite Highveld coals and found char volatile matter contents ranging from 0.8 to 3.3 wt% (d.b).

The large char moisture error can be explained by the fact that the first char analysis was done shortly after the char was prepared and the second analysis six months later. The samples were exposed to the atmosphere during handling and weighing of samples which allowed atmospheric moisture to adsorb to the char surface.

Calculating the coal fixed carbon content on a dry mineral matter free basis gives a value of 72 %. On the ASTM coal classification ranking such a coal is classified as a medium volatile bituminous coal, which is typical of the Highveld seam 4 coal (Hattingh *et al*., 2011). This is also a high ash coal (23 wt% d.b.) according to SABS ISO standard 1171 of 1997. The proximate analysis results compare well to other studies that have been conducted on coals from the same seam (Hattingh *et al*., 2011), (Hlatshwayo et al., 2009), (Pinheiro, 1999).

3.5.2 Ultimate analysis

The ultimate analysis was done on both the coal and the char, the obtained analysis results are summarised in Table 3-4.

Table 3-4: Ultimate analysis results

Variable [wt%]	Coal [d.a.f.]	Char [d.a.f.]
Carbon	78.4 ± 0.1	96.0 ± 0.1
Hydrogen	4.0 ± 0.1	0.1 ± 0.1
Nitrogen	2.0 ± 0.1	1.6 ± 0.1
Oxygen[1]	14.7 ± 0.4	1.6 ± 0.2
Sulphur	0.9 ± 0.3	0.7 ± 0.1

[1] Obtained by difference

As expected both the oxygen and hydrogen contents of the coal were significantly reduced during de-volatilisation, which is consistent with other studies (Kajitani *et al*., 2002), (Roberts and Harris, 2006), (Matsuoka *et al*., 2009).

The sulphur and nitrogen contents only decreased slightly during the charring process. This shows that the nitrogen and sulphur species found in the coal are tightly bound to the carbon structure and unlikely to form volatile compounds when exposed to high temperatures in an inert atmosphere. This observed behaviour during de-volatilisation relates well to other gasification studies with bituminous coals *i.e.* (Roberts and Harris, 2000, 2006, 2007), (Kajitani *et al*., 2002), (Wu *et al*., 2006), (Van Niekerk and Mathews, 2010). The reported values in Table 3-4 also relate well to other studies involving the same coal seam (Hattingh *et al*., 2011), (Van Niekerk and Mathews, 2010).

3.5.3 Calorific value

Results of the calorific value analysis of the char and the parent coal are presented in Table 3-5 and compared to calorific values calculated using the Dulong formula (Speight, 2005). This formula relates coal chemical composition to calorific value and is represented by:

$$CV\ [MJ/kg] = 33.86 * C\ wt\% + 144.4 * \left(H\ wt\% - \frac{O\ wt\%}{8}\right) + 9.428 * S\ wt\% \quad (3.1)$$

The calculated values correspond well to the values reported by ACT.

Table 3-5: Gross calorific value

Variable [MJ/kg]	Coal [a.d.b.]	Char [a.d.b.]
Calorific value [ACT]	21.7 ± 0.3	24.2 ± 0.3
Calorific value [Dulong]	22.2 ± 0.3	23.0 ± 0.3

From literature it is observed that a typical Highveld coal has a gross calorific value ranging from 19 – 23 MJ/kg on an air dried basis (Van der Merwe, 2010), (Hattingh *et al*., 2011), which is in agreement with the analysis values reported in Table 3-5.

3.5.4 Petrographic analysis

Both the petrographic maceral composition and the vitrinite reflectance results are discussed in this section. The maceral composition analyses values are reported in Table 3-6. From the analysis it is evident that the coal has high inertinite content (69% m.m.f.b.) and a low liptinite content, which is typical for Highveld coal (Van Niekerk and Mathews, 2010), (Hattingh *et al*., 2011).

Table 3-6: Maceral point count results

	Coal	
% Vitrinite		17 ± 1
% Liptinite		2 ± 1
% Inertinite		81 ± 1
% Fusinite + Secrenite	2	
% Micrinite	< 1	
% Minerals	13	
% Reactive Semifusinite	28	
% Inert Semifusinite	39	
% Total Reactives		47 ± 1
% Vitrinite	17	
% Liptinite (Exinite)	2	
% Reactive Semifusinite	28	
% Total Inerts		54 ± 1
% Inert Semifusinite	39	
% Inertinite	2	
% Mineral Matter	13	

For bituminous coals, it is generally accepted that the reactive macerals include only vitrinite and liptinite. However, some macerals that are classified as inertinites do contribute to the reactive materials, such as reactive semifusinite. The total reactive macerals make up 46% of the coal maceral content. The vitrinite reflectance histogram for the investigated coal is shown in Figure 3-1.

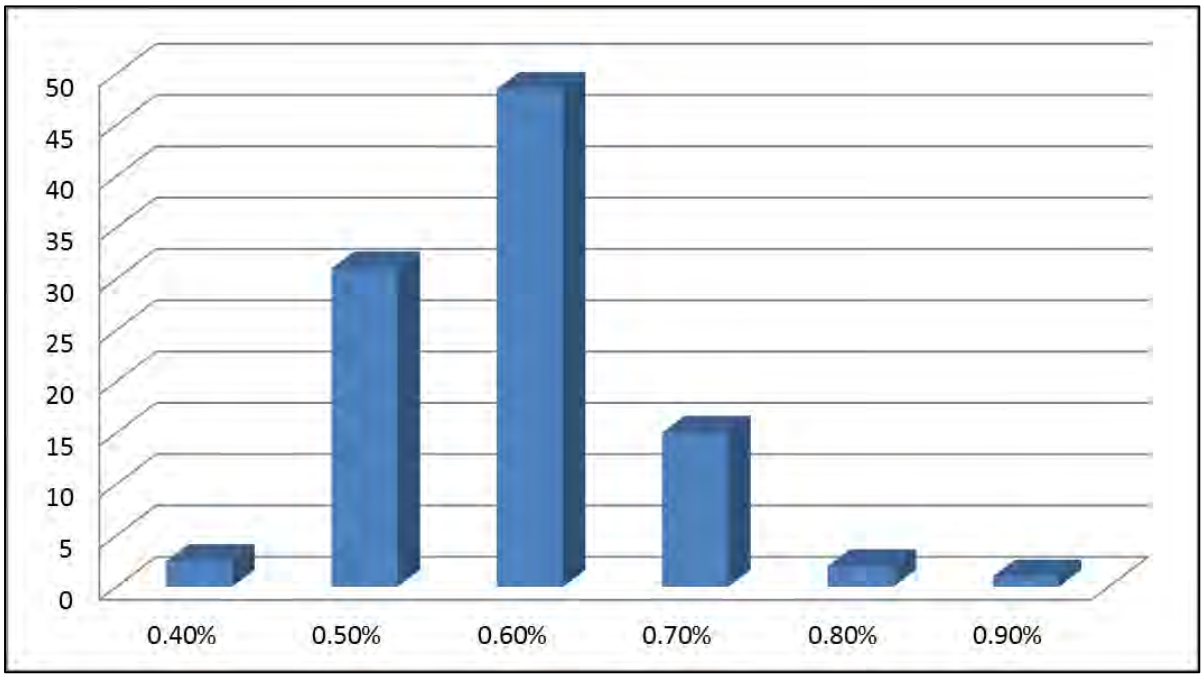

Figure 3-1: Vitrinite reflectance histogram

It is evident that the vitrinite reflectance falls predominantly in the 0.50 to 0.79 % (V5 to V7) reflectance bands. From the vitrinite reflectance data the mean vitrinite reflectance was calculated as 0.64 % with a standard deviation of 0.08 %. The small standard deviation (<0.1 %) is typical of a single seam, non-blended coal. When comparing the reported vitrinite mean reflectance value to the ISO standard 11760(2005), the coal ranks as a bituminous medium rank C, which is typical of a Highveld seam 4 coal (Hattingh *et al*., 2011).

3.5.5 Gas adsorption analysis

The micro pore surface area and the monolayer capacity were calculated using the Dubinin-Radushkevich (D-R) equation and Langmuir surface areas were calculated from isotherm data. The CO_2 adsorption experimental results are summarised in Table 3-7.

Table 3-7: Gas adsorption analysis results

	Coal	Char
D-R Surface area [m^2/g]	161 ± 5	182 ± 5
D-R Monolayer capacity [cm^3/g]	35 ± 1	40 ± 1
Langmuir [m^2/g]	117 ± 5	126 ± 5
Pore volume [cm^3/g]	4.2 ± 2 x10^{-5}	3.3 ± 2 x10^{-5}

Hattingh *et al*., (2011) found surface areas for three Highveld seam 4 coals to be between 181-197 m^2/g when calculated using the Dubinin-Radushkevich equation. This corresponds to the CO_2 surface areas calculated by Feng & Bhatia (2003) for bituminous chars of 100-300 m^2/g.

It is clear that the charring of the coal increases the total micro pore surface area of the particle. The average pore volume and pore size is decreased during the charring / de-volatilisation process. These results may be explained by the opening and creation of more micro pores during the heat treatment of the de-volatilisation process. An increase in the amount of smaller pores will lower the average pore diameter and increase the total surface area (Sangtong-Ngam and Narasingha, 2009). Everson *et al*. (2008_a) found an increase in BET surface area when comparing chars prepared at 700 °C and 900 °C to its parent coal.

3.5.6 Mercury porosimetry analysis

To determine the coal and char structural properties such as density and meso pore area, mercury porosimetry was performed (Giesche, 2006). The results obtained from the Mercury intrusion analyses are summarised in Table 3-8.

Table 3-8: Mercury intrusion results

Properties	Coal	Char
Total meso pore volume (ml/g)	0.09 ± 0.01	0.12 ± 0.01
Total pore area (m^2/g)	21.2 ± 0.8	8.7 ± 0.2
Average pore diameter (Å)	162 ± 16	532 ± 24
Porosity (%)	12.5 ± 0.8	17.2 ± 1.2
Bulk density @ 3.52 kPa (g/mL)	1.45 ± 0.1	1.48 ± 0.1
Apparent (skeletal) density (g/mL)	1.67 ± 0.1	1.79 ± 0.1

The meso pore volumes and surface areas reported in Table 3-8 correspond well to values reported for bituminous coals by Czechowski and Kidawa (1991).

The coal used in this study is seen to have a lower porosity when compared to bituminous coals reported in the literature (Bliek *et al*., 1986), (Ye *et al*., 1997), this could be due to the high inertinite content resulting in a more dense char (Everson *et al*., 2006_a).

The following deductions can be made from the mercury intrusion results shown in Table 3-8. All the measured and calculated parameters increased with de-volatilisation, of which the pore diameter increased by the most (± x3). Only the total pore area was observed to decrease

by more than half. These results can be explained by the widening and merging of the central pores during de-volatilisation, resulting in higher particle porosity. Due to the pore size increase the pores merged, resulting in a decrease in the measured surface area of the sample (Yu *et al.*, 2007).

3.6 Summary of char properties

The characterisation results are summarised in Table 3-9. All reported results are typical of South African Highveld seam 4 coal and compares well to values reported in literature for similar coals.

Pore structure analysis of the parent coal and the resulting char showed that charring at 950 °C results in a decrease in meso pore surface area but an increase in micro pore area. This means that the heat treatment and volatile matter release caused more micro pores to form in the char structure, while the larger meso pores grew and merged.

Taking all factors into account, this coal is classified as a high ash, high inertinite, medium rank C bituminous coal.

Table 3-9: Summary of coal and char characterisation results

Properties		Coal	Char
Proximate analysis [wt% a.d.b.]			
	Moisture	5.6	3.0
	Volatile matter	23.8	1.9
	Fixed carbon	49.1	70.4
	Ash	21.6	24.8
Ultimate analysis [wt%, d.a.f.]			
	Carbon	78.4	96.0
	Hydrogen	4.0	0.1
	Nitrogen	2.0	1.6
	Oxygen	14.7	1.6
	Sulphur	0.9	0.7
Calorific value [MJ/kg a.d.b.]		21.7	24.2
Petrography [%]			
	Vitrinite	17	
	Liptinite	2	
	Inertinite	81	
Physical analysis			
	CO_2 surface area D-R [m^2/g, d.a.f]	161	182
	Mercury intrusion Pore area [m^2/g]	21.2	8.7
	Porosity [%]	12.5	17.2

Chapter 4: Experimental

4.1 Introduction

In this chapter the experimental equipment, the experimental parameters as well as the collection method for char gasification data is presented. In Section 4.2 the raw materials used for gasification experiments are described. In Section 4.3 a detailed description of the experimental setup is given. In Section 4.4 the experimental methods followed to gather data is presented and the data processing procedures are given in Section 4.5. In Section 4.6 the experimental limitations for temperature, reagent flow and sample mass are presented. In Section 4.7 all the experimental parameters are presented and summarised.

4.2 Materials used

For the purposes of this study only one coal was used. 1 ± 0.2 mm coal particles were charred beforehand to create a uniform starting material as discussed in Section 3.3. The characteristic properties of the coal and char are summarised in Table 3.9.
The gases CO_2 and N_2 were supplied by AFROX South Africa. Nitrogen was selected as the inert gas during de-volatilisation and as diluent in the reactivity experiments. Reagent gas specifications are summarised in Table 4-1

Table 4-1: Gas reagent specifications

Gas	Item number	Purity	Grade
Carbon Dioxide	40-RC	>99.0	Technical
Nitrogen	511203-SE-C	>99.999 %	Baseline 5.0

Compressed air from a main line connected to a compressor was used to burn off residual carbon after gasification experiments were completed. De-ionised water supplied by Immuno-Vet services (Pty) Ltd was used for steam generation.

4.3 General description of experimental setup

In this study an existing in-house large particle TGA design was used. This apparatus was used since no commercial TGA was readily available that could incorporate steam. The apparatus was originally designed for particles up to 45 mm, but since operation in the chemically controlled regime was desired, smaller particle sizes were used. A schematic representation of the experimental setup is presented in Figure 4-1.

The flow of gaseous reagents (6) was controlled by a bank of Brooks model 0254 mass flow controllers (5). The separate mass flow controllers connect to a manifold which in turn connects to the tube furnace. All mass flow controllers were individually calibrated with a bubble flow meter.

A 20 *l* water reservoir (1) was connected to a 323 S/D Watson-Marlow Bredel high-performance variable speed peristaltic pump (2) which fed water through a non-return valve (3) to a clamp oven. The 1400 W custom built clamp oven (4) supplied by Hi-Tech elements (Pty) Ltd was operated at 340 °C to produce steam.

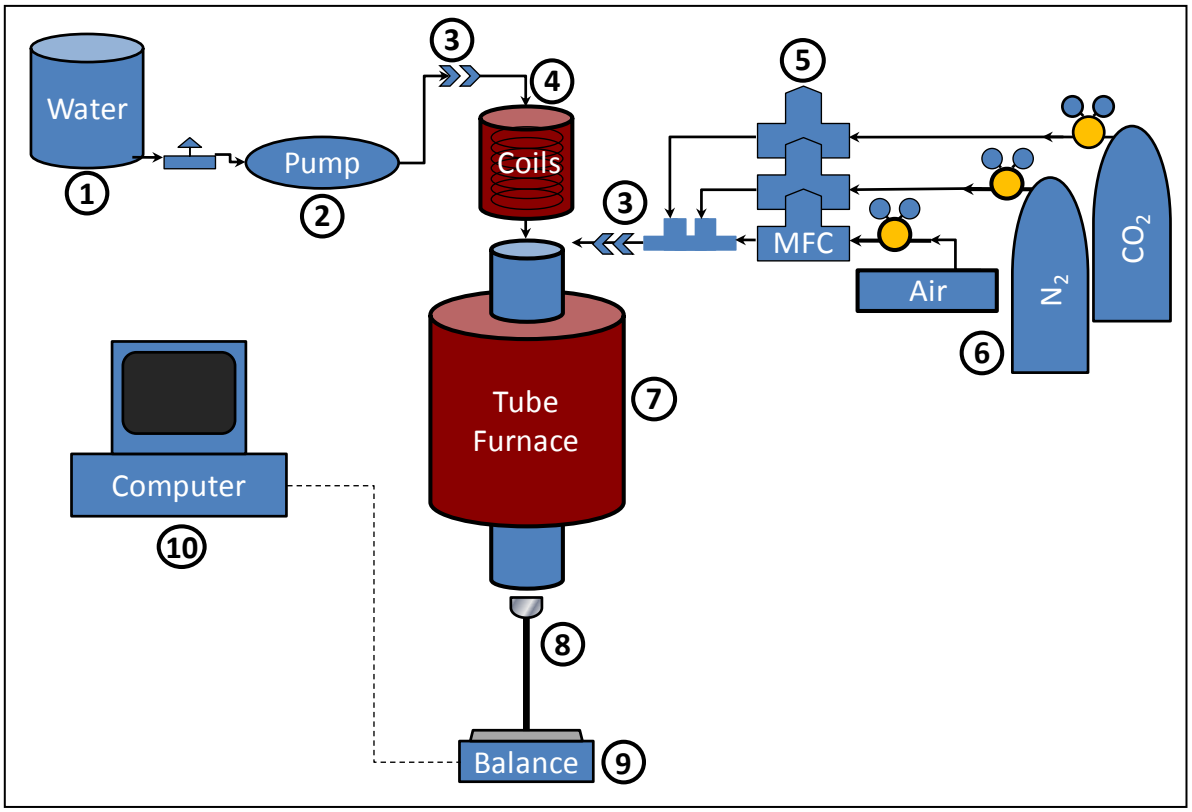

Figure 4-1: Schematic representation of the experimental setup

All reagents were fed to the top of a 50 mm ID Kanthal pipe fitted into a TSV15/50/180 tube furnace (7) supplied by Elite Thermal Systems Ltd which served as the heat source for the reactions. The furnace can be controlled to operate at temperatures from ambient to 1500 °C and with heating rates ranging from 1 to 25 °C/min. A 3 mm K-type [1] thermocouple was inserted from the top of the reactor to measure the temperature. The thermocouple was placed ± 5 mm above the sample during experiments.

Care was taken to ensure that the sample was in the thermal stable (constant temperature) region of the reactor (Appendix 7.1) and that the particles were converted under isothermal conditions (Appendix 7.2). A specially designed quartz bucket (8) was used to introduce the char sample into the reactor. Bucket design specifications are given in Appendix 7.3.

The sample bucket was placed on an ADAM PGW 453e milli balance (9) which continually (every 5 seconds) logged the mass of the sample in the reactor. The balance was linked to a personal computer (10) with an RS-232 connection cable. Using ADAM Data Capture Utility software, the mass values were saved in a .csv file format to later be exported and evaluated in Microsoft Office Excel. The ADAM PGW 453e mass balance is rated to have repeatability (accuracy) of 0.001 g and linearity (standard deviation) of 0.002 g. These specifications were confirmed by taking the standard deviation of 280 readings from an 8 hour blank experiment. The calculated standard deviation was 0.002 g.

4.4 Experimental method

Char samples were weighed off beforehand and kept in polytop vials. The reactor temperature was set to the desired experimental temperature. A constant nitrogen flow of 1800 Nml/min was used during heating and cooling of the reactor. The sample stand was prepared with the sieve and quartz wool and placed on the balance. The balance was zeroed and two readings were logged to the computer. The char sample was then loaded onto the quartz bucket and spread out to form a layer of uniform thickness (2-3 particles thick). Two more readings are logged to establish the exact sample mass. The bucket was raised into the bottom (cold) section of the oven under constant nitrogen flow. The data logging software was then set to capture the mass. Then the oven was lowered until the bucket was inside the hot zone and just below the thermocouple. Once all adsorbed moisture had been driven off the sample and the mass has been stable for 5 minutes the nitrogen flow was turned off. The

[1] The K-type thermocouple has an effective temperature measurement range from -200°C to 1350°C.

sample mass without reagent flow was logged for 2 minutes before the gasification reagents (Steam/N_2/CO_2) was introduced.

Experimental runs were left to either achieve complete conversion or for the slowest runs, the experiment was terminated after ± 48 hours regardless of conversion achieved. The gasification reagent flows were then stopped and an air flow was introduced to burn off residual carbon. Once no significant mass loss was observed, all flow was stopped and the ash value without reagent flow was logged.

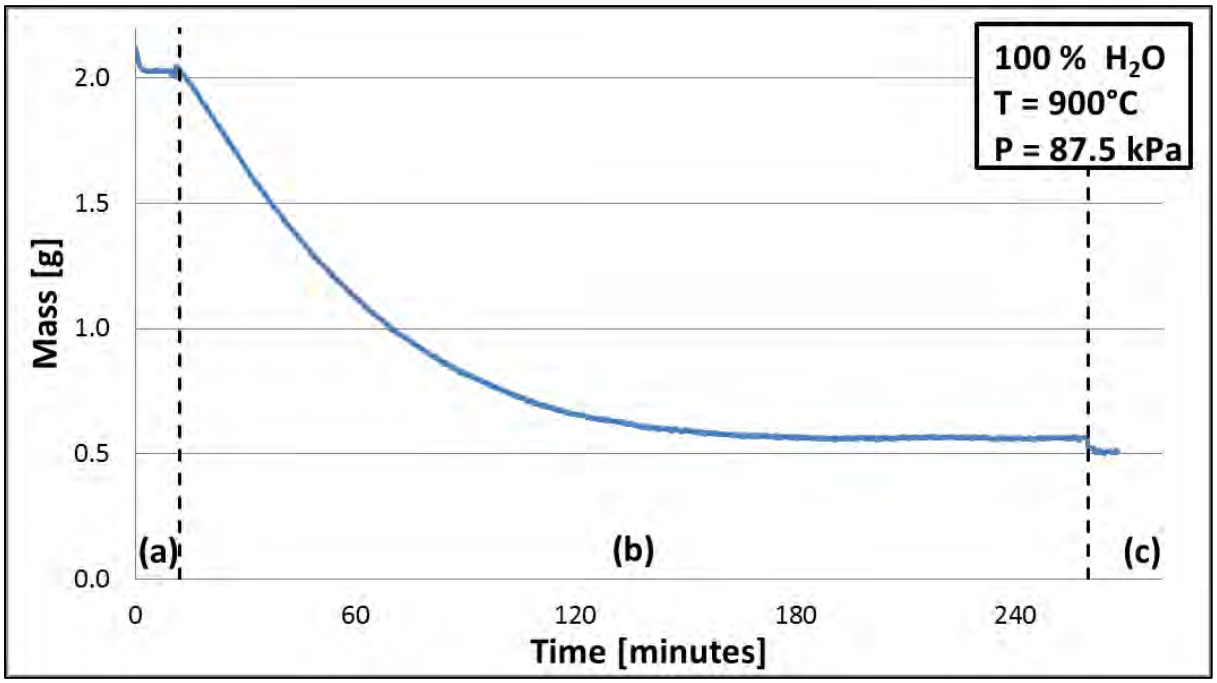

Figure 4-2: Typical steam gasification TGA data

Figure 4-2 shows the raw data for a steam gasification TGA experiment at 900°C. The data consists of three sections, (a) an initial section where moisture is driven off in a nitrogen atmosphere. The main part of the data is the gasification region (b) and then the last part (c) where the residual carbon is combusted and the ash value is measured. For a 2.0 gram sample the ash values ranged from 0.50g to 0.55g (25-27 wt% d.v.m.f.), which correlates well with the char proximate analysis ash value of 26 % (moisture + volatile matter free) as reported in Table 3-3.

4.5 Data processing

In this section the data processing steps following the data acquisition are described. These steps include; data sampling, correction for gas flow effects, normalization, data accuracy, calculation of conversion and conversion rate.

4.5.1 Sampling

The raw data sheets contain data points for every five seconds. To ease data processing, data was sampled from the original data set to have a frequency of one data point every 10 minutes. Sampling was started at the first data point after gasification was initiated.

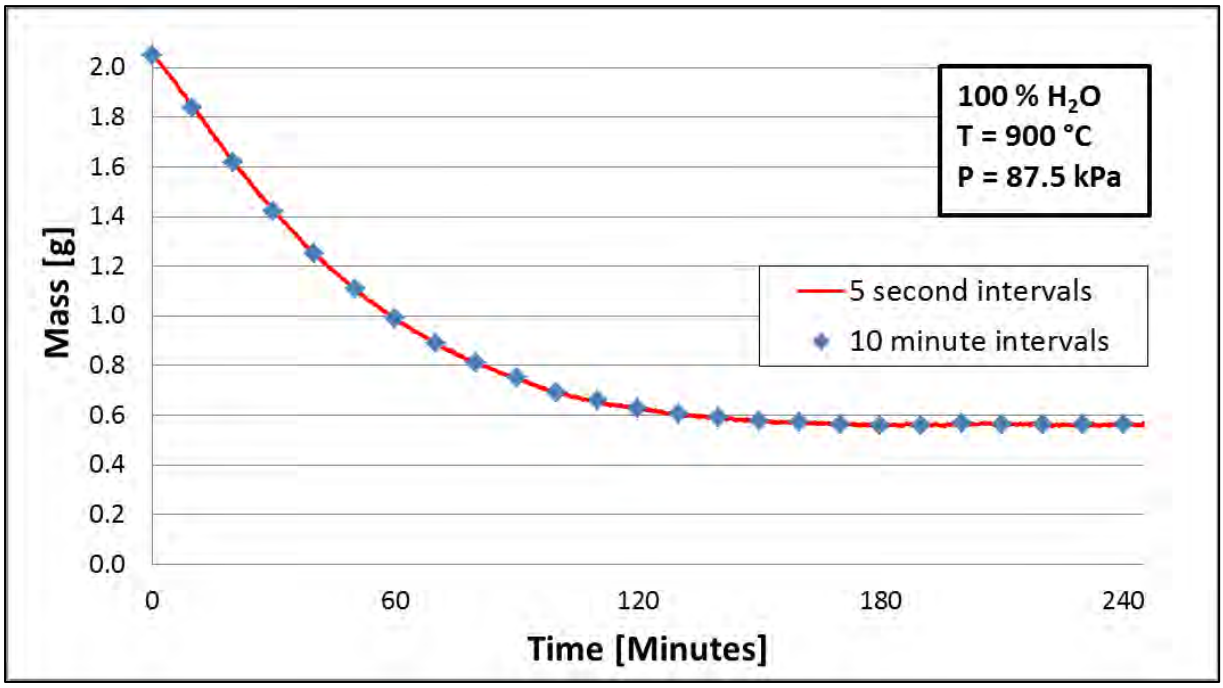

Figure 4-3: Experimental data timescale comparison

From the graph in Figure 4-3 it is clear that sampling the data every 10 minutes still represents the experimental data accurately.

4.5.2 Gas flow effect

Gas flow effects include the variations in mass observed when gasification reagent flow is started or stopped. To determine the significance of gas flow during an experiment, the mass of the char sample in the reactor with no flow is subtracted from the average sample mass just after gasification has been initiated. It has been observed that the variation in the logged mass

at the initiation and termination of experiments is within 0.5 % of the initial sample mass. Figures 4-4 and 4-5 show the first and last couple of minutes of gasification using 100 % steam at 900 °C.

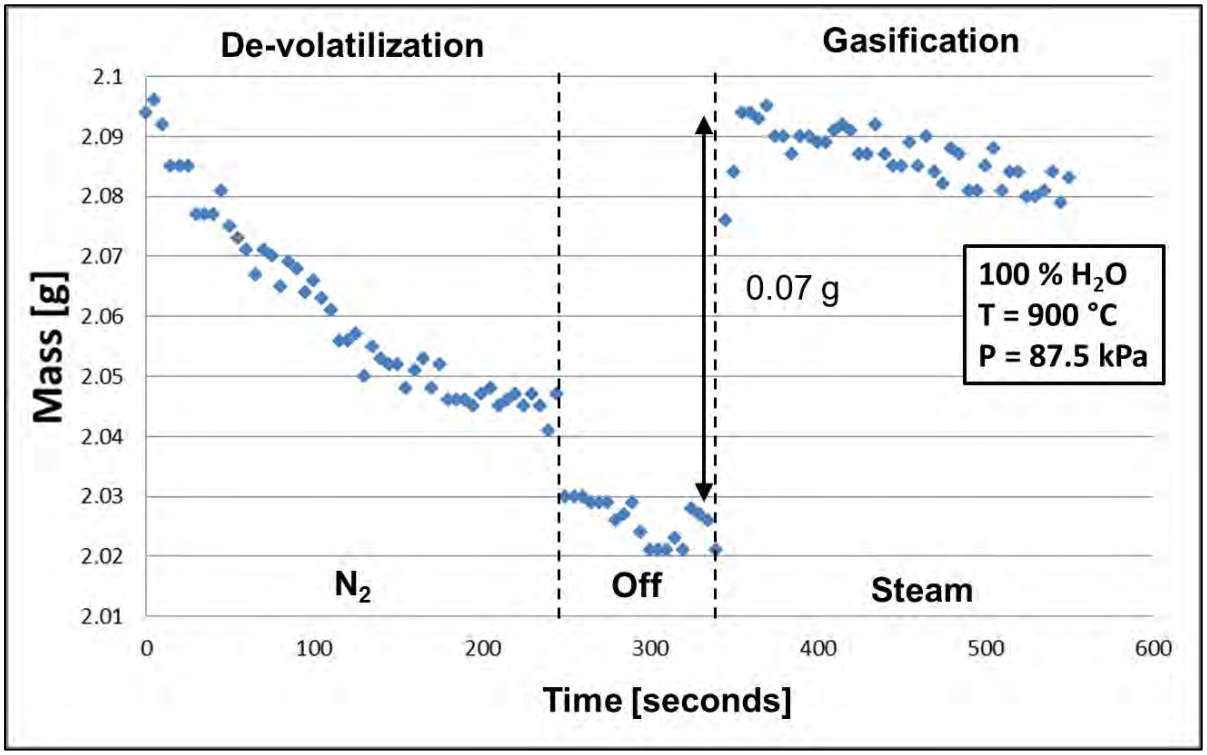

Figure 4-4: Experimental gasification initiation

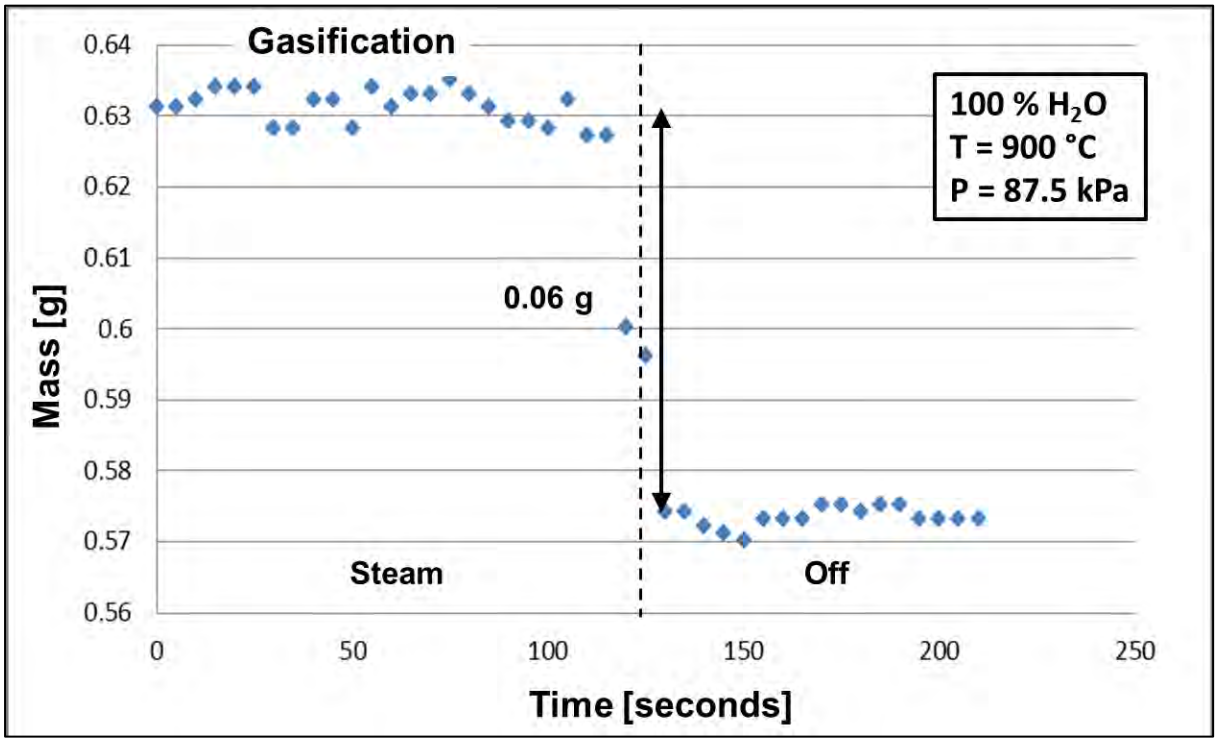

Figure 4-5: Experimental gasification termination

The observed change in mass is ascribed to the change in momentum of the reaction gas flowing downward over the sample bucket. The mass change has been observed to only be dependent on reagent flow rate, and not sample size or temperature.

4.5.3 Normalisation

In order to compare different experimental results, the sampled data was normalised with regard to the initial sample mass:

$$n_i = \frac{M_i}{M_o} \qquad (4.1)$$

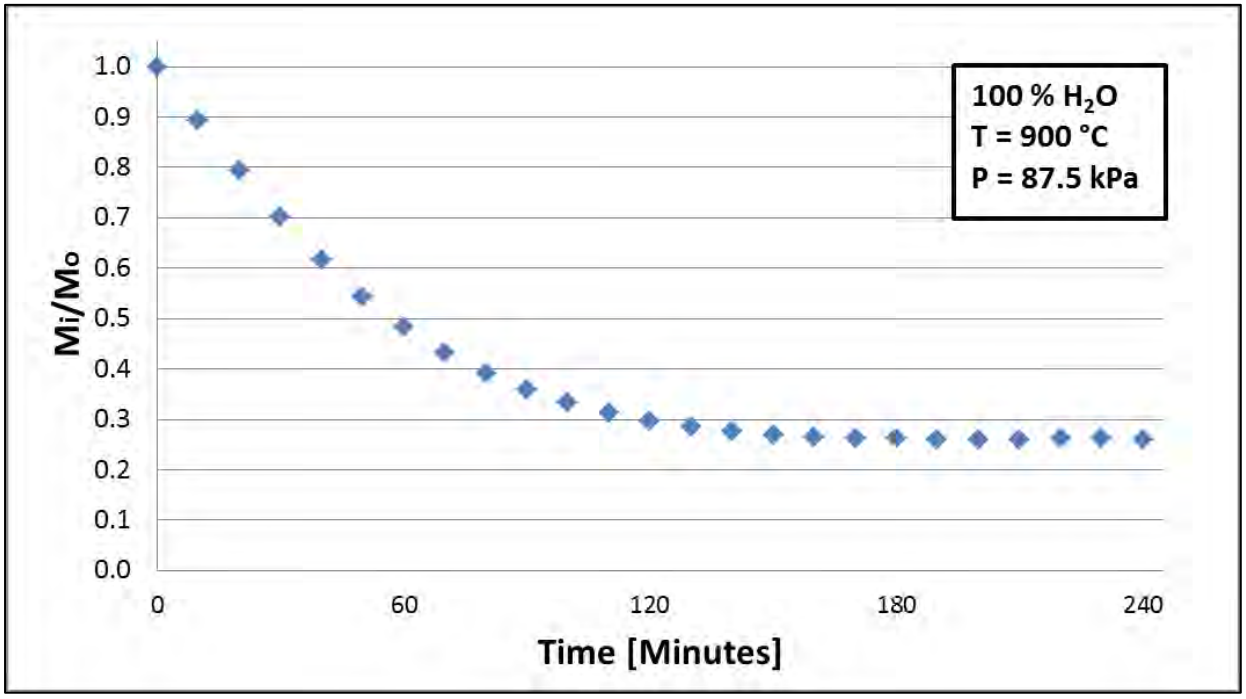

Figure 4-6: Normalised mass versus time graph

Figure 4-6 shows a normalised conversion plot for 100% steam at 900 °C. The normalised value starts at one and decreases to the ash value fraction.

4.5.4 Conversion

To give the conversion (*X*) for each experiment, the mass data was normalised between the initial sample mass and the sample ash value. This method gives the conversion on a daf basis as shown in Equation 4.2:

$$X = \frac{M_o - M_i}{M_o - M_f} \qquad (4.2)$$

A typical conversion versus time graph is shown in Figure 4-7. The conversion equation takes the ash value into account. The conversion values start at 0 and progress to 1 corresponding to 100 % conversion.

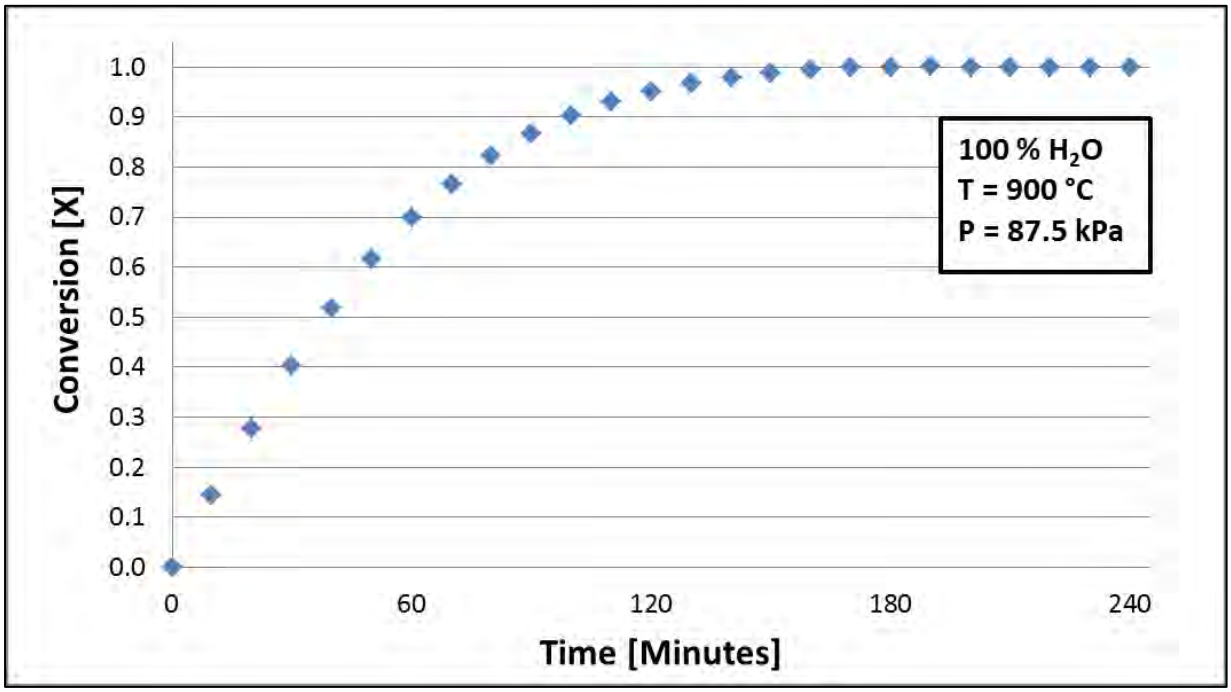

Figure 4-7: Conversion versus time graph

The conversion rate is equal to the slope of the conversion vs. time graph at any specific time. Conversion rate can be calculated using Equation 4.3:

$$\frac{dX}{dt} = \frac{\Delta X}{\Delta t} = \frac{X_i - X_{i-1}}{t_i - t_{i-1}} \qquad (4.3)$$

4.6 Experimental limitations and ranges

One of the objectives defined in Section 1.5 was to determine the reaction kinetics for steam and CO_2 gasification in the chemical reaction controlled regime. In this section the operational constraints and the methods used to determine experimental parameter limits are discussed. Because steam was found to react about five times faster than CO_2 *i.e.* (Ye *et al*., 1997), (Kajitani *et al*., 2002), (Everson *et al*., 2006_a), steam was used for all preliminary experiments. Parameters that were investigated included external diffusion, optimal sample mass for accurate TGA operation and reaction temperature.

4.6.1 Influence of gas flow rate

To determine the influence of external mass diffusion on the gasification rate the reagent flow rate around the particles was altered. A reagent composition of 50 mol% steam and 50 mol% nitrogen was chosen to evaluate the diffusion effects at 900 and 950 °C. The total flow rates were selected to be 3300 Nml/min, 6600 Nml/min and 9900 Nml/min. Figures 4-8 and 4-9 show the conversion versus time graphs for the three flow rates at 950 °C and 900 °C. All the runs were done using a sample mass of 2.0 g.

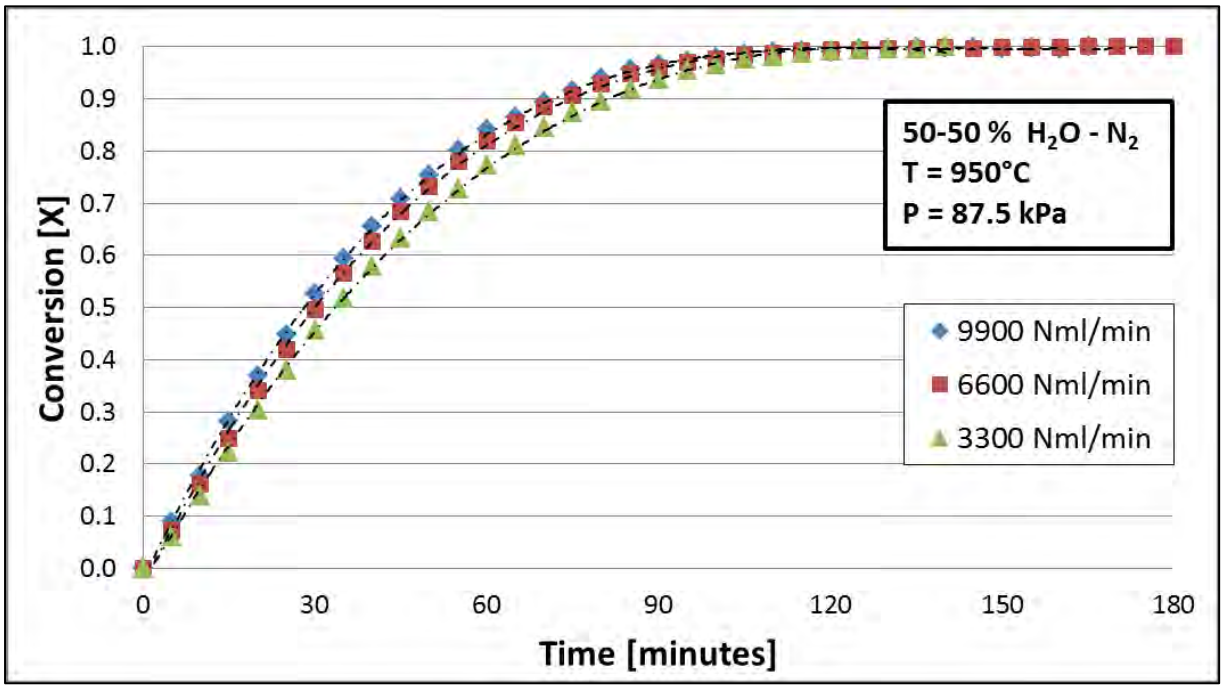

Figure 4-8: Char conversion as a function of gas flow rate at 950 °C

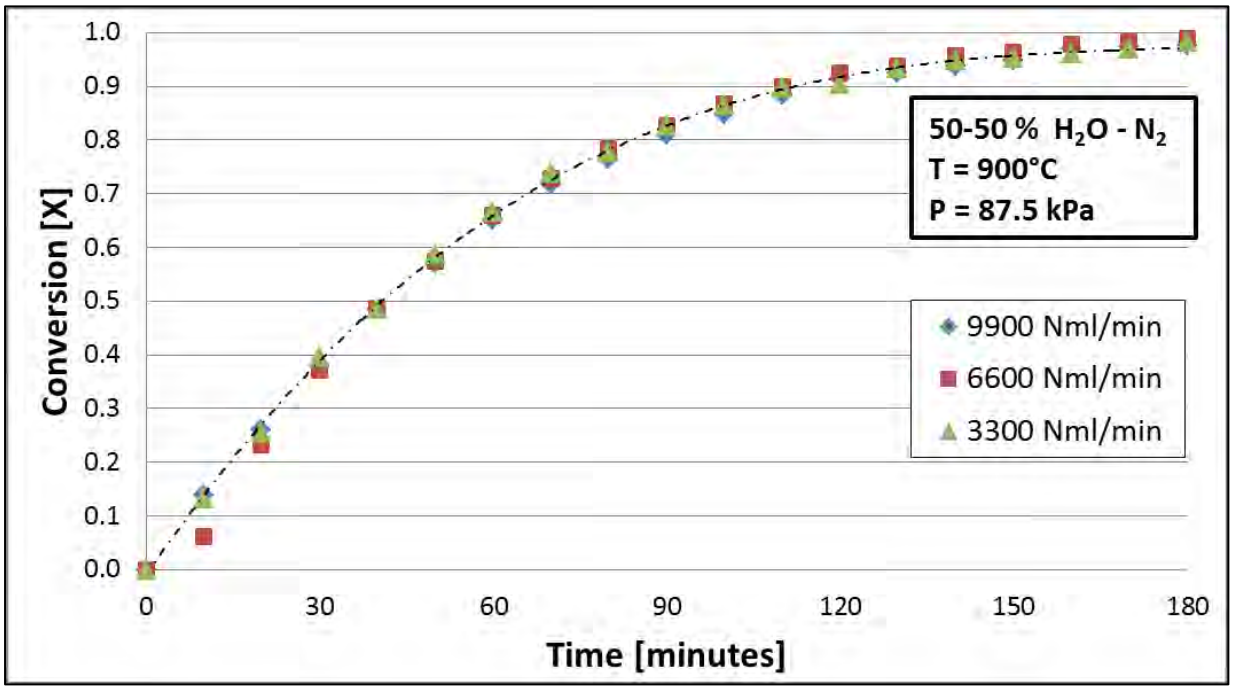

Figure 4-9: Char conversion as a function of gas flow rate at 900 °C

In Figure 4-8 some variation in the conversion profiles of the respective flow rates are observed at 950 °C. In Figure 4-9 no significant variations in the conversion profiles for the respective flow rates are observed. The conclusion is made that from 900 °C and lower, that the variations in flow rate do not influence the rate of gasification and that external mass diffusion does not play a significant role in the gasification rate at the investigated temperatures and flow rates.

For all ensuing experiments a total reactant flow rate of 6600 Nml/min was selected. This flow rate is equal to the stoichiometric amount of reagent necessary for complete conversion fed to the reactor every minute.

4.6.2 Influence of temperature

To investigate the influence of temperature on reaction rate, kinetic data over a broad temperature range needed to be collected. Instead of doing multiple experiments, one experiment was conducted using multiple temperatures. From preliminary experiments, it was observed that the reaction rate for steam and CO_2 gasification did not change significantly over the first 50 % conversion period, therefore the experiment was stopped before 50 % conversion was achieved.

The experiment was started at 750 °C and kept there for 5 % conversion. Then the reaction temperature was increased by 25 °C for every 5 % conversion achieved. This procedure was

repeated up to 950 °C. To ensure the accuracy of this method a second experiment was conducted where the temperature was decreased from 950 °C to 750 °C.

From these results the reaction rate (r_s) was estimated for each temperature by using Equation 2.5. Using an Arrhenius rate relation (Equation 2.23), a plot of $\ln(r_s)$ versus $(1/T)$ gives an indication of the temperature dependence of the reaction rate .

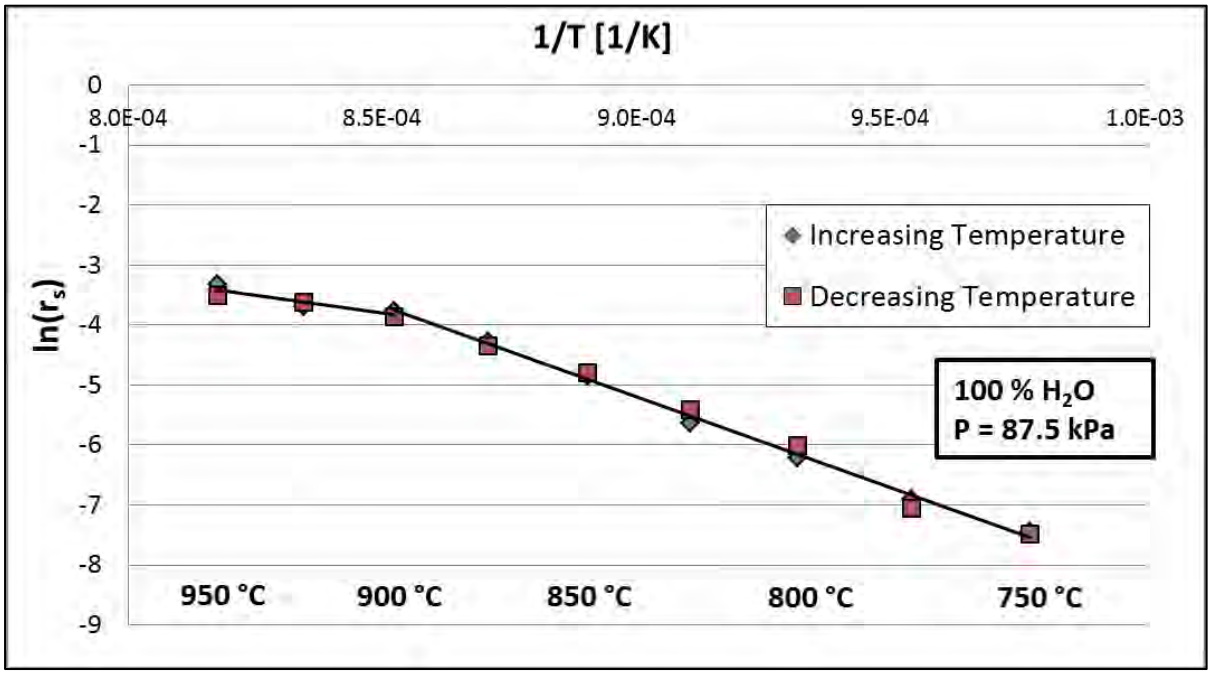

Figure 4-10: Steam gasification $\ln(r_s)$ vs 1/T plot

From Figure 4-10 it is clear that the slope of the graph changes at about 900 °C. This change in slope is an indication of a change in the temperature dependence of the kinetic rate, meaning that at a temperature above 900 °C, diffusion effects start to influence the kinetic rate. The results for a similar experiment conducted for CO_2 gasification is shown in Figure 4-11.

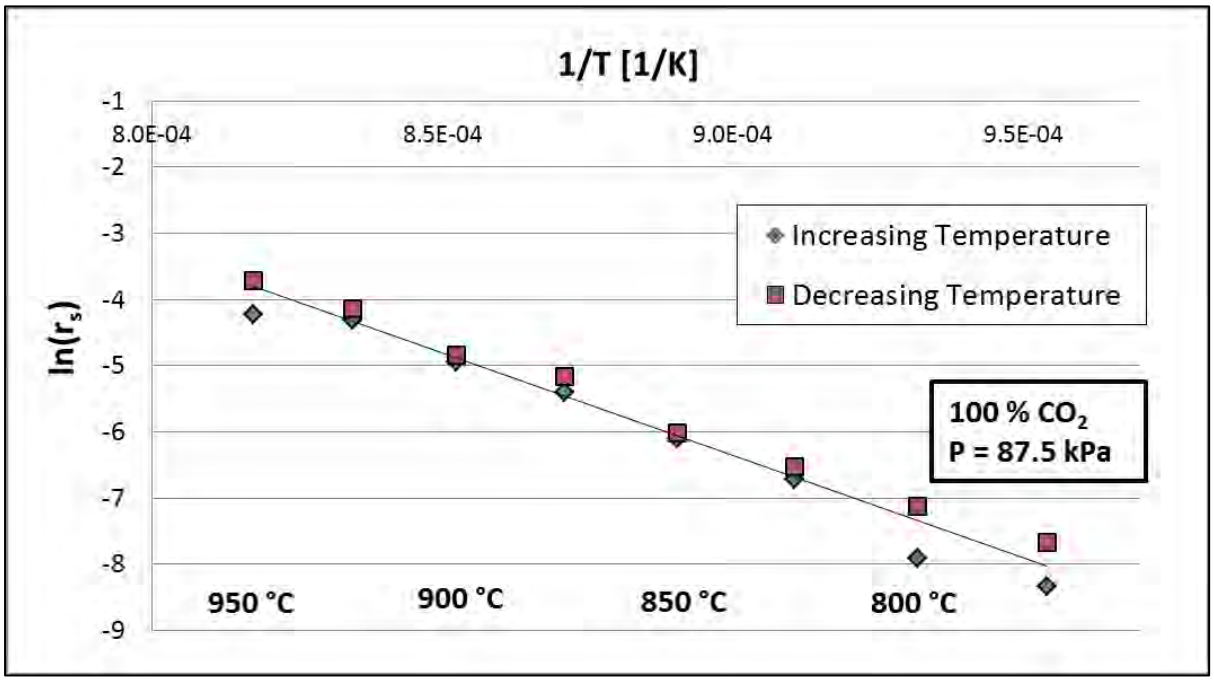

Figure 4-11: CO_2 gasification $\ln(r_s)$ vs 1/T plot

Because the CO_2 gasification rate at 750 °C was unobservable after 1 hour, the minimum temperature for the CO_2 gasification tests was set at 775 °C. Figure 4-11 shows a linear plot for both CO_2 gasification experiments, which means that there is no observed regime change in the investigated temperatures.

Thus it is established that steam and CO_2 gasification of this char under the investigated conditions is chemical reaction controlled at and below 900 °C. The CO_2 gasification rate at 750 °C was extremely low, therefore the following temperatures would be investigated: 900, 850, 825, 800, and 775 °C.

4.6.3 Influence of sample mass

In this section the influence of varying sample mass is investigated. Samples of 2.0, 1.0 and 0.5 grams were gasified at 900 °C with a reagent composition of 50 mol% steam and 50 mol% nitrogen.

Preliminary experiments showed that smaller sample masses resulted in higher experimental instability. This was investigated by doing three repeat runs for each sample mass and then evaluating the experimental errors of the repeat runs with a confidence interval of 95 %. The calculated error values were 14.3 %, 7.9 % and 6.3 % for the 0.5 g, 1.0 g and 2.0 g

experiments respectively. These results showed that an increase in sample mass lowers the experimental error. A comparison of these experiments is presented in Figure 4-12.

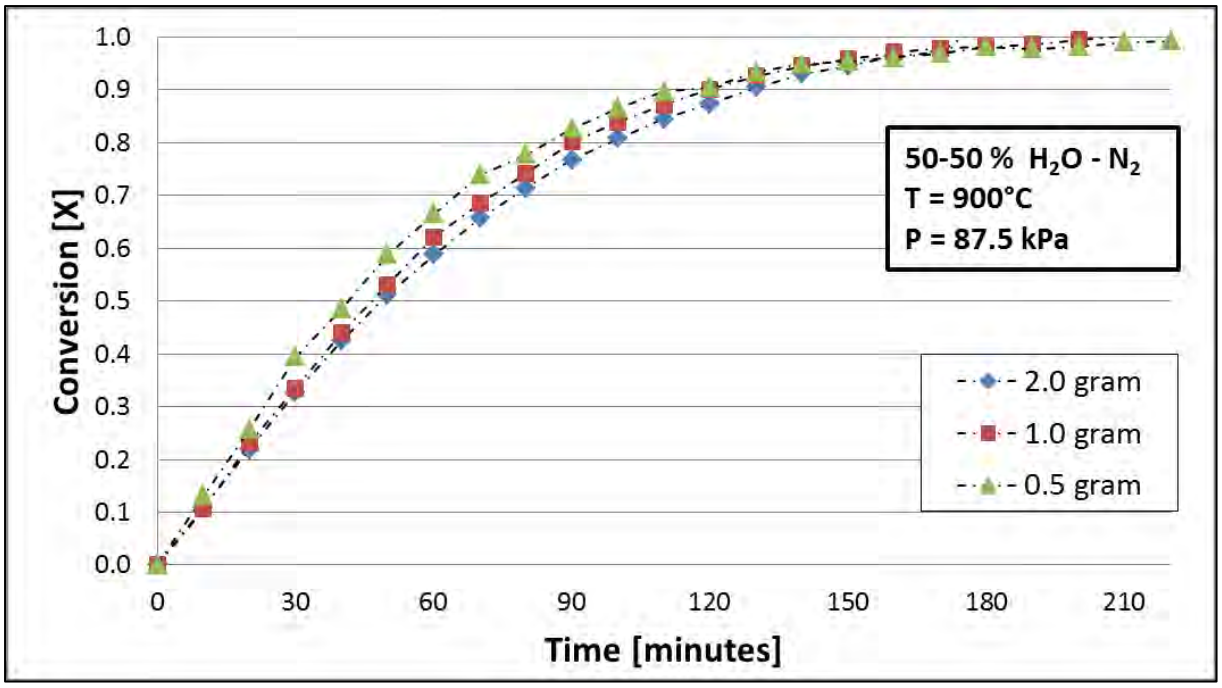

Figure 4-12: Conversion vs time graphs for different sample sizes

From Figure 4-12 some discrepancy in reaction rate is observed for the different sample masses evaluated. This is an indication that a degree of bed diffusion is present. These effects were observed to be constant for repeated experiments with a maximum error of 11 % and an average error of 4.7 %. It was decided that a constant error would have less detrimental effects on the reaction rate than experimental instability would have. Therefore in the interest of accuracy and experimental repeatability the bed diffusion discrepancy was accepted and a sample mass of 2.0 g was chosen for all ensuing experiments.

4.6.4 Repeat runs

This study required a large amount of experimental data to be gathered. During the course of the study only selected experiments were repeated to determine the accuracy of the experimental data. Figure 4-13 shows the conversion data for four steam gasification experiments at 850 °C.

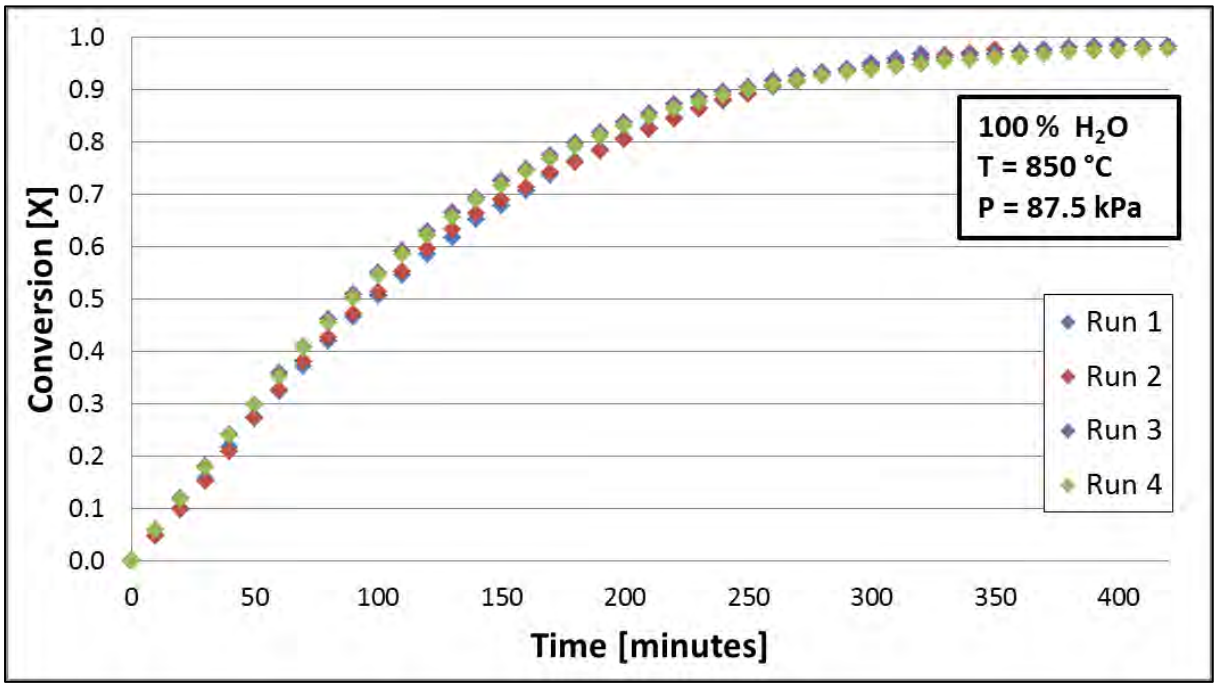

Figure 4-13: TGA steam gasification conversion data at 850 °C

The experimental error for the four runs was calculated by doubling the standard deviation of the experiments and then dividing the value with the average mass at the given time. This resulted in an average error value of 6.6 % with a 95 % confidence interval for the whole graph. From these results and the values reported in Section 4.6.3, the assumption was made that the accuracy of the apparatus was sufficient not to require repeat runs for all the experiments to be conducted.

4.6.5 Gasification reagent concentrations

To investigate the influence of CO_2 addition to steam gasification, the following experimental approach was followed. The parameters that were varied during experimentation included: temperature, gasification reagent partial pressure and gas mixtures. Table 4-2 summarises the different mixtures and concentrations that were used.

Table 4-2: Experimental reagent concentrations (mol%)

Steam / N_2	Steam / CO_2	CO_2 / N_2
100 % / 0 %	-	100 % / 0 %
75 % / 25 %	75 % / 25 %	75 % / 25 %
50 % / 50 %	50 % / 50 %	50 % / 50 %
25 % / 75 %	25 % / 75 %	25 % / 75 %

By comparing the reactivity of steam-CO_2 mixtures with that of steam-N_2 and CO_2-N_2, the contribution that an individual reagent makes to the overall gasification rate can be determined.

4.7 Summary

Experiments were conducted using an in house designed large particle TGA. 1 ± 0.2 mm char particles of a Highveld seam 4, medium rank C bituminous coal were used. Data readings were taken every 5 seconds, corrected for gas flow effects, and sampled to have 10 minute intervals. No external diffusion effects were observed below 900 °C. A reagent flow rate of ± 6600 Nml/min was selected. 2.0 gram samples were used because it delivered the most repeatable results. Reagent concentrations varied according to the values shown in Table 4-2. The experimental parameters set in this chapter are summarised and presented in Table 4-3.

Table 4-3: Experimental parameter summary

Experimental parameter	Value
Coal	Highveld seam 4
Particle diameter (d_p)	1 ± 0.2 mm
Reagents	CO_2, Air, de-ionised water
Reagent concentrations	25 – 100 mol%
Reagent flow rate	6600 Nml/min
Temperature range	775 – 900 °C
Sample mass	2.0 g
Experimental error	6.6 %

Chapter 5: Results and discussion:

5.1 Introduction

In this chapter the experimental results and its modelling is presented. In Section 5.2 an evaluation of the factors influencing steam gasification as well as an evaluation of an appropriate structural model is discussed. In Section 5.3 a similar discussion with regards to CO_2 gasification is presented. In Section 5.4 a comparison of steam- and CO_2 gasification is made and its kinetic modelling is evaluated. In Section 5.5 the mixed reagent conversion data is fitted to a chosen structural and kinetic model. In Section 5.6 the results of the experiments are summarised.

5.2 Steam gasification

5.2.1 Influence of temperature and partial pressure

The temperature dependence of steam gasification reactivity was determined by comparing the steam gasification conversion at the various temperatures. The conversion graph for pure steam gasification is shown in Figure 5-1.

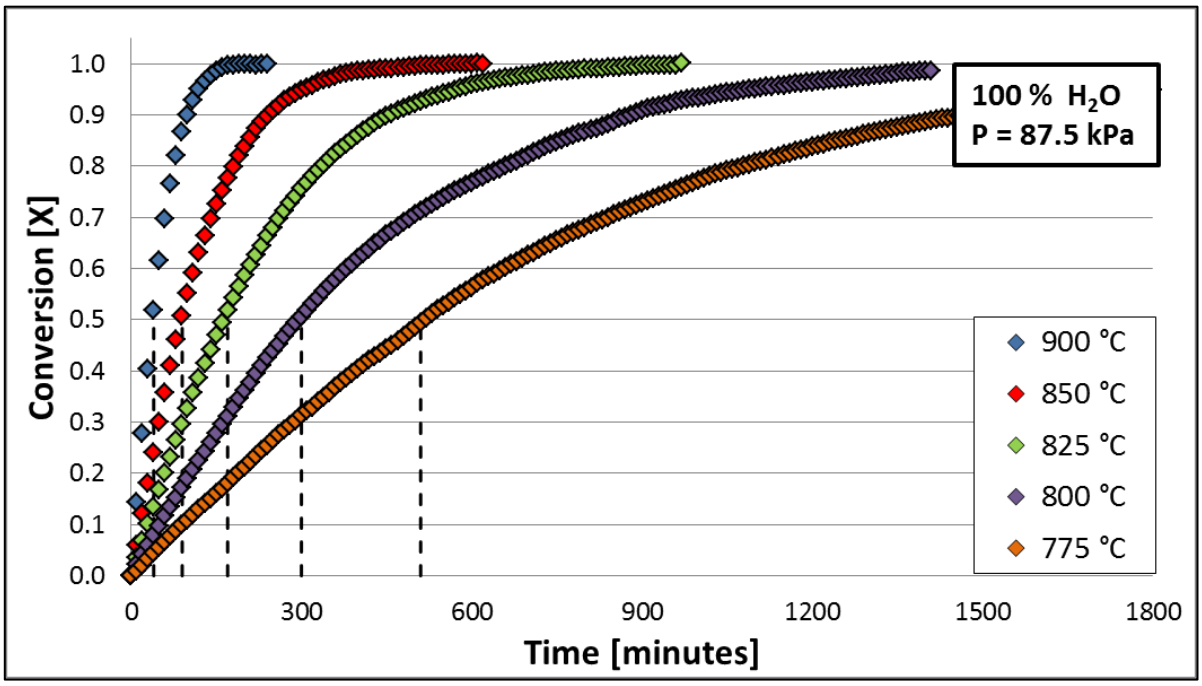

Figure 5-1: Steam gasification as a function of temperature

In Figure 5-1 it is shown that the conversion graphs are linear up to 50 % conversion. It is also observed that a decrease in temperature significantly increases the conversion time. Similar behaviour was observed for the other investigated partial pressures as shown in Appendix 7.4.1. The observed temperature dependence of gasification reactivity compares well with what is reported in literature *i.e.* (Everson *et al*., 2006_a), (Ye *et al*., 1997), (Xu *et al*., 2011_a). The mathematical relation of temperature and reaction rate, as defined by the Arrhenius equation is discussed in Section 5.4.3.

To study the influence of reagent partial pressure the specific reaction rate (R_s) was calculated from mass versus time data and is defined by Equation 5.1 as:

$$R_S = -\frac{1}{M_i}\frac{dM}{dt} \qquad (5.1)$$

Before applying Equation 5.1, the mass data was first smoothed by fitting a polynomial with the sum of least squares method. Figure 5-2 shows a comparative plot of specific reaction rate against conversion for the various steam concentrations investigated at 850 °C.

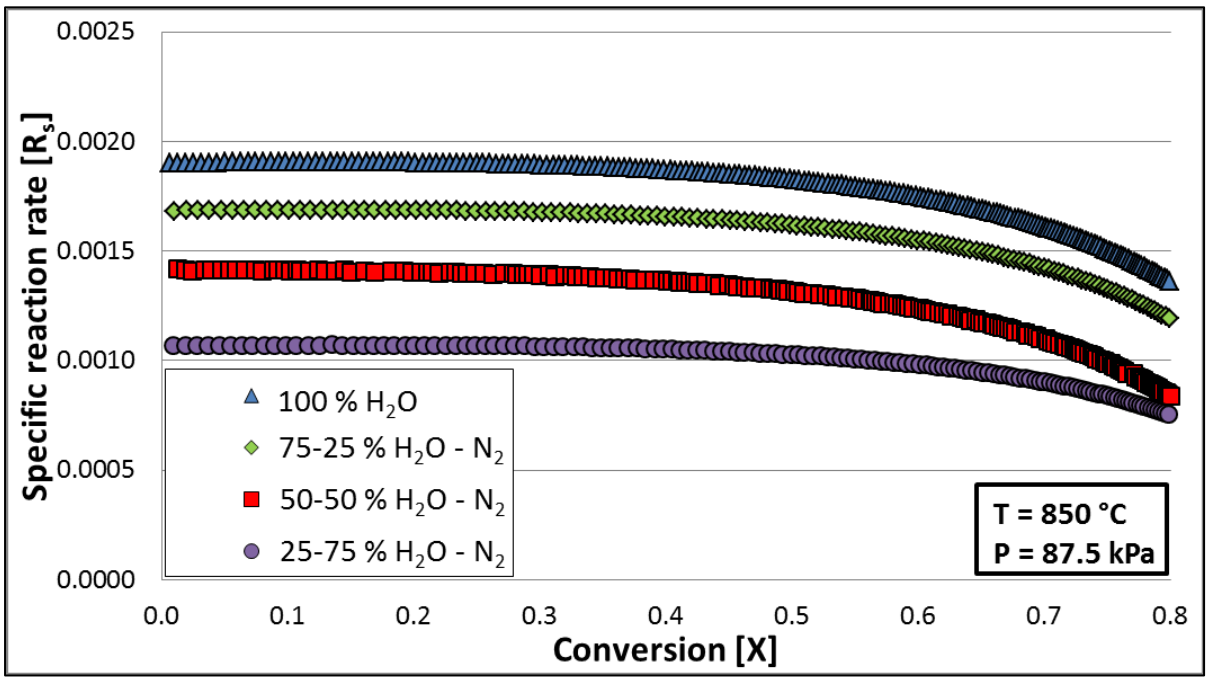

Figure 5-2: Partial pressure dependence of steam gasification rate at 850 °C

Figure 5-2 shows that an increase in steam partial pressure results in a definite increase in conversion rate. This dependence of gasification rate on reagent partial pressure relates well to what is reported in literature *i.e.* (Lee and Kim, 1995), (Matsuoka *et al*., 2009), (Karimi *et al*., 2011). Similar observations were made for all the investigated temperatures, see Appendix 7.4.1. The mathematical relation of reaction rate to partial pressure is further discussed in Section 5.4.3.

It is also observed from Figure 5-2 that the reactivity rate remains constant up to 50% conversion. This indicated that the reactivity index for 50 % conversion (Equation 2.1) could be used to compare steam gasification experiments as shown in Table 5-1.

Table 5-1: Reactivity index values for steam gasification

R_{50} [1/hr]	100 % H_2O	75-25 % H_2O-N_2	50-50 % H_2O-N_2	25-75 % H_2O-N_2
900 °C	0.79	0.71	0.56	0.41
850 °C	0.34	0.28	0.23	0.19
825 °C	0.18	0.17	0.12	0.11
800 °C	0.10	0.09	0.08	0.06
775 °C	0.06	0.05	0.04	0.03

From the reactivity index values reported in Table 5-1 it is seen that the reaction rate almost doubles with a temperature increase of 25 °C. With regard to partial pressure it is observed that the reaction rate decreases by 10, 30 and 45 % for every 25 mol% decrease in reagent concentration.

5.2.2 Structural model evaluation for steam gasification

In this section a selection of structural models are applied and compared to the experimental results. The models are evaluated based on its carbon conversion quality of fit, the relevance of the calculated kinetic constants and the application of the model. To determine the accuracy of the applied model the quality of fit parameter was defined as:

$$QOF\ (\%) = 100\left[1 - \frac{\sum_1^N \frac{|x_{calc} - x_{exp}|}{x_{exp}}}{N}\right] \quad (5.2)$$

The QOF of an experiment was evaluated up to 95 % conversion, or the maximum conversion achieved.

Homogeneous model

To evaluate the applicability of the Homogeneous model, Equation 2.5 was fitted for an r_s value by implementing the sum of least squares method.

$$t = -\frac{1}{r_s}\ln(1 - X) \quad (2.5)$$

The modelled conversion time graph was then compared to the experimental data. Conversion time plots for pure steam gasification are compared to the homogeneous model conversion predictions in Figure 5-3.

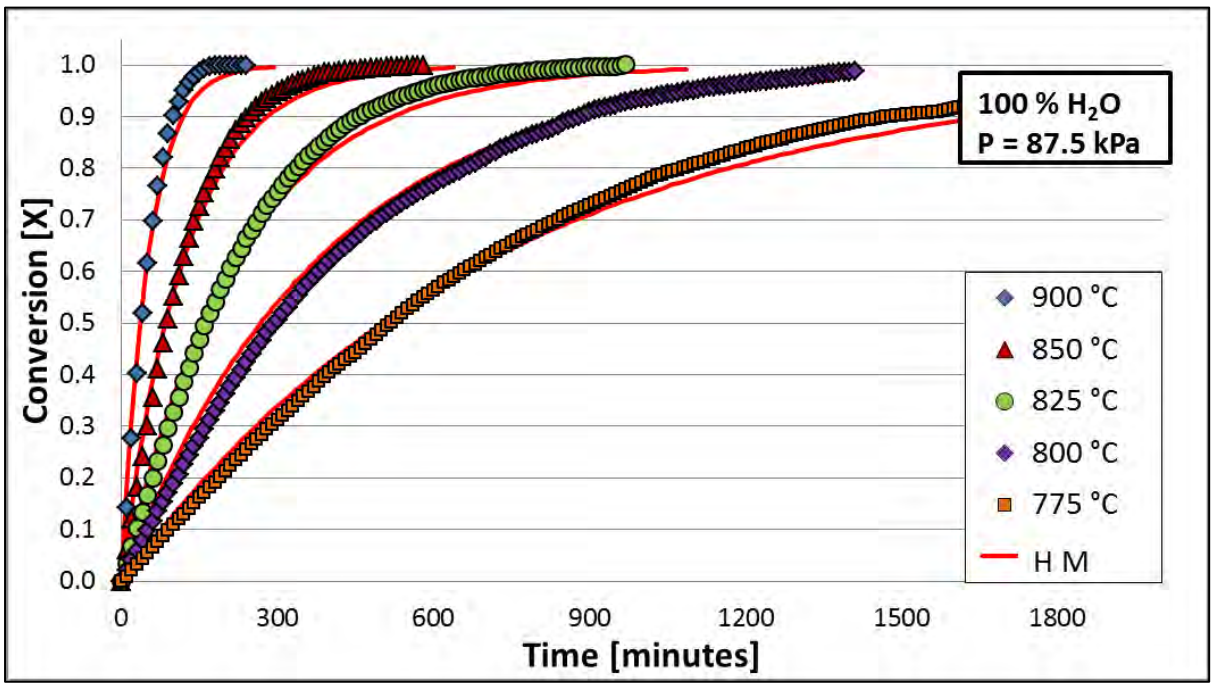

Figure 5-3: Homogeneous model steam gasification conversion data fitting

The homogeneous model is seen to slightly under predict the gasification conversion values after 60 % conversion. This same trend is observed for all steam partial pressures investigated (Appendix 7.4.2). The QOF for steam gasification modelling with the homogeneous model was 94.4 %. The calculated r_s values are presented in Table 5-2.

Table 5-2: Homogeneous model r_s [1/min] values for steam gasification

r_s [1/min]	100 % H_2O	75-25 % H_2O-N_2	50-50 % H_2O-N_2	25-75 % H_2O-N_2
900 °C	2.0×10^{-2}	1.8×10^{-2}	1.4×10^{-2}	1.0×10^{-2}
850 °C	8.2×10^{-3}	6.8×10^{-3}	5.6×10^{-3}	4.5×10^{-3}
825 °C	4.4×10^{-3}	4.1×10^{-3}	3.0×10^{-3}	2.6×10^{-3}
800 °C	2.4×10^{-3}	2.2×10^{-3}	1.8×10^{-3}	1.4×10^{-3}
775 °C	1.4×10^{-3}	1.2×10^{-3}	9.2×10^{-4}	7.4×10^{-4}

The calculated r_s values decrease with a decrease in temperature and partial pressure, which correspond to the rate relations found in Section 5.2.1. This trend also corresponds to trends reported in literature *i.e.* (Lee and Kim, 1995), (Ye *et al*., 1997), (Fermoso *et al.*, 2010).

Shrinking Un-reacted Core Model

To evaluate the applicability of the SUCM to steam gasification Equations 2.10, 2.11 and 2.12 were compared to the experimental conversion time data as proposed by Everson *et al*. (2006_a).

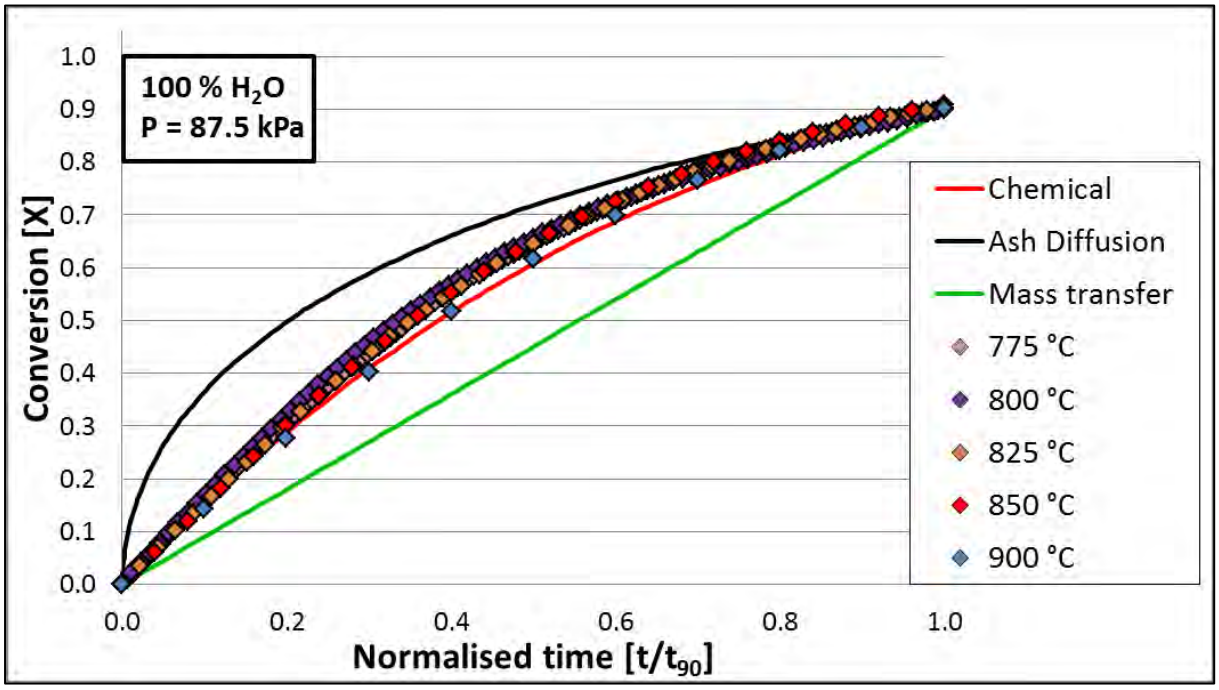

Figure 5-4: SUCM rate controlling step evaluation for steam gasification

The experimental data shown in Figure 5-4 is seen to fit the chemically controlled shrinking core mechanism, with some deviation to the ash diffusion controlled mechanism. Similar results were found for all investigated steam partial pressures (Appendix 7.4.3). Since the experimental data predominantly follows a chemically controlled mechanism, the chemically controlled shrinking core model (Equation 2.7) was applied to model the steam gasification data.

$$t = \frac{1}{\tau}\left[1 - (1 - X)^{1/3}\right] \qquad (2.7)$$

Figure 5-5 shows conversion time data for pure steam gasification modelled to the chemically controlled shrinking core model.

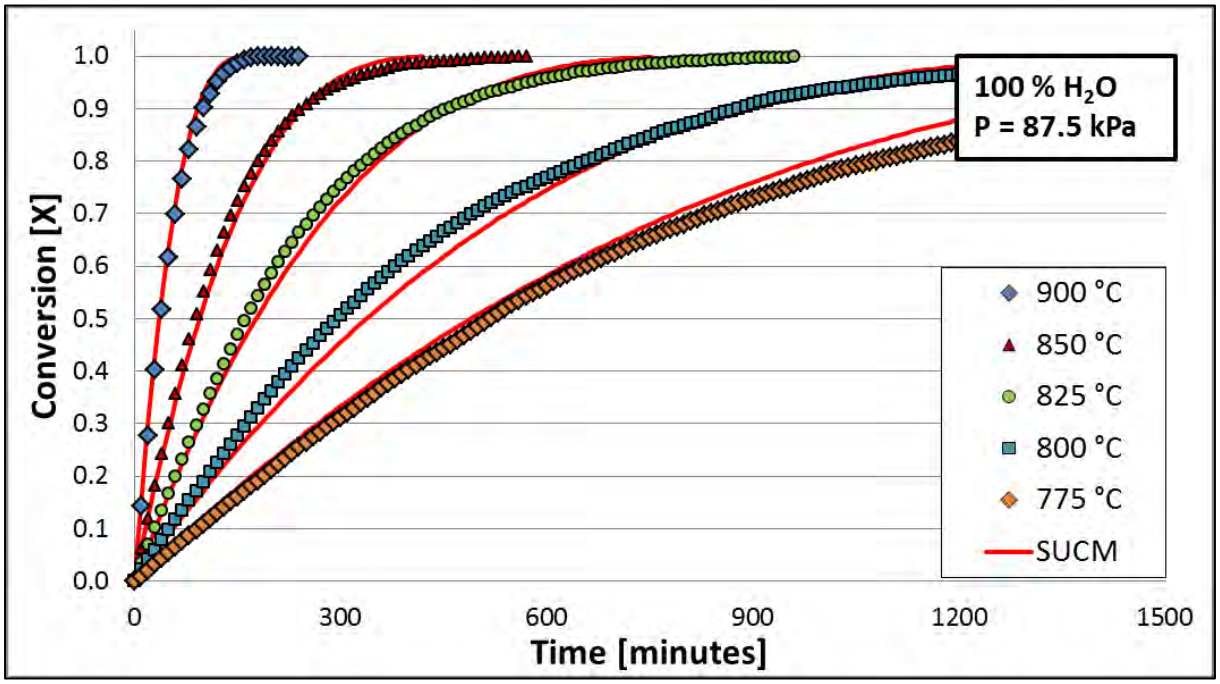

Figure 5-5: Chemically controlled SUCM steam gasification conversion data fitting

The chemically controlled SUCM model fits the experimental data adequately for all temperatures and partial pressures (see Appendix 7.4.3). A QOF value of 95.9 % was calculated for the chemically controlled SUCM. In Table 5-3 the calculated τ values for all the steam gasification experiments are presented.

Table 5-3: SUCM τ values for steam gasification

τ [(mol^2 K)/(min m^4)]	100 % H_2O	75-25 % H_2O-N_2	50-50 % H_2O-N_2	25-75 % H_2O-N_2
900 °C	5.4 x10^{-3}	5.0 x10^{-3}	3.8 x10^{-3}	2.9 x10^{-3}
850 °C	2.3 x10^{-3}	1.9 x10^{-3}	1.6 x10^{-3}	1.3 x10^{-3}
825 °C	1.2 x10^{-3}	1.1 x10^{-3}	8.5 x10^{-4}	7.1 x10^{-4}
800 °C	6.4 x10^{-4}	5.9 x10^{-4}	4.9 x10^{-4}	4.3 x10^{-4}
775 °C	3.8 x10^{-4}	3.3 x10^{-4}	2.5 x10^{-4}	2.1 x10^{-4}

As described in Section 2.5.2 τ is used as an indication of reaction rate. The τ values are seen to decrease as temperature and partial pressure decrease. These results correspond to the

findings of Section 5.2.1 as well as reported trends from literature *i.e.* (Lee and Kim, 1995), (Wu *et al*., 2006), (Everson *et al*., 2006_a), (Fermoso *et al*., 2010).

Random Pore Model

Using the method as defined by Everson *et al*. (2008_b) and discussed in Section 2.5.2, the RPM structural parameter is evaluated by applying Equation 2.17 and regressing a value for the structural parameter for each experiment with the sum of least squares method.

$$\frac{t}{t_{90}} = \frac{\sqrt{1-\Psi \ln(1-X)}-1}{\sqrt{1-\Psi \ln(1-0.9)}-1} \qquad (2.17)$$

Figure 5-6 shows normalised steam gasification experimental data compared to the Equation 2.17.

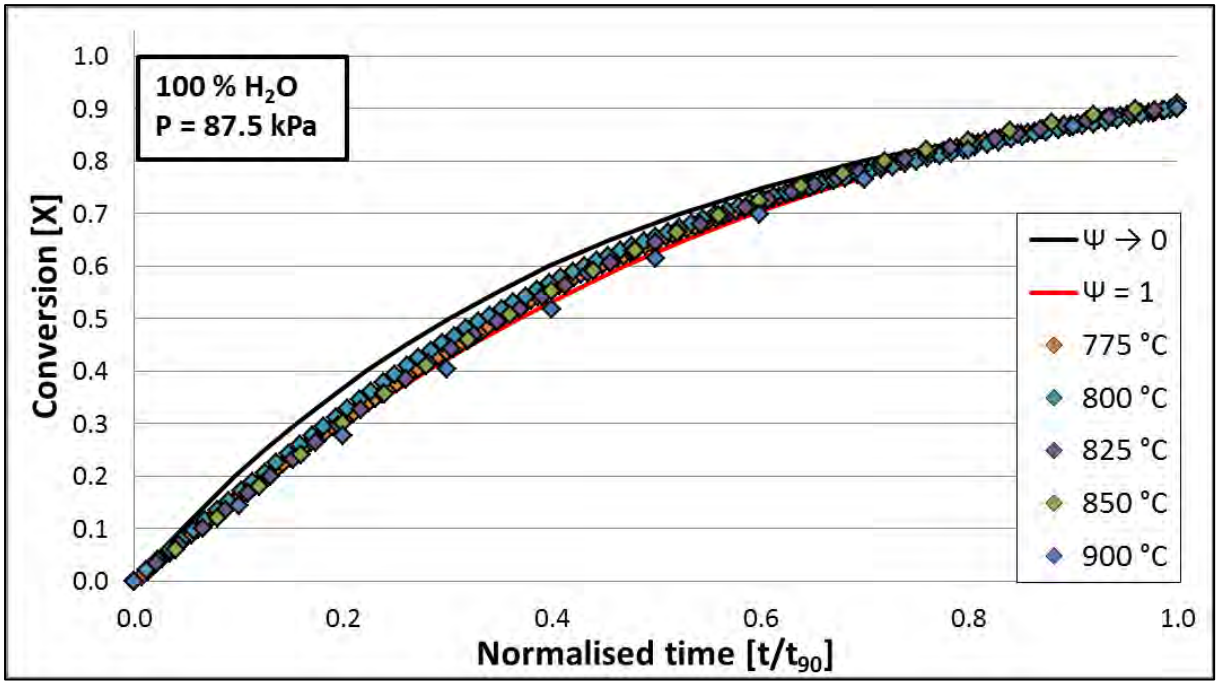

Figure 5-6: Structural parameter regression

From the comparison in Figure 5-6 it is observed that the RPM structural parameter for steam gasification is between zero and one. Structural parameter comparative plots for other steam partial pressures are presented in Appendix 7.4.4. The fitted structural parameters for all steam experiments are presented in Table 5-4.

Table 5-4: Steam gasification structural parameter values

Ψ	100 % H_2O	75-25 % H_2O-N_2	50-50 % H_2O-N_2	25-75 % H_2O-N_2	Average Ψ
900 °C	1.4	0.9	0.6	1.5	**1.1**
850 °C	0.5	1.0	0.6	0.7	**0.7**
825 °C	0.6	0.6	0.8	0.6	**0.6**
800 °C	0.6	0.1	0.5	0.6	**0.4**
775 °C	0.6	0.8	0.4	0.6	**0.5**

In Table 5-4 the average structural parameter is observed to decrease with reaction temperature. Theoretically the structural parameter Ψ as defined by Equation 2.13 is only dependent on the physical parameters of the parent char. Therefore one structural parameter value should be applicable to all the experiments. An average structural parameter of 0.7 was calculated. Depending on the type and rank of the coal investigated, reported structural parameter values for steam gasification ranged between 0.6 and 26 (Sangtong-Ngam and Narasingha, 2009), (Fermoso *et al*., 2010), (Kajitani *et al*., 2002), (Zang *et al*., 2010), (Xu *et al*., 2011_b).

$$t = \frac{2(1-\varepsilon_o)}{r_s S_o \Psi}\left(\sqrt{1-\Psi \ln(1-X)}-1\right) \qquad (2.15)$$

The averaged structural parameter ($\Psi = 0.7$) was used in Equation 2.15 and the RPM conversion predictions were compared to the experimental conversion data.

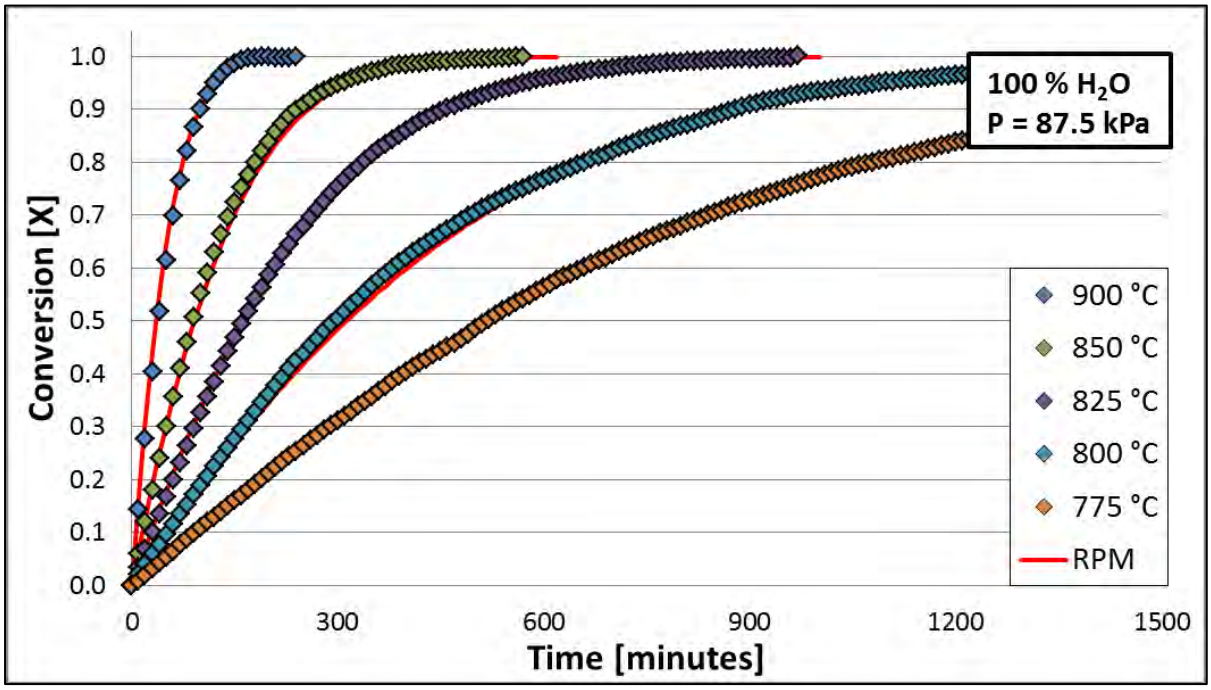

Figure 5-7: RPM Steam gasification conversion data fitting (Ψ = 0.7)

From Figure 5-7 it is observed that the RPM with an average structural parameter of 0.7 predicts the experimental conversion data accurately. A QOF value of 96.7 % was calculated for steam gasification modelling with the chemically controlled RPM. RPM conversion modelling for the other investigated partial pressures is presented in Appendix 7.4.4. The RPM time factor values for steam gasification are presented in Table 5-5.

Table 5-5: RPM steam gasification time factor values

t_f [m^2/min]	100 % H_2O	75-25 % H_2O-N_2	50-50 % H_2O-N_2	25-75 % H_2O-N_2
900 °C	2.2×10^{-3}	1.8×10^{-3}	1.4×10^{-3}	1.0×10^{-3}
850 °C	8.4×10^{-4}	7.0×10^{-4}	5.6×10^{-4}	4.6×10^{-4}
825 °C	4.7×10^{-4}	4.4×10^{-4}	3.3×10^{-4}	2.8×10^{-4}
800 °C	2.5×10^{-4}	2.3×10^{-4}	1.9×10^{-4}	1.5×10^{-4}
775 °C	1.5×10^{-4}	1.3×10^{-4}	9.7×10^{-5}	8.0×10^{-5}

The calculated time factor values decrease with temperature and partial pressure similarly to the findings of Section 5.2.1 and trends reported in literature (Kajitani *et al*., 2002), (Everson et al., 2008_a), (Sangtong-Ngam and Narasingha, 2009), (Fermoso *et al*., 2010).

Wen model

The semi-empirical Wen model was evaluated to determine its applicability to steam gasification reactions under the investigated conditions. Equation 2.19 was applied to the experimental data and values for r_s and m was regressed by using the sum of least squares method.

$$t = -\frac{1}{r_s}\left[\frac{(1-X)^{1-m}}{1-m} - \frac{1}{1-m}\right] \quad (2.19)$$

The Wen model fitting parameters for gasification with 100% steam are presented in Table 5-6.

Table 5-6: Rate constant (r_s) and solid reaction order (m) values for steam gasification

r_s [1/min]	100 % H_2O	75-25 % H_2O-N_2	50-50 % H_2O-N_2	25-75 % H_2O-N_2
900 °C	**1.8 x10^{-2}**	**1.7 x10^{-2}**	**1.3 x10^{-2}**	**9.3 x10^{-3}**
m	0.83	0.81	0.85	0.81
850 °C	**7.7 x10^{-3}**	**5.8 x10^{-3}**	**5.0 x10^{-3}**	**4.1 x10^{-3}**
m	0.82	0.78	0.77	0.80
825 °C	**4.1 x10^{-3}**	**3.7 x10^{-3}**	**2.8 x10^{-3}**	**2.3 x10^{-3}**
m	0.81	0.78	0.79	0.85
800 °C	**2.3 x10^{-3}**	**2.1 x10^{-3}**	**1.7 x10^{-3}**	**1.3 x10^{-3}**
m	0.90	0.91	0.89	0.87
775 °C	**1.2 x10^{-3}**	**1.2 x10^{-3}**	**8.4 x10^{-4}**	**7.2 x10^{-4}**
m	0.98	1.16	1.02	1.05

A general trend is observed for the rate constants (r_s), *i.e.* an increase in temperature and partial pressure increases the r_s value *i.e.* (Lee and Kim, 1995), (Kajitani *et al*., 2002). The fitting parameter m is defined as the solid particle reaction order and is observed to increase marginally as the temperature decreases. An average m value of 0.87 ± 0.2 was calculated from the data in Table 5-6. The Wen model rate constants were re-calculated for the constant m value of 0.87 and are presented in Table 5-7.

Table 5-7: Steam rate constant values for the Wen model with *m* = 0.87

r_s [1/min]	100 % H_2O	75-25 % H_2O-N_2	50-50 % H_2O-N_2	25-75 % H_2O-N_2
900 °C	1.8×10^{-2}	1.7×10^{-2}	1.3×10^{-2}	9.3×10^{-3}
850 °C	7.6×10^{-3}	6.3×10^{-3}	5.2×10^{-3}	4.2×10^{-3}
825 °C	4.1×10^{-3}	3.8×10^{-3}	2.8×10^{-3}	2.4×10^{-3}
800 °C	2.2×10^{-3}	2.1×10^{-3}	1.7×10^{-3}	1.3×10^{-3}
775 °C	1.3×10^{-3}	1.2×10^{-3}	8.6×10^{-4}	6.9×10^{-4}

From a comparison of Table 5-6 and 5-7, no significant change in rate constant values was observed. Therefore the average *m* value was used in Equation 2.19 and compared to all the experiments as shown in Figure 5-8.

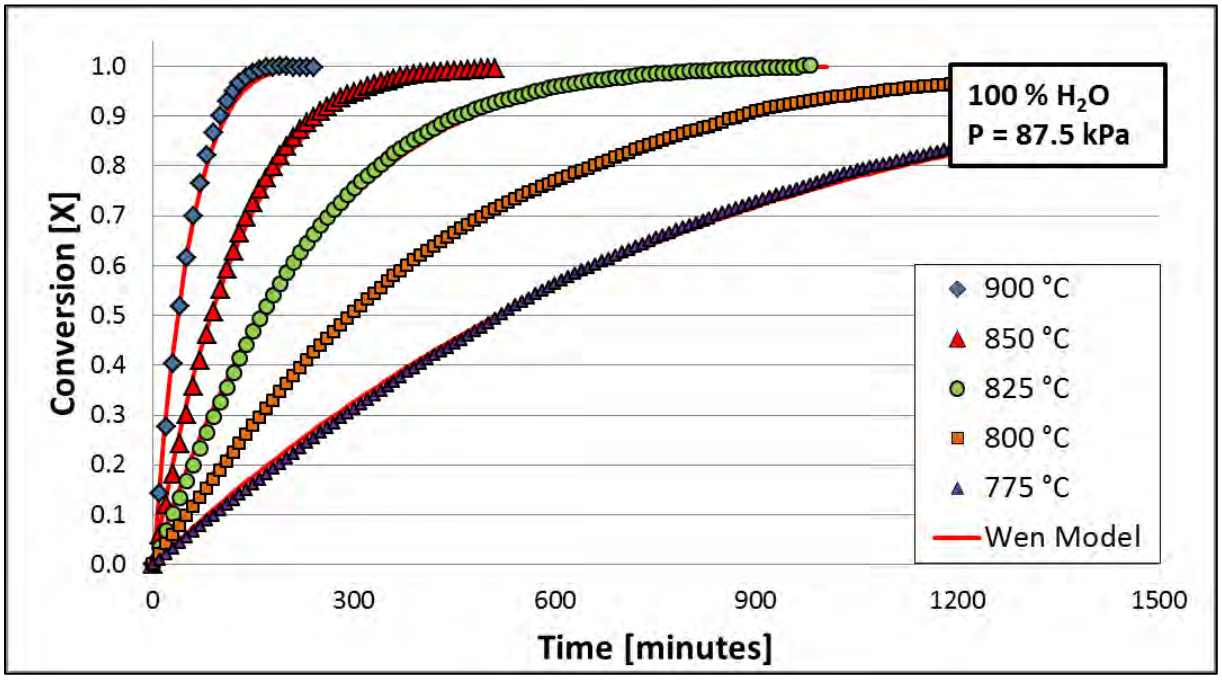

Figure 5-8: Wen model steam gasification conversion data fitting (*m* = 0.87)

The Wen model with an averaged m value is seen to fit the experimental data well. A QOF parameter value of 96.1 % was calculated for steam gasification fittings when using the Wen model. Similar results were observed for the other partial pressures investigated, see Appendix 7.4.5.

5.3 CO_2 gasification

5.3.1 Influence of temperature and partial pressure

The temperature dependence of CO_2 gasification was evaluated by comparing the conversion lines at different temperatures. The conversion time lines for pure CO_2 gasification at the various investigated temperatures are presented in Figure 5-9.

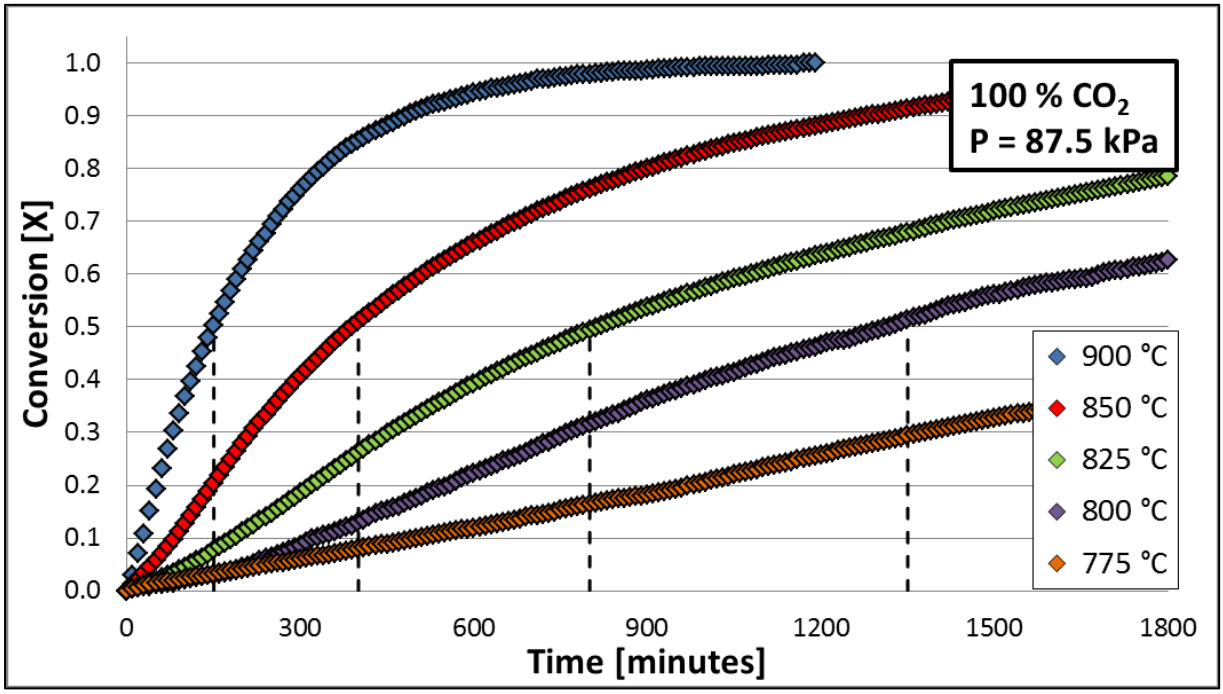

Figure 5-9: CO_2 gasification as a function of temperature

From Figure 5-9 it is apparent that the CO_2 gasification rate is strongly dependent on reaction temperature. This strong temperature dependence is an indication that the gasification rate is controlled by the chemical reactions on the char surface (Roberts and Harris, 2000), (Everson *et al*., 2008_a), (Xu *et al*., 2011_b).

The specific reaction rate versus conversion graphs for CO_2 gasification at different partial pressures was compared to evaluate the influence of partial pressure on gasification rate. Figure 5-10 shows one of these graphs at 850 °C.

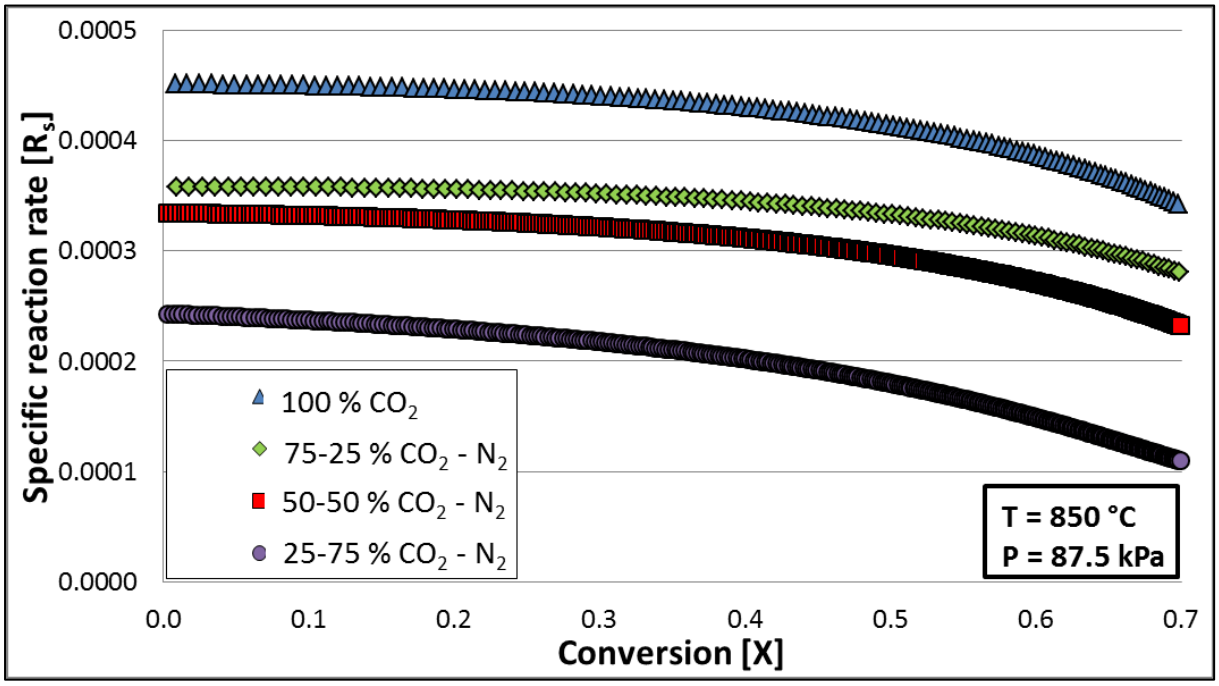

Figure 5-10: Partial pressure dependence of CO_2 gasification rate at 850 °C

Similar to the findings for steam gasification (Section 5.2.5), the CO_2 gasification rate is seen to be highly dependent on the CO_2 partial pressure. Partial pressure comparative conversion graphs for all the investigated temperatures are presented in Appendix 7.5.1. The R_{50} values for CO_2 gasification as calculated by Equation 2.1 are presented in Table 5-8.

Table 5-8: Reactivity index values for CO_2 gasification

R_{50} [1/hr]	100 % CO_2	75-25 % CO_2-N_2	50-50 % CO_2-N_2	25-75 % CO_2-N_2
900 °C	0.20	0.17	0.15	0.091
850 °C	0.077	0.066	0.052	0.035
825 °C	0.037	0.033	0.025	0.018
800 °C	0.023	0.021	0.016	0.010
775 °C	0.012	0.010	0.008	-

The reactivity index values indicate that the reaction rate doubles with a 25 °C increase in temperature, similar to the findings for steam gasification (Section 5.2.1). The reactivity index is seen to decrease by 12, 31 and 54 % respectively for every 25 mol% reduction in CO_2 concentration. At 775 °C and 25-75 mol% CO_2-N_2, the experiment did not reach 50 % conversion after 48 hours, therefore no R_{50} value could be calculated for that experiment.

5.3.2 Structural model evaluation for CO_2 gasification

This section evaluates a selection of structural models to determine its applicability to CO_2 gasification (similar to Section 5.2.2). The models are evaluated on the basis of its ability to predict carbon conversion with time, Quality of Fit and the relevance of the calculated kinetic parameters.

Homogeneous model

Following the same procedure as with steam gasification (Section 5.2.2), the homogeneous model was fitted to the CO_2 gasification experimental data. The model fittings for pure CO_2 at the investigated temperatures are presented in Figure 5-11.

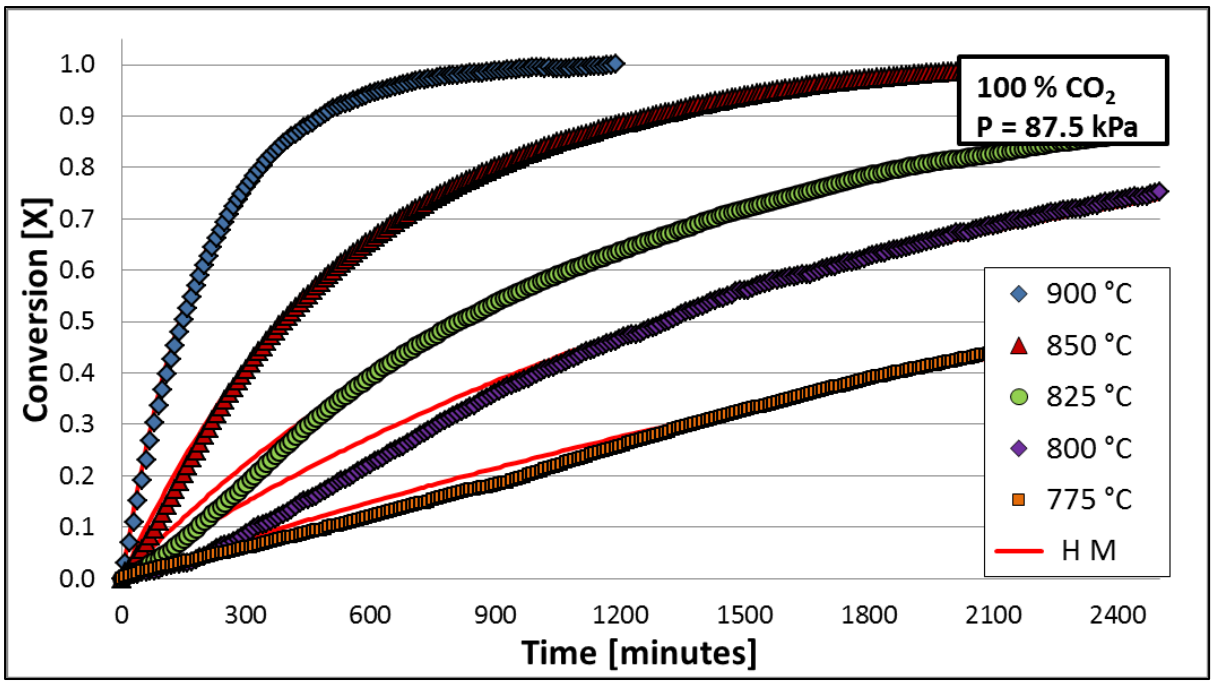

Figure 5-11: Homogeneous model CO_2 gasification conversion data fitting

From Figure 5-11 it is seen that the homogeneous model predicts the conversion behaviour for CO_2 gasification well for high temperatures, but tends to significantly over predict the initial conversion values for low temperature CO_2 gasification. The calculated QOF value for CO_2 gasification modelling with the homogeneous model was 90.1 %. The homogeneous model rate constants are presented in Table 5-9.

Table 5-9: Homogeneous model r_s [1/min] values for CO_2 gasification

r_s [1/min]	100 % CO_2	75-25 % CO_2-N_2	50-50 % CO_2-N_2	25-75 % CO_2-N_2
900 °C	4.7×10^{-3}	4.2×10^{-3}	3.4×10^{-3}	2.1×10^{-3}
850 °C	1.8×10^{-3}	1.5×10^{-3}	1.2×10^{-3}	8.0×10^{-4}
825 °C	8.4×10^{-4}	7.6×10^{-4}	5.7×10^{-4}	4.1×10^{-4}
800 °C	5.4×10^{-4}	4.6×10^{-4}	3.7×10^{-4}	2.3×10^{-4}
775 °C	2.7×10^{-4}	2.3×10^{-4}	1.7×10^{-4}	1.3×10^{-4}

The reaction rate constants decrease with temperature and partial pressure similar to the steam gasification values presented in Table 5-2. Similar trends of CO_2 reactivity dependence has been reported in literature *i.e.* (Ye *et al*., 1997), (Lee and Kim, 1995), (Matsuoka *et al.*, 2009), (Hattingh *et al*., 2011). The Homogeneous model fit for the other investigated partial pressures are presented in Appendix 7.5.2.

Shrinking Un-reacted Core Model

To determine the rate controlling step for CO_2 gasification with regards to the SUCM, the same procedure used in Section 5.2.2 for steam gasification was applied. CO_2 conversion data versus normalised time is compared to Equations 2.10, 2.11 and 2.12 in Figure 5-12.

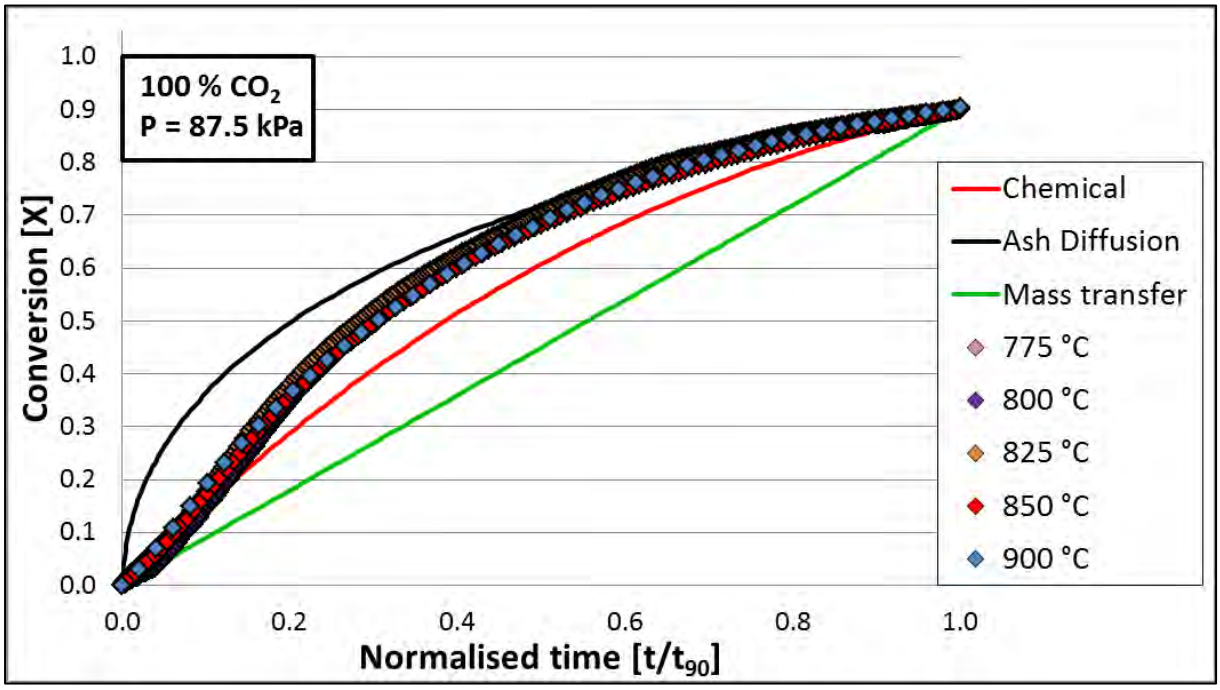

Figure 5-12: SUCM rate controlling step evaluation for CO_2 gasification

If the SUCM was applicable, the data from Figure 5-12 would suggest that CO_2 gasification starts being off chemical reaction controlled, but to the latter part of 10 % conversion, ash diffusion starts to play a prominent role in the rate controlling mechanism.

In both Figures 5-11 and 5-12 it is observed that the conversion data tend to show inflections (S shaped curves). These inflections become more prominent as the reaction rate of the experiments decreased. This phenomenon is thought to be caused by the slow initialisation of the reaction causing discrepancies in when the reaction is thought to start (t_0).

In Section 4.6.2 it has been shown that CO_2 gasification under the investigated conditions are chemical reaction controlled, this coupled with the findings from literature (Ye *et al.*, 1997), (Matsuoka *et al.*, 2009), (Hattingh *et al.*, 2011) make it unlikely that CO_2 gasification would follow an ash diffusion controlled mechanism, and therefore the SUCM was found inappropriate to describe the CO_2 gasification conversion behaviour.

Random Pore Model

Following the method described in Section 5.2.2, the RPM structural parameter value for CO_2 gasification was regressed from Equation 2.17. The normalised conversion plots and the RPM regression lines are shown in Figure 5-13.

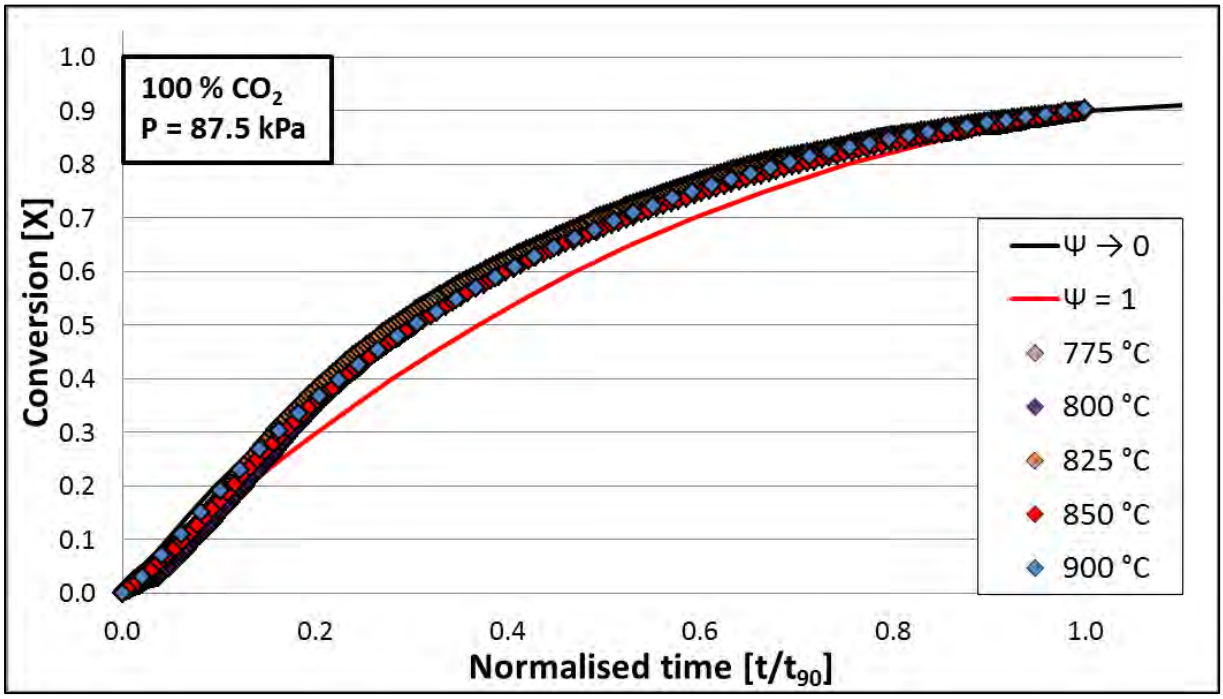

Figure 5-13: CO_2 gasification structural parameter regression

In Figure 5-13 the normalised CO_2 gasification data is compared to the RPM conversion predictions with structural parameters of one and zero. The experimental data is seen to completely cover the ($\Psi \rightarrow 0$) line. The regressed structural parameter values are presented in Table 5-10.

Table 5-10: CO_2 gasification structural parameter values

Ψ	100% CO_2	75-25 % CO_2-N_2	50-50 % CO_2-N_2	25-75 % CO_2-N_2
900 °C	0.2	0.2	0.1	0.2
850 °C	0.3	0.0	0.0	0.0
825 °C	0.5	0.0	0.0	0.0
800 °C	0.9	0.0	0.0	0.4
775 °C	0.0	0.0	0.0	0.0

The fitted structural parameter values reduce to zero for most of the CO_2 gasification experiments. Viable structural parameters could only be fitted for a couple of experiments. As the structural parameter reduces to zero, the RPM becomes the same as the HM (Zang *et al*., 2010). Therefore the RPM was not further evaluated to model CO_2 gasification.

Wen model

The Wen model was compared to the experimental data with the same method as followed in Section 5.2.2. The Wen model was fitted to the experimental CO_2 gasification data for r_s and m, the fitted values are presented in Table 5-11.

Table 5-11: Rate constant (r_s) and solid reaction order (m) values for CO_2 gasification

r_s [1/min]	100 % CO_2	75-25 % CO_2-N_2	50-50 % CO_2-N_2	25-75 % CO_2-N_2
900 °C	**4.3×10^{-3}**	**3.9×10^{-3}**	**3.1×10^{-3}**	**1.9×10^{-3}**
m	0.80	0.84	0.77	0.71
850 °C	**1.5×10^{-3}**	**1.5×10^{-3}**	**1.2×10^{-3}**	**7.7×10^{-3}**
m	0.70	0.93	0.75	0.91
825 °C	**8.8×10^{-4}**	**8.7×10^{-4}**	**6.4×10^{-4}**	**4.2×10^{-4}**
m	0.86	1.17	1.05	0.89
800 °C	**5.4×10^{-4}**	**5.1×10^{-4}**	**3.0×10^{-4}**	**2.7×10^{-4}**
m	1.02	0.96	0.54	1.04
775 °C	**2.2×10^{-4}**	**2.2×10^{-4}**	**1.2×10^{-4}**	**1.1×10^{-4}**
m	0.70	0.80	0.65	0.50

The Wen model predicted rate constants that exhibit the same trend as was observed for steam gasification (Table 5-6), as well as solid particle reaction orders ranging from 0.5 to 1.17. The calculated m values from Table 5-11 were averaged to a value of 0.83 ± 0.3, the rate constant values were recalculated as given in Table 5-12.

Table 5-12: CO_2 rate constant values for the Wen model with m = 0.83

r_s [1/min]	100 % CO_2	75-25 % CO_2-N_2	50-50 % CO_2-N_2	25-75 % CO_2-N_2
900 °C	4.3×10^{-3}	3.9×10^{-3}	3.1×10^{-3}	1.9×10^{-3}
850 °C	1.7×10^{-3}	1.4×10^{-3}	1.1×10^{-3}	7.5×10^{-3}
825 °C	7.8×10^{-4}	7.0×10^{-4}	5.0×10^{-4}	3.8×10^{-4}
800 °C	5.0×10^{-4}	4.3×10^{-4}	3.5×10^{-4}	2.2×10^{-4}
775 °C	2.6×10^{-4}	2.0×10^{-4}	1.6×10^{-4}	1.3×10^{-4}

The rate constants are not observed to change significantly by using an average m value, when compared to the individual m values. Therefore the Wen model with an average m value of 0.83 and the r_s values from Table 5-12 were fitted to conversion data for pure CO_2 gasification using Equation 2.19.

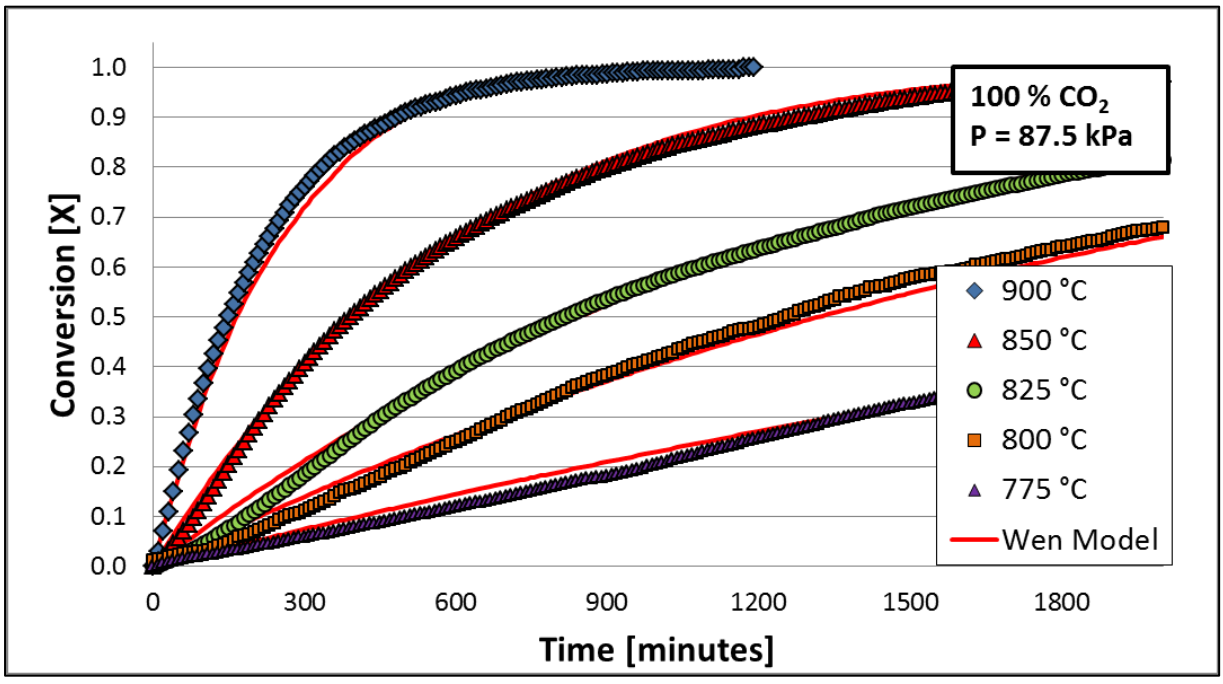

Figure 5-14: Wen model CO_2 gasification conversion data fitting (m = 0.83)

The Wen model is seen to predict the CO_2 gasification conversion data accurately in Figure 5-14. Some over prediction is observed for the initial conversion at 775 °C. A QOF value of 91.8 % was calculated for the Wen model fitting for all the CO_2 gasification experiments. Similar fittings were observed for the other investigated partial pressures as shown in Appendix 7.5.5.

5.4 Steam and CO_2 gasification comparison

In this section the results obtained for steam and CO_2 gasification (given in Sections 5.2 and 5.3) are summarised and compared. An appropriate structural and kinetic model is selected for the modelling of both steam and CO_2 gasification.

5.4.1 Reaction rate comparison

The reaction rate for both steam and CO_2 gasification was found to be strongly dependant on temperature and reagent partial pressure. A comparison of the pure steam and pure CO_2 gasification reactivity indices are presented in Table 5-13.

Table 5-13: Reactivity index comparison for steam and CO_2 gasification

R_{50} [1/hr]	100% H_2O	75-25 % H_2O-N_2	50-50 % H_2O-N_2	25-75 % H_2O-N_2
900 °C	0.79	0.71	0.56	0.41
850 °C	0.34	0.28	0.23	0.19
825 °C	0.19	0.17	0.12	0.11
800 °C	0.10	0.094	0.076	0.058
775 °C	0.058	0.052	0.039	0.031
R_{50} [1/hr]	**100 % CO_2**	**75-25 % CO_2-N_2**	**50-50 % CO_2-N_2**	**25-75 % CO_2-N_2**
900 °C	0.20	0.17	0.15	0.091
850 °C	0.077	0.066	0.052	0.035
825 °C	0.037	0.033	0.025	0.018
800 °C	0.023	0.021	0.016	0.010
775 °C	0.012	0.010	0.008	-

From the data in Table 5-13 it was calculated that steam gasification is 4-6 times faster than CO_2 gasification in the studied temperature and partial pressure range. Initial reaction rates for steam gasification reported by Roberts and Harris, (2006) was more than 3 times faster than the corresponding CO_2 gasification rates. Everson *et al*. (2006_a) found similar results, with steam gasification being 3-4 times faster than CO_2 gasification of an inertinite rich coal.

Kajitani *et al*. (2002) observed steam gasification to be about 7 times faster than CO_2 gasification.

5.4.2 Structural model comparison

The structural models evaluated for steam and CO_2 gasification (given in Section 5.2.2 and 5.3.2) are summarised and compared in Table 5-14.

Table 5-14: Structural model comparison

	Steam	**CO_2**
	Model evaluation	
HM QOF	93.9 %	90.1 %
SUCM QOF	95.0 %	-
Rate controlling	Chemical reaction control	Ash + Chemical control
RPM QOF	96.7 %	-
	$\Psi = 0.7$	$\Psi \rightarrow 0.0$
Wen Model QOF	96.2 %	91.8 %
Solid reaction order	$m = 0.87$	$m = 0.83$

It can be seen that the homogeneous model fitted both steam and CO_2 gasification conversion data with adequate accuracy. The chemically controlled SUCM fitted steam gasification conversion data well, but (incorrectly) predicted ash diffusion controlled kinetics for CO_2 gasification. The RPM fitted the steam gasification data the best (QOF = 96.7 %) with a structural parameter value of 0.7, but when predicting CO_2 gasification, the RPM structural parameter tended to regress to zero, indicating homogeneous model kinetics. The semi empirical Wen model fitted both steam and CO_2 conversion data with a high level of accuracy and similar solid reaction orders, $m = 0.87$ and 0.83 respectively.

Regarding the results from Table 5-14, only the homogeneous and the Wen model were found to fit both steam and CO_2 experimental conversion data with the same equation and similar kinetic constants. The Wen model had a higher QOF value than the homogeneous model for both steam and CO_2 gasification conversion modelling. Because of the high

accuracy and the similar solid reaction orders, the semi empirical Wen model was selected to be applied to model steam-CO_2 mixed reagent gasification data.

For the gasification modelling of steam-CO_2 mixtures, the solid reaction order was averaged to 0.85 ± 0.3 and the rate constants recalculated as presented in Table 5-15.

Table 5-15: Wen model rate constants for *m* = 0.85

r_s [1/min]	100% H_2O	75-25 % H_2O-N_2	50-50 % H_2O-N_2	25-75 % H_2O-N_2
900 °C	1.8 x10^{-2}	1.7 x10^{-2}	1.3 x10^{-2}	9.3 x10^{-3}
850 °C	7.6 x10^{-3}	6.3 x10^{-3}	5.2 x10^{-3}	4.2 x10^{-3}
825 °C	4.1 x10^{-3}	3.8 x10^{-3}	2.8 x10^{-3}	2.4 x10^{-3}
800 °C	2.2 x10^{-3}	2.1 x10^{-3}	1.7 x10^{-3}	1.3 x10^{-3}
775 °C	1.3 x10^{-3}	1.2 x10^{-3}	8.6 x10^{-4}	6.9 x10^{-4}
r_s [1/min]	**100 % CO_2**	**75-25 % CO_2-N_2**	**50-50 % CO_2-N_2**	**25-75 % CO_2-N_2**
900 °C	4.3 x10^{-3}	3.9 x10^{-3}	3.1 x10^{-3}	1.9 x10^{-3}
850 °C	1.7 x10^{-3}	1.4 x10^{-3}	1.1 x10^{-3}	7.5 x10^{-3}
825 °C	7.8 x10^{-4}	7.0 x10^{-4}	5.0 x10^{-4}	3.8 x10^{-4}
800 °C	5.0 x10^{-4}	4.3 x10^{-4}	3.5 x10^{-4}	2.2 x10^{-4}
775 °C	2.6 x10^{-4}	2.0 x10^{-4}	1.6 x10^{-4}	1.3 x10^{-4}

The Wen model rate constants were not observed to change significantly with the application of the average *m* value for steam and CO_2 gasification.

5.4.3 Kinetic rate equation evaluation

In this section both the power rate law and the L-H kinetic equations are evaluated to be applied to predict the rate constants for steam and CO_2 gasification using the semi empirical Wen model with an *m* value of 0.85.

Power rate law

The *n*-th order power rate law is a simplified kinetic rate equation and has been widely applied for low temperature (< 1200 °C) applications and for single gaseous reactants *i.e.* (Everson *et al*., 2008_b), (Kajitani *et al*., 2006), (Roberts and Harris, 2006). By linearising Equation 2.20, the reaction order with respect to the gaseous reagent partial pressure can be calculated. The linearised power rate law is given by:

$$\ln(r_s) = \ln(k_o) + n\ln(p_A) \qquad (5.2)$$

By plotting the natural logarithm of the rate constants $\ln(r_s)$ from Table 5-15 versus the natural logarithm of the respective partial pressures $\ln(p_{H_2O})$ and $\ln(p_{CO_2})$, the reaction order (n) with respect to partial pressure is equal to the slope of the plot, and the natural logarithm of the intrinsic rate constant $\ln(k_o)$ is the y intercept of the graphs. Figure 5-16 and 5-16 shows the respective plots for steam and CO_2 gasification.

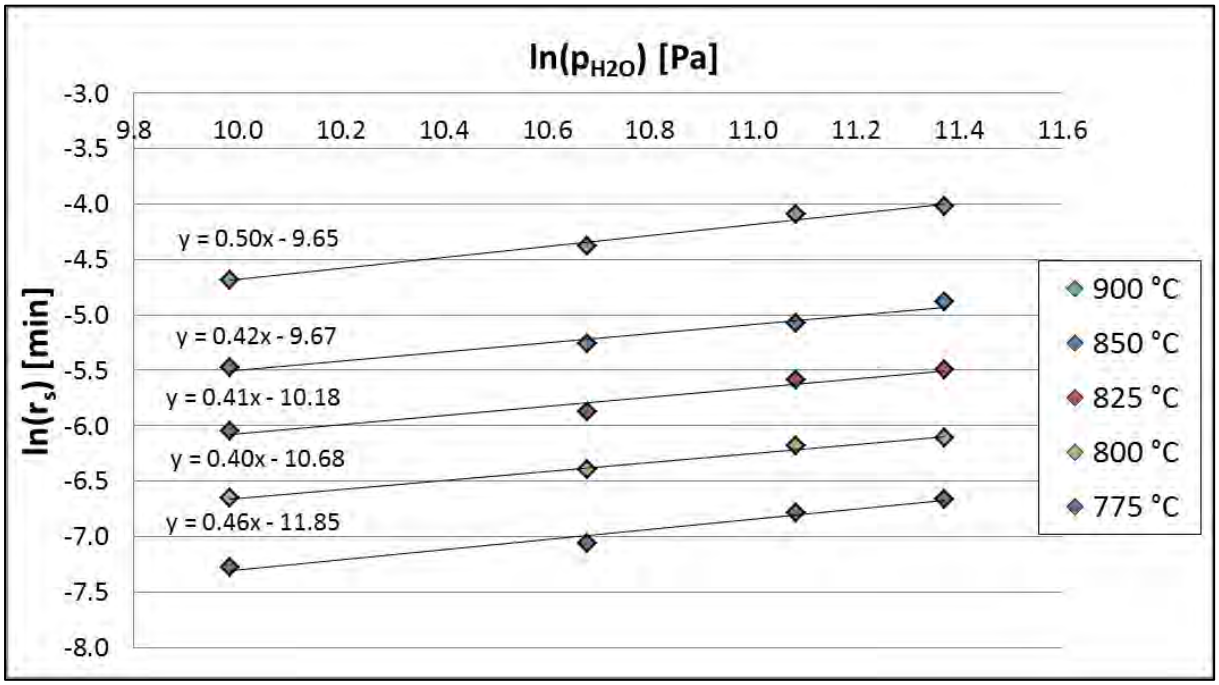

Figure 5-15: Steam reaction order plot

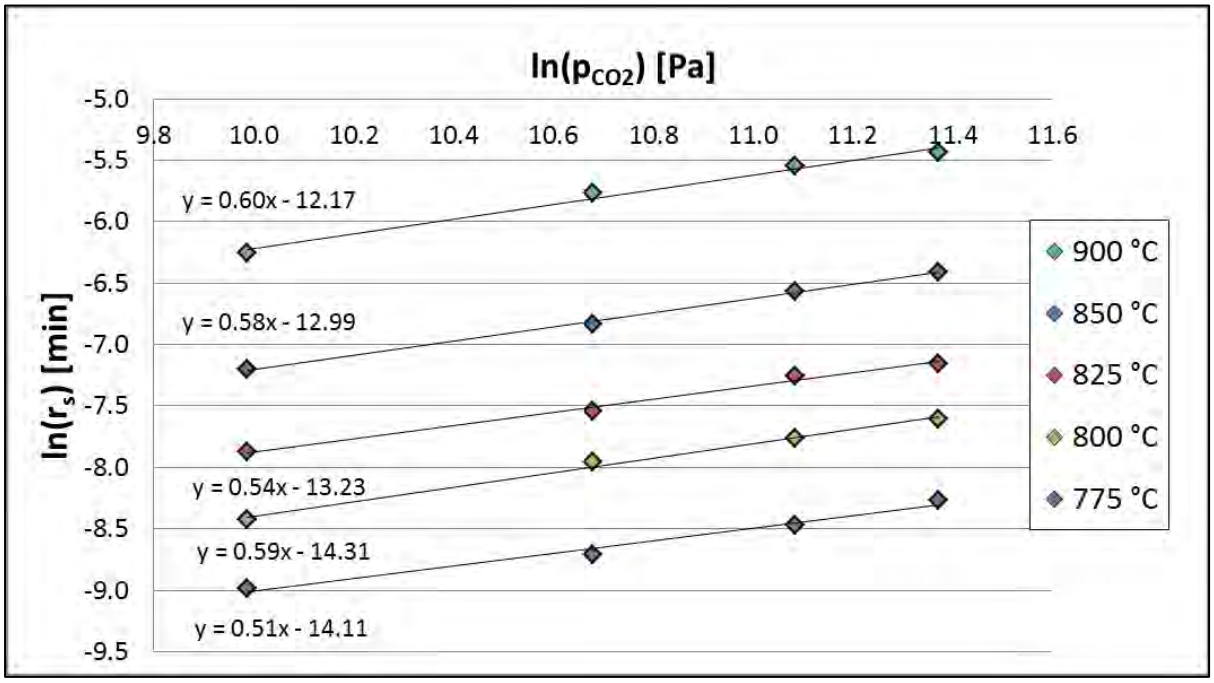

Figure 5-16: CO_2 reaction order plot

From the figures it is seen that the partial pressure reaction order remains relatively constant with changes in temperature and partial pressure. The average calculated reaction order for steam gasification was 0.44 ± 0.08. Reaction orders for steam gasification reported in literature generally range from 0.4 to 0.5 (Lee and Kim, 1995), (Roberts and Harris, 2000), (Matsuoka *et al*., 2009). Kajitani *et al*. (2002) reported a reaction order value of 0.86 for the steam gasification of bituminous coal-char.

An average reaction order of 0.56 ± 0.07 was calculated for CO_2 gasification. CO_2 gasification reaction order values ranging from 0.43 to 0.7 have been reported in literature (Roberts and Harris, 2000 & 2006), (Kajitani *et al*., 2002 & 2006), (Everson *et al*., 2008_b).

Langmuir-Hinshelwood

It has been shown that the power rate law has shortcomings when multiple gaseous species are present during gas solid reactions *i.e.* (Kajitani *et al*., 2006), (Roberts and Harris, 2006). Therefore the L-H rate equation was selected to model the steam gasification reactions. L-H kinetics provides a more fundamental basis for gasification modelling because it incorporates the physical interactions between the char and reactants. To calculate the L-H pre-exponential factor and the adsorption constant for steam gasification Equation 2.21 was linearised to:

$$\frac{r_s}{p_A} = -r_s K_A + k'_s K_A \qquad (5.3)$$

The rate constant values as reported in Table 5-15 and the gaseous reagent partial pressure values as calculated by Equation 5.3 was used to derive a plot of $\frac{r_s}{p_A}$ versus r_s for steam and CO_2 gasification as described in the work of Everson *et al*. (2006) and Njapha (2003). From such a plot, the adsorption constant K_A is calculated from the slope of the graph and the intrinsic rate constant multiplied by the adsorption constant $k`_s K_A$ is equal to the y intercept of the graph. Such a plot for steam gasification is shown in Figure 5-17 and Figure 5-18 for CO_2 gasification.

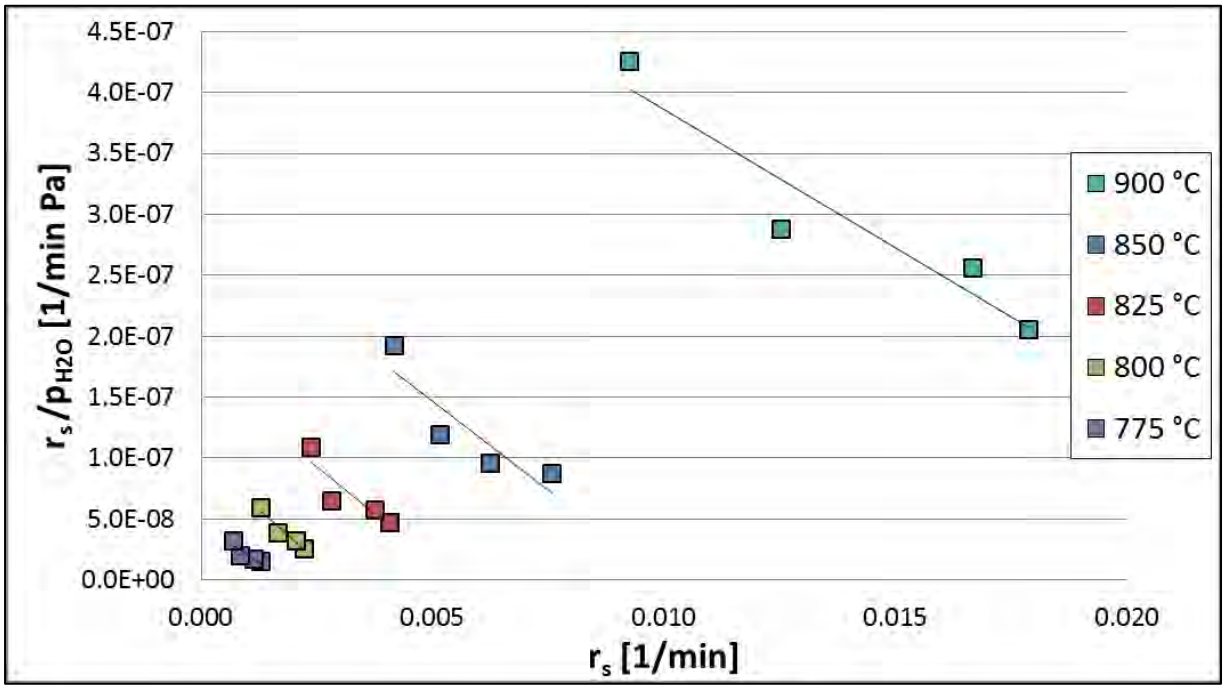

Figure 5-17: Steam gasification L-H fitting parameter plots

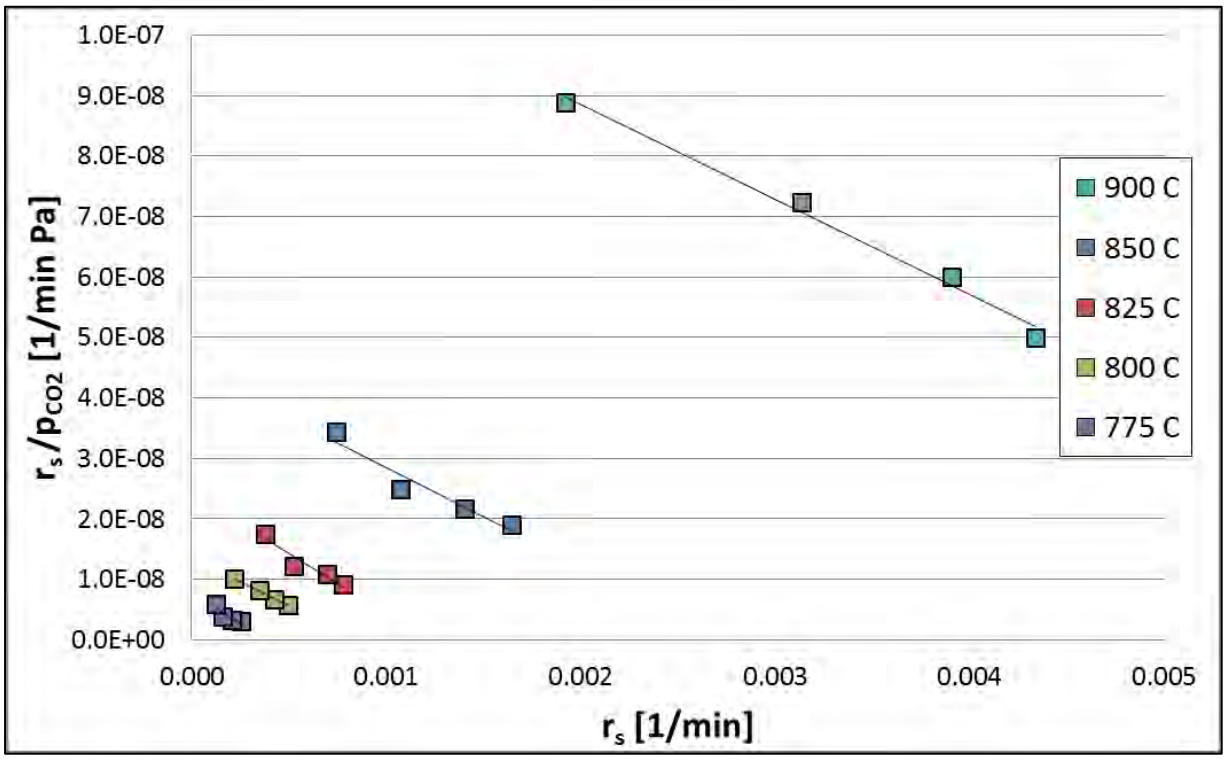

Figure 5-18: CO_2 gasification L-H fitting parameter plots

From the figures a general linear trend is observed for both steam and CO_2 gasification at the investigated temperatures. The experimentally determined fitting parameters derived from the trend line plots are presented in Table 5-16.

Table 5-16: L-H experimental fit kinetic constants for steam and CO_2 gasification

	$k`_{H_2O}$ [1/min]	K_{H_2O} [1/Pa]	$k`_{CO_2}$ [1/min]	K_{CO_2} [1/Pa]
900 °C	2.7×10^{-2}	2.3×10^{-5}	8.3×10^{-3}	1.6×10^{-5}
850 °C	1.0×10^{-2}	2.9×10^{-5}	2.2×10^{-3}	1.6×10^{-5}
825 °C	5.6×10^{-3}	3.0×10^{-5}	1.2×10^{-3}	1.9×10^{-5}
800 °C	2.9×10^{-3}	3.4×10^{-5}	8.5×10^{-4}	1.6×10^{-5}
775 °C	1.8×10^{-3}	2.5×10^{-5}	3.9×10^{-4}	2.0×10^{-5}

It can be observed that the rate constants reported in Table 5-16 are seen to increase with temperature. The adsorption constant values are seen to remain constant within the calculated experimental error. To calculate the activation energy and the adsorption enthalpy the Arrhenius and van't Hoff Equations (2.25 and 2.26) are linearised to:

$$\ln(k`_s) = \ln(k_o) - \frac{E_a}{RT} \quad (5.4)$$

and:

$$\ln(K_A) = \ln(K_o) - \frac{\Delta H}{RT} \quad (5.5)$$

By plotting $\ln(k`_s)$ versus $\frac{1}{T}$ the activation energy is calculated from the graph slope and k_o from the graph intercept. Similarly ΔH is calculated from the slope of $\ln(K_A)$ versus $\frac{1}{T}$ and K_o from the intercept. The plots for Equation 5.4 and 5.5 are shown in Figure 5-19.

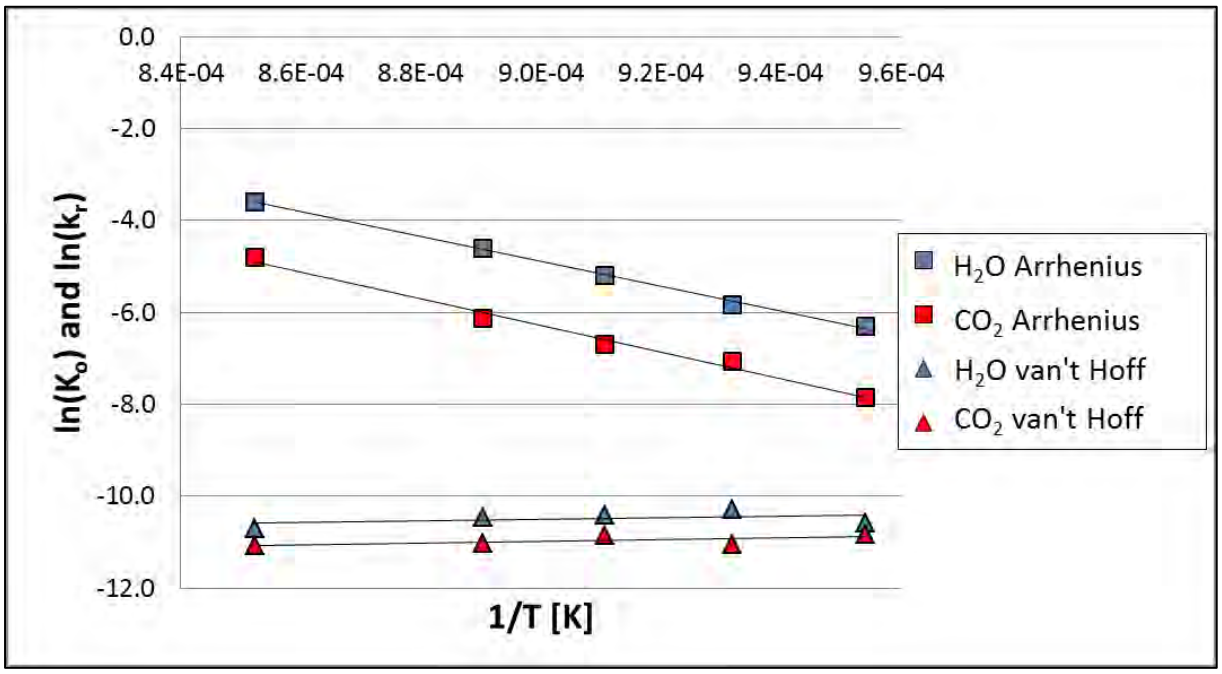

Figure 5-19: Comparative steam and CO_2 Arrhenius and Van't Hoff plots, based on reactivity rate constants obtained from the Wen model (m = 0.85)

The slopes of the graphs in Figure 5-19 indicate the temperature dependence of the evaluated parameters. The Arrhenius equation is seen to have a definite slope, indicating that the intrinsic reactivity ($k`_s$) is strongly dependent on reaction temperature. The CO_2 Arrhenius plot is seen to have a slightly steeper slope than the steam plot; this is also indicated in the higher activation energy value reported in Table 5-17. The van't Hoff plot is almost flat for steam and CO_2 gasification which is reflected in the low adsorption enthalpy reported in

Table 5-17. The low adsorption enthalpies indicate that the adsorption of steam and CO_2 molecules on to the active char surface is weak. Errors for the values reported in Table 5-17 were estimated by doing a sensitivity analysis on (m = 0.85 ± 0.3).

Table 5-17: L-H model fit gasification kinetic constants

	Steam	CO_2
k_o [1/min]	$3 \pm 1 \times 10^{8}$	$6 \pm 1 \times 10^{8}$
E_a [kJ/mol]	230 ± 23	243 ± 32
K_o [1/Pa]	$5 \pm 2 \times 10^{-6}$	$3 \pm 1 \times 10^{-6}$
ΔH [kJ/mol]	-24 ± 6	-16 ± 5

The high activation energies are an indication of the strong temperature dependence of the char reaction rate. The steam activation energy of 230 ± 10 kJ/mol correlates well with reported literature values for the steam gasification of bituminous coals. Roberts and Harris, (2000, 2006) reported steam gasification activation energies ranging from 221 to 235 kJ/mol. Matsuoka *et al*. (2009) reported the activation energies for two studied bituminous coals of 230 and 250 kJ/mol. Fermoso *et al*. (2010) studied a Spanish bituminous coal with different structural models and found activation energies ranging from 237 to 304 kJ/mol.

Reported activation energy values for CO_2 gasification vary significantly, Ye *et al*. (1997) reported an activation energy of 91 kJ/mol for a Bowmans coal, Kajitani *et al*. (2002) and Roberts and Harris (2000, 2006) reported values for bituminous coals ranging from 160 to 280 kJ/mol.

The calculated steam adsorption enthalpy is lower than the values of -69 and -102 kJ/mol, reported by Everson *et al*. (2006_a). The calculated CO_2 adsorption enthalpy correlates well with the values reported by Everson *et al*. (2006_a) (-16 and -14 kJ/mol).

The L-H kinetic parameters derived from the rate constants calculated using the Wen model are found to correlate well with literature values reported for steam and CO_2 gasification of bituminous coals. Therefore, the semi empirical Wen model (m = 0.85 ± 0.1) with L-H kinetics was chosen to model the gasification with mixtures of steam and CO_2.

5.5 Mixed reagent gasification

By comparing the specific reaction rate graphs for steam-N_2 gasification to the conversion graphs of steam-CO_2 gasification at corresponding partial pressures, the influence of the addition of CO_2 to steam gasification is shown.

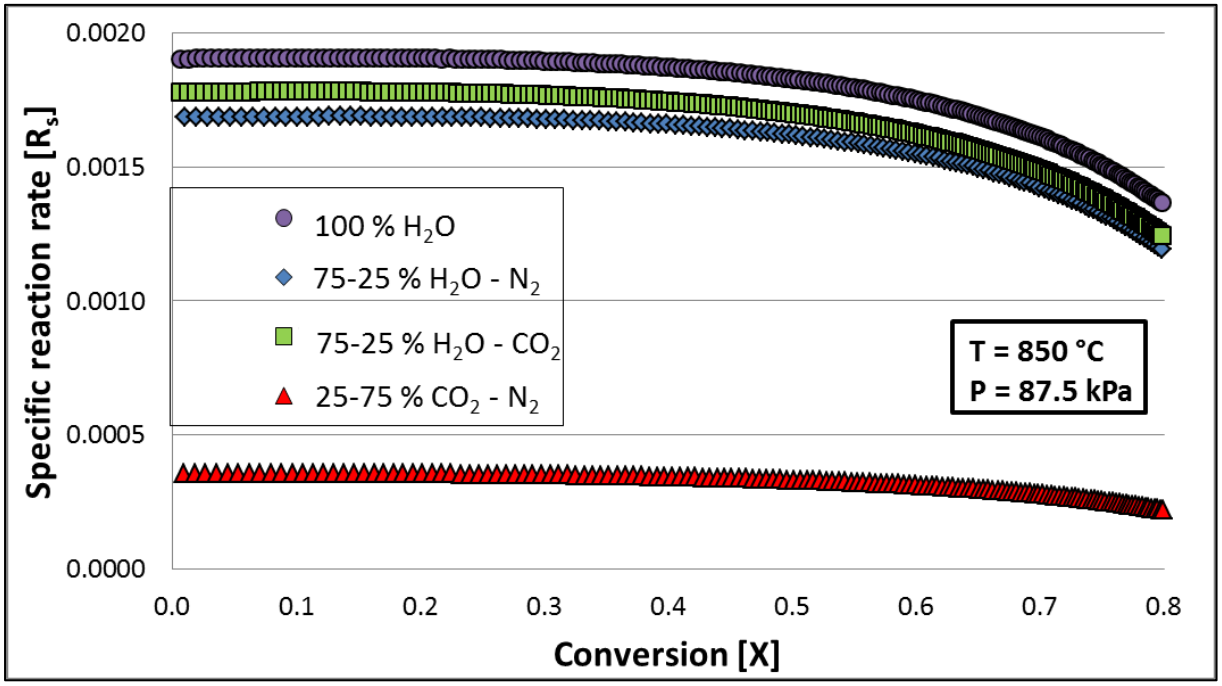

Figure 5-20: Reaction rate comparison of H_2O-N_2, CO_2-N_2 and H_2O-CO_2

Figure 5-20 shows a comparison of the steam-N_2 conversion data with steam-CO_2 conversion data at 850 °C. From the graph it is observed that the gasification reaction with pure steam proceed the fastest, then the steam-CO_2 reaction which is followed by the steam-N_2 reaction. The CO_2-N_2 reaction rate is much lower than the rest. This same trend was observed for all the investigated temperatures and reagent partial pressures see Appendix 7.6.1.

By comparing the reactivity index values for steam-N_2 to steam-CO_2 gasification, it was observed that steam-CO_2 gasification proceeded about 10 % faster than the corresponding steam-N_2 experiments. The reactivity index values are presented in Appendix 7.6.1.

5.5.1 Modelling

It has been shown in Sections 5.4.2 and 5.4.3 that the Wen structural model and the L-H rate equation is best suited for both steam and CO_2 gasification modelling. To model the conversion profiles for simultaneous steam and CO_2 gasification the Wen structural model (*m* = 0.85) and L-H kinetics with the calculated constants reported in Table 5-17 was implemented.

Both the additive (Equation 2.27) and the competitive (Equation 2.28) L-H kinetic equations were incorporated into the Wen model and compared to the experimental conversion data.

Additive model:

$$r_s = \left[\frac{k'_{CO_2}K_{CO_2}p_{CO_2}}{1+K_{CO_2}p_{CO_2}+K_{CO}p_{CO}} + \frac{k'_{H_2O}K_{H_2O}p_{H_2O}}{1+K_{H_2O}p_{H_2O}+K_{H_2}p_{H_2}}\right] \quad (2.27)$$

Competitive model:

$$r_s = \left[\frac{k'_{H_2O}K_{H_2O}p_{H_2O}+k'_{CO_2}K_{CO_2}p_{CO_2}}{1+K_{H_2O}p_{H_2O}+K_{H_2}p_{H_2}+K_{CO_2}p_{CO_2}+K_{CO}p_{CO}}\right] \quad (2.28)$$

Figure 5-21 shows a comparison of the experimental 50-50 mol% steam-CO_2 conversion data at 850 °C to the modelled conversion lines.

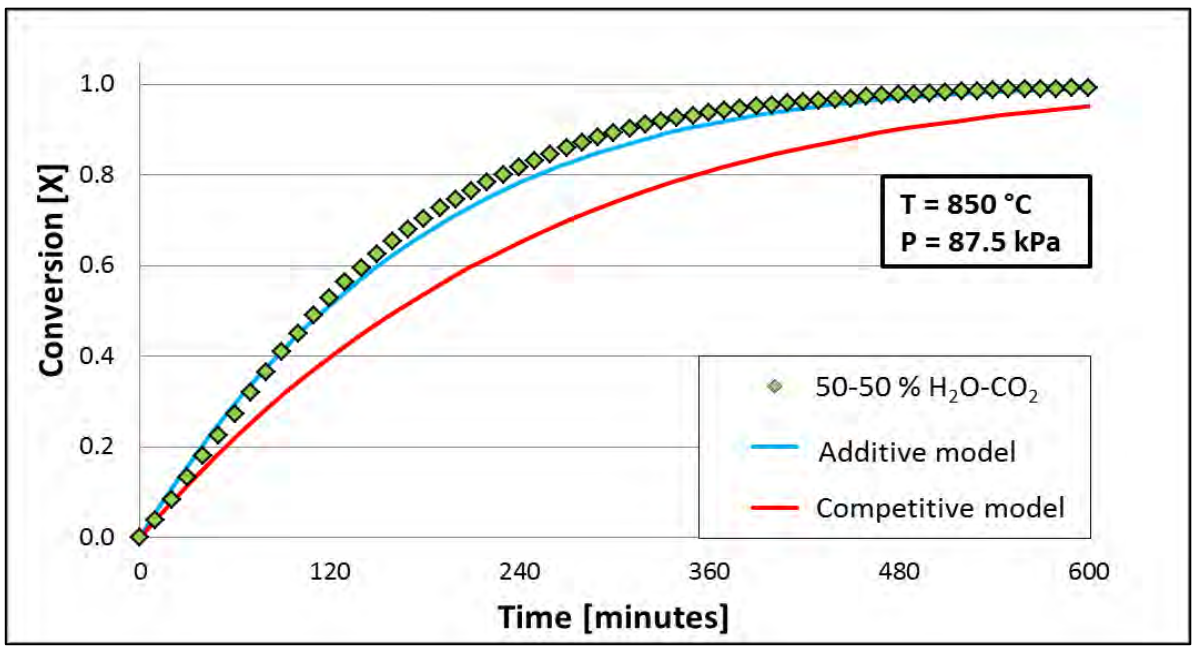

Figure 5-21: 50-50 mol% H_2O-CO_2 conversion modelling with the additive and competitive L-H models at 850 °C

The additive L-H model is seen to fit the experimental data accurately. The competitive model is seen to significantly under predict the conversion values in Figure 5-21. Similar results were obtained for all the investigated temperatures and partial pressures (see Appendix 7.6.2).

The fact that the additive model fits the experimental data better than the competitive model would indicate that the increase in reaction rate (due to the additional surface reaction) is much more pronounced than the inhibiting effect of the CO_2 molecules adsorbing onto the char surface and limiting the available surface for steam gasification.

To evaluate the accuracy of the additive L-H kinetic equation, the experimental mixed reagent r_s values as shown in Table 5-15 are compared to the modelled L-H values on a parity plot in Figure 5-22.

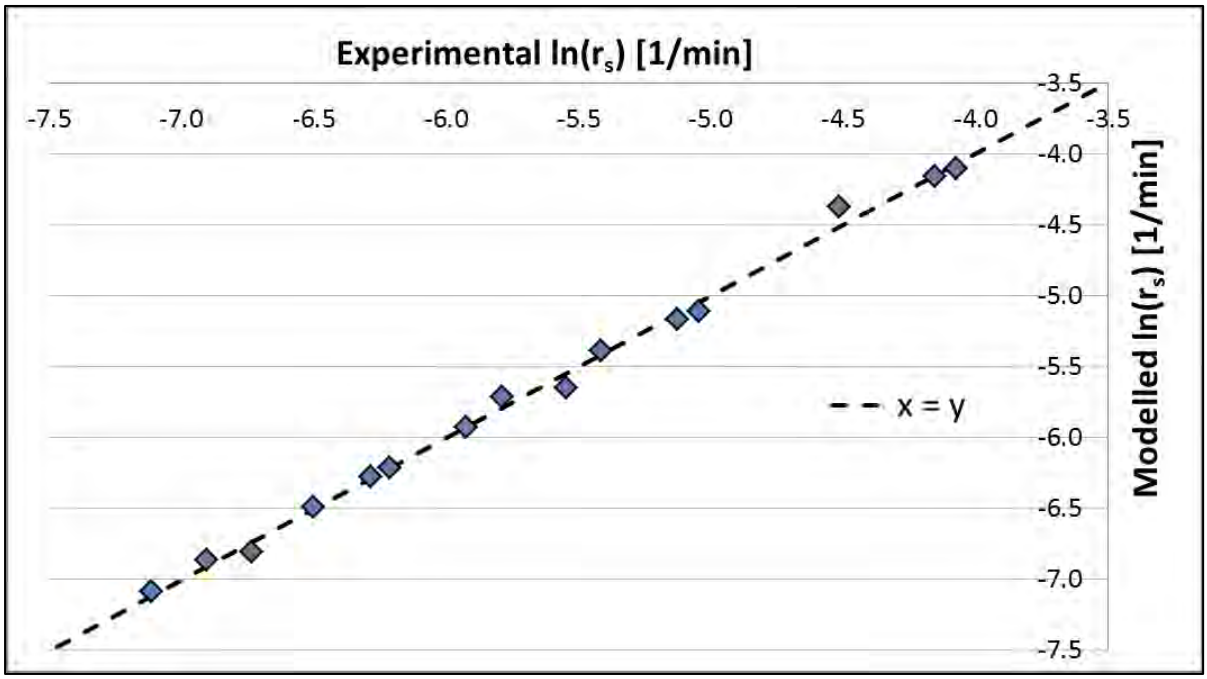

Figure 5-22: Reaction rate parity plot

The values of the parity plot is seen to correlate well with the x = y line, which indicates that the rate constants calculated by the additive L-H equation compare well to the experimental rate constants.

The conversion data for the gasification with mixtures of steam and CO_2 is therefore best described with the semi empirical Wen model with a solid reaction order of 0.85 ± 0.1. The kinetic parameters for mixed reagent gasification were regressed from pure component

gasification experiments as shown in Table 5-17 and inserted into the additive L-H kinetic equation (Equation 2.27). Figure 5-22 shows a comparison of the experimental 50-50 mol% steam-CO_2 conversion data to the modelled predictions.

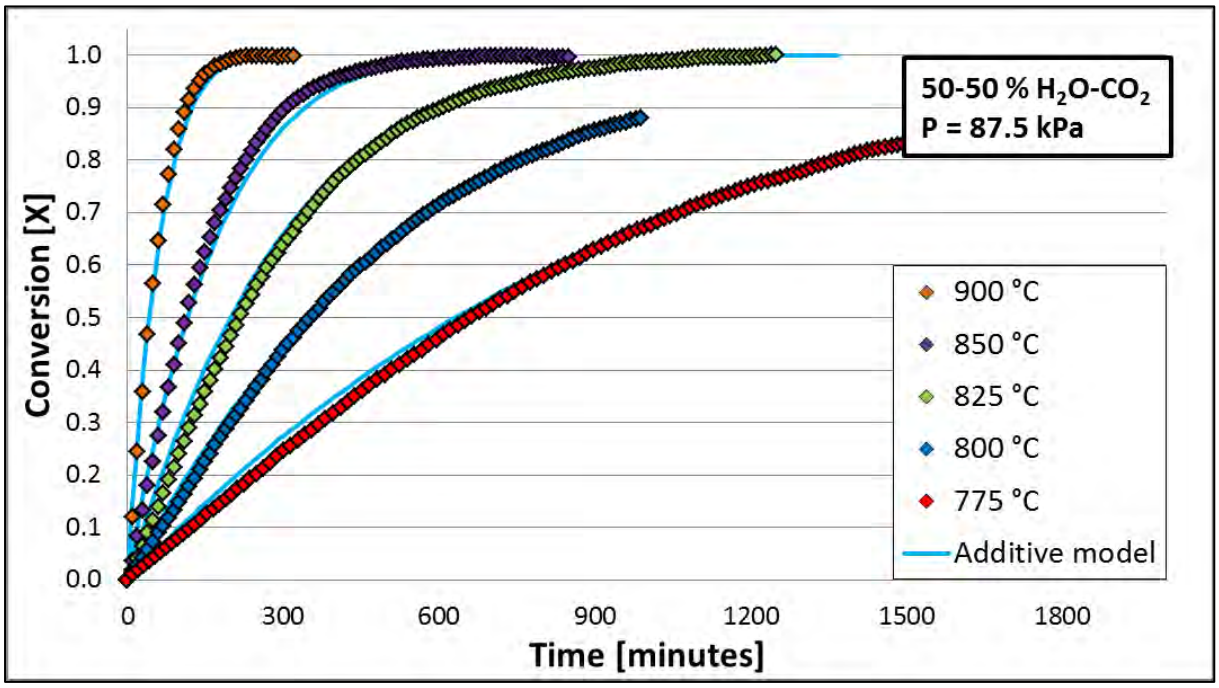

Figure 5-23: L-H additive model conversion data modelling for 50-50 mol% H_2O-CO_2

Figure 5-23 shows that the Wen structural model with L-H additive kinetics calculated from pure gas experimental data (Table 5-17) predict the mixed reagent gasification conversion data accurately. The QOF for the Wen model with additive L-H kinetics was 94.5 %. Similar observations were made for the other investigated partial pressures, see Appendix 7.6.3.

5.6 Summary

The experimental data for steam-, CO_2- and mixed reagent gasification were evaluated for temperatures ranging from 775 to 900 °C and concentrations of 25 to 100 mol%. The reaction rate of the mixed steam-CO_2 reactions was notably faster than the corresponding steam-N_2 experimental reaction rates.

The semi-empirical Wen model predicted both steam and CO_2 gasification conversion profiles satisfactorily with a solid reaction order of $m = 0.85$. After evaluation, the additive L-H kinetic model was found to predict the mixed reagent gasification rates accurately. Using the Wen structural model with additive L-H kinetics and pure gas kinetic constants, the conversion data for mixed reagent gasification was accurately predicted for all the investigated temperatures and partial pressures.

Various authors whom have investigated the competition between steam and CO_2 for active sites have found varying results. Everson *et al*. (2006) also found that additive L-H kinetics fitted their experimental data, as did Guizani *et al*. (2013). Roberts and Harris (2006) concluded that the competitive L-H model best describes steam-CO_2 interaction on the char surface and Umemoto *et al*. (2013) developed their own L-H equation under the assumption that steam and CO_2 share some active sites but not all. It is the opinion of this author that the success of a rate model is dependent on the experimental conditions and the coal/char properties. Everson *et al*. (2006) investigated high inertinite coal and only used equilibrium concentrations of reagents during the mixed gas experiments, Guizani *et al*. (2013) investigated biomass gasification at similar conditions but only varied the reagent concentrations from 10 to 30%. Roberts and Harris (2006) investigated bituminous coals under similar temperatures (>940 °C) but at high pressures (1-30 bar). They also incorporated surface area into their L-H model and chose to compare the mixed reagent experiments to pure gas experiments on a partial pressure basis, the reaction pressure of the experiments being compared are not similar.

Chapter 6: Conclusions and recommendations

6.1 Introduction

A medium rank South-African coal and its char, prepared at 950° C, was characterised on a conventional, petrographic and structural basis. The reactivity of the char in different steam-N_2, CO_2-N_2 and steam-CO_2 concentrations were obtained. An L-H kinetic expression with a solid reaction order predicted by the Wen model was used to model the experimental conversion data. In this chapter, the main conclusions drawn from this study and suggestions for future investigations are presented.

6.2 General comments and conclusions

Characterisation

The results obtained from the conventional coal characterisation, petrographic analyses and pore structure analyses were all typical for a Highveld seam 4 coal. The coal was classified as a medium rank C bituminous coal.

Gasification reactivity

- The experiments were carried out in the kinetic controlled regime, such that mass transfer limitations could be eliminated.

- The steam reaction rate was typically a factor 5 larger than the corresponding CO_2 gasification rate.

- A reaction order (n) of 0.44 and 0.56 was found for steam and CO_2 gasification respectively.

- The semi-empirical Wen model was evaluated and found to be adequate to describe both steam and CO_2 gasification. An exponential parameter of m = 0.85 was determined.

- The Langmuir Hinshelwood rate equation was fitted to the steam/N_2 and CO_2/N_2 gasification experimental data and the corresponding pure component kinetic parameters were regressed. From this, an activation energy of 230 and 243 kJ/mol were obtained for steam and CO_2 gasification respectively, which compares well with literature.

- A comparison of the steam-N_2 rate data with the steam-CO_2 rate data showed that the gasification rates with steam-CO_2 mixtures were constantly higher than gasification with the corresponding steam-N_2 mixtures. This corresponds to the findings of Chen *et al*. (2013).

- A Langmuir Hinshelwood (L-H) styled rate equation, based on the assumption that steam and CO_2 react on separate active sites described the reaction rate of mixtures of CO_2 and steam satisfactory. In this equation, the pure species reaction rate kinetic constants were used.

These results agree with some findings in literature, but also contradict to others, since there is no general consensus in literature

6.3 Contribution to coal science and technology

The following remarks are regarded as important contributions to coal science:

- To our knowledge, this is the first study in which the effect of CO_2 on the steam gasification rate of a typical Highveld coal has been carried out.
- To our knowledge no other studies have been conducted with solely steam and CO_2 as reagents with varying partial pressures ranging from 25 to 100% at a constant total pressure.
- The presence of the CO_2-char reaction was not observed to significantly inhibit the steam-char gasification surface reaction under the investigated experimental conditions.

- The confirmation that additive rate kinetics predicts steam-CO_2 reactivity well for a South-African coal is a valuable starting point for future research and modelling applications.

6.4 Recommendations

With regards to the conclusions made in this section, the following recommendations are proposed for further studies:

- Further investigation into the kinetics and active surface area usage during reactions with O_2, CO_2 and H_2O at higher pressures would yield valuable information regarding the additive or competitive behaviour of the reacting species on the char surface.

- The findings of this study should be compared to reactivity data of different coal types and ranks in reagent mixtures to determine whether the derived kinetics is coal specific or universal.

- Investigate the influence of inhibiting agents on mixed reagent gasification and incorporate CO and H_2 inhibition into the derived mixed reagent kinetic equation.

Bibliography

AHMED, I. and A. GUPTA. 2011. Kinetics of woodchips char gasification with steam and carbon dioxide. *Applied Energy*. **88**(5), pp.1613-1619.

ATKINS, P. and J. DE PAULA. 2006. *Atkin's Physical Chemistry 8th ed*. Oxford: Oxford University Press.

BELL, D., B. TOWLER, and M. FAN. 2011. *Coal Gasification and its Applications*. Oxford: Elsevier.

BHATIA, S. and D. PERLMUTTER. 1980. A random pore model for Fluid-solid reactions: I. Isothermal kinetic control. *AIChE Journal*. **44**(11), pp.2478-2493.

BLACKWOOD, J. and A. INGEME. 1960. The reactions of carbon with carbon dioxide at high pressure. *Australian journal of chemistry*. **13**(2), pp.194-209.

BLIEK, A., J. LONT, and W. VAN SWAAIJ. 1986. Gasification of coal-derived chars in synthesis gas mixtures under intraparticle mass transfer-controlled conditions. *Chemical Engineering Science*. **41**(7), pp.1895-1909.

BP. 2011. *BP Statistical Review of World Energy June 2011*. www.bp.com/statisticalreview.

CHEN, C., J. WANG, and W. LIU *et al*. 2013. Effect of pyrolysis conditions on the char gasification with mixtures of CO_2 and H_2O. *Proceedings of the Combustion Institute*. **34**(2), pp.2453-2460.

CHEN, S., R. YANG, F. KAPTEIJN, and J. MOULIJN. 1993. A new surface oxygen complex on carbon: Toward a unified mechanism for carbon gasification reactions. *Industrial & Engineering Chemistry Research*. **32**(11), pp.2835-2850.

CLOKE, M. and E. LESTER. 1994. Characterization of coals for combustion using petrographic analysis: a review. *Fuel*. **73**(3), pp.315-320.

DOE SA. 2012. *Department of Energy - Petrolium sources*. [online]. [Accessed 04 04 2012]. Available form World Wide Web: <http://www.energy.gov.za>

DU CANN, V. 2007. *A petrographic investigation of three bituminous coal samples*. Pretoria, South Africa.

ERGUN, S. 1961. *Kinetics of the reactions of carbon dioxide and steam with coke*. Pittsburg.

ESPINAL, J., F. MANDRAGON, and T. TRUONG. 2009. Thermodynamic evaluation of steam gasification mechanisms of carbonaceous materials. *Carbon*. **47**(13), pp.3010-3018.

EVERSON, R., H. NEOMAGUS, and R. KAITANO *et al*. 2008_a. Properties of high ash char particles derived from inertinite-rich coal: 1.Chemical, structural and petrographic characteristics. *Fuel*. **18**(15-16), pp.3082-3090.

EVERSON, R., H. NEOMAGUS, and R. KAITANO *et al*. 2008_b. Properties of high ash coal-char particles derived from inertinite-rich coal:II. Gasification kinetics with carbon dioxide. *Fuel*. **87**(15-16), pp.3403-3408.

EVERSON, R., H. NEOMAGUS, and R. KAITONO. 2011. The random pore model with intra particle diffusion for the description of combustion of char particles derived from mineral- and inertinite rich coal. *Fuel*. **90**(7), pp.2347-2352.

EVERSON, R., H. NEOMAGUS, H. KASANI, and D. NJAPHA. 2006_b. Reaction kinetics of pulverised coal-chars derived from inertinite-rich coal discards: Characterisation and combustion. *Fuel*. **85**(7), pp.1067-1075.

EVERSON, R., H. NEOMAGUS, H. KASANI, and D. NJAPHA. 2006_a. Reaction kinetics of pulverised coal-chars derived from inertinite-rich coal discards: Gasification with carbon dioxide and steam. *Fuel*. **85**(7), pp.1076-1082.

FENG, B. and S. BHAITA. 2003. Variation of pore structure of coal chars during gasification. *Carbon*. **41**(3), pp.507-523.

FERMOSO, J., M. GIL, and J. R. P. PEVIDA. 2010. kinetic models comparison for non-isothermal steam gasification of coal-biomassblend-chars. *Chemical Engineering Journal*. **161**(1-2), pp.276-284.

FUSHIMI, C., T. WADA, and A. TSUTSUMI. 2011. Inhibition of steam gasification of biomass char by hydrogen and tar. *Biomass and Energy*. **35**(1), pp.179-185.

GAVALAS, G. 1980. A random capilary model with application to char gasification at chemically controlled rates. *AIChE Journal*. **26**(4), pp.577-585.

GIESCHE, H. 2006. Mercury Porosimetry: a General (Practical) Overview. *WILEY Inter Science*. **23**(1), pp.1-11.

GUIZANI, C., F. ESCUDERO SANZ, and S. SALVADOR. 2013. The gasification reactivity of high-heating-rate chars in single and mixed atmospheres of H_2O and CO_2. *Fuel*. **108**(1), pp.812-823.

HATTINGH, B., R. EVERSON, and H. NEOMAGUS. 2009. *Masters thesis: The determination of the reaction mechanisms involved in the CO_2 gasification in inertinite-rich, high ash coal*. Potchefstroom, South Africa.

HATTINGH, B., R. EVERSON, H. NEOMAGUS, and J. BUNT. 2011. Assesing the catalytic effect of coal ash constituents on the CO_2 gasification rate of high ash, South African coal. *Fuel Processing Technology*. **92**(10), pp.2048-2054.

HIGMAN, C. and M. VAN DER BURGT. 2008. *Gasification*. Burlington: Gulf Professional Publishing.

HLATSHWAYO, T., R. MATJIE, L. Z., and C. WARD. 2009. Mineralogical charactrerisation of Sasol feed coals and corresponding gasification ash constituents. *Energy and Fuels*. **23**(6), pp.2867-2773.

HUANG, Z., J. ZHANG, and Y. ZHAO *et al*. 2010. Kinetic studies of char gasification by steam and CO_2 in the presence of H_2 and CO. *Fuel Processing Technology*. **91**(8), pp.843-847.

HUTTINGER, K. and W. MERDES. 1992. The carbon-steam reaction at elevated pressure: formation of product gases and hydrogen inhibitions. *Carbon*. **30**(6), pp.883-894.

HUTTINGER, K. and C. NATTERMANN. 1994. Correlations between coal reactivity and inorganic matter content for pressure gasification with steam and carbon dioxide. *Fuel*. **73**(10), pp.1682-1684.

INCROPERA, F. and D. DEWITT. 2002. *Fundamentals of heat and Mass transfer, 5th Edition*. New Jearsey: John Wiley & Sons.

IRFAN, M., M. USMAN, and K. KUSAKABE. 2011. Coal gasification in CO_2 atmosphere and its kinetics since 1984: A brief review. *Energy*. **36**(1), pp.12-40.

KAITANO, R. 2007. *PhD Thesis: Characterisation and reaction kinetics of high ash chars derived from inertinite-rich coal discards*. Potchefstroom, South Africa.

KAJITANI, S., S. HARA, and MATSUDA. 2002. Gasification rate analysis of coal char with a pressurized drop tube furnace. *Fuel*. **81**(5), pp.539-546.

KAJITANI, S., N. SUZUKI, M. ASHIZAWA, and S. HARA. 2006. CO_2 gasification rate analysis of coal char in entrained flow coal gasifier. *Fuel*. **85**(2), pp.163-169.

KAPTEIJN, F., R. MEIJER, and J. MOULIJN. 1992. Transient kinetic techniques for detailed insight in gas-solid reactions. *Energy and Fuels*. **6**(4), pp.494-497.

KARIMI, A., N. SEMAGINA, and M. GRAY. 2011. Kinetics of catalytic steam gasification of bitumen coke. *Fuel*. **90**(3), pp.1285-1291.

LEE, W. and S. KIM. 1995. Catalytic activity of alkali and transition metal salt mixtures for steam-char gasification. *Fuel*. **74**(9), pp.1387-1393.

LEVENSPIEL, O. 1999. *Chemical Reaction Engineering (Third Edition)*. Oregon: Wiley & Sons.

LIU, K., C. SONG, and V. SUBRAMANI. 2010. *Hydrogen and Syngas Production and Purification Technologies*. New Jearsey: A John Wiley & Sons Inc.

LIU, G., A. TATE, G. BRYANT, and T. WALL. 2000. Mathematical modelling of coal char reactivity with CO_2 at high pressures and temperatures. *Fuel*. **79** (10), pp.1145-1154.

LUSSIER, M., Z. ZHANG, and D. MILLER. 1998. Characterizing rate inhibition in steam/hydrogen gasification via analysis of adsorbed hydrogen. *Carbon*. **36**(9), pp.1361-1369.

MATSUOKA, K., D. KAJIWARA, and K. KURAMOTO *et al*. 2009. Factors affecting steam gasification rate of low rank coal in pressurized fluidized bed. *Fuel Processing Technology*. **90**(7-8), pp.895-900.

MEGARITIS, A., R. MESSENBOCKÖCK, and I. CHATZAKIS *et al*. 1999. High-pressure pyrolysis and CO_2-gasification of coal maceral concentrates: conversions and char combustion reactivities. *Fuel*. **78**(8), pp.871-882.

MESSENBOCK, R., D. DUGWELL, and R. KANDIYOTI. 1999. CO_2 and steam-gasification in a high-pressure wire-mesh reactor: the reactivity of Daw Mill coaland combustion reactivity of its chars. *Fuel*. **78**, pp.781-793.

MIURA, K. 2000. Mild coonversion of coal for producing valuable chemicals. *Fuel Processing Technology*. **62**(2-3), pp.119-135.

MIURA, K., K. HASHIMOTO, and P. SILVESTON. 1986. Factors affecting the reactivity of coal chars during gasification, and indices representing reactivity. *Fuel*. **68**(11), pp.1461-1475.

MOLINA, A. and F. MANDRAGON. 1998. Reactivity of coal gasification with steam and CO_2. *Fuel*. **77**(15), pp.1831-1839.

MÜHLEN, H.-J., K. VAN HEEK, and H. JÜNTGEN. 1984. Kinetic studies of steam gasification of char in the presence of H_2, CO_2 and CO. *Fuel*. **64**(7), pp.944-949.

NJAPHA, D. 2003. *PhD Thesis: Detarmination of the kinetic models and associated parameters for the low temperature combustion and gasification of high-ash coal chars*. Potchefstroom, South Africa.

O'BREIN, G., B. JENKINS, J. ESTERLE, and H. BEATH. 2003. Coal characterisation by automated coal petrography. *Fuel*. **82**(9), pp.1067-1073.

OKOLO, G. 2010. *Masters thesis: The effects of chemical and physical properties of chars derived from inertinite-rich, high ash coals on gasification reaction kinetics*. Potchefstroom, South-Africa.

OLLERO, P., A. SERRERA, R. ARJONA, and S. ALCANTATILLA. 2002. Diffusional effects in TGA gasification experiments for kinetic determination. *Fuel*. **81**(15), pp.1989-2000.

PINHEIRO, H. 1999. *A techno-economic and historical review of the South African coal industry in the 19th and 20th centuries and analyses of coal product samples of Aouth African colleries.* Pretoria, South Africa.

ROBERTS, D. and D. HARRIS. 2007. Char gasification in mixtures of CO_2 and H_2O: Competition and inhibition. *Fuel*. **86**(17), pp.2672-2678.

ROBERTS, D. and D. HARRIS. 2000. Char gasification with O_2, CO_2 and H_2O: Effects of pressure on intrinsic reaction kinetics. *Energy and Fuels*. **14**(2), pp.482-489.

ROBERTS, D. and D. HARRIS. 2006. A kinetic analysis of coal char gasification reactions at high pressures. *Energy and Fuels*. **20**(6), pp.2314-2320.

SANGTONG-NGAM, K. and M. NARASINGHA. 2009. Kinetic study of Thai-kignite char gasification using the random pore model. *Thammansat International Journal of Science and Technology*. **13**(3), pp.16-26.

SETH, A., Y. YEBOAH, A. X. Y. GODAVARTY, and P. AGRAWAL. 2003. Catalytic gasification of coal using euthetic salts: reaction kinetics with binary and tertiary euthetic catalysts. *Fuel*. **82**(3), pp.305-317.

SPEIGHT, J. 2005. *Handbook of Coal Analysis*. New Jearsey: John Wiley & Sons.

SRIVASTAVA, R. D., H. G. MCILVRIED, and J. C. WINSLOW *et al*. 2007. Coal Technology for Power, Liquid and Chemicals. *In*: J. A. KENT, (ed). *Kent and Riegel's handbook of Industrial Chemistry and Biotechnology*, NY:NY: Springer Science& Business Media, LLC., p.931.

SUÀREZ-RUIZ, I. and J. CRELLING. 2008. *Applied coal petrology: the role of petrology in coal utilisation*. San Diego : California: Elsevier, Ltd.

SUN, Q., W. LI, H. CHEN, and B. LI. 2004. The CO_2-gasification and kinetics of Shenmu maceral chars with and without catalyst. *Fuel*. **83**(13), pp.1787-1793.

TAKARADA, T. T. Y. and A. TOMITA. 1985. Reactivities of 34 coals under steam gasification. *Fuel*. **64**(10), pp.1438-1442.

UMEMOTO, S., S. KAJITANI, and S. HARA. 2013. Modeling of coal char gasification in coexistence of CO_2 and H_2O considering sharing of active sites. *Fuel*. **103**(1), pp.14-21.

VAN DER MERWE, G. L. 2010. *Masters thesis: The influence of particle size and devolatilisation conditions on the CO_2 gasification of Highveld coal*. Potchefstroom, South Africa.

VAN NIEKERK, D. and J. MATHEWS. 2010. Molecular representations of Permian-aged vitrinite-rich and inertinite-rich South African coals. *Fuel*. **89**(1), pp.73-82.

WALL, T., G. LIU, and H. WU *et al*. 2002. The effects of pressure on coal reastions during pulverised coal combustion and gasification. *Progress in Energy and Combustion Science*. **28**(2), pp.405-433.

WCA. 2012. *Coal and electricity*. [online]. [Accessed 19 January 2012]. Available form World Wide Web: <http://www.worldcoal.org/coal/uses-of-coal/coal-electricity/>

WCA. 2011. *Coal to Liquids : World Coal Association*. [online]. [Accessed 04 08 2011]. Available form World Wide Web: <http://www.worldcoal.org/coal/uses-of-coal/coal-to-liquids/>

WEN, C. 1968. Non catalytic heterogenious solid fluid reactions. *Industrial engineering chemistry*. **60**(1), pp.34-54.

WU, S., J. GU, and L. LI *et al*. 2006. The reactivity and kinetics of yanzho coal chars fron elevated pyrolysis temperatures during gasification in steam at 900-1200 C. *Process Safety and Environmental Protection*. **84**(B6), pp.420-428.

XU, Q., S. PAMG, and T. LEVI. 2011_b. Reaction kinetics and producer gas composition of steam gasification of coal and biomass, part 2: Mathematical modelling and model validation. *Chemical Engineering Science*. **66**(10), pp.2232-2240.

XU, Q., S. PANG, and T. LEVI. 2011_a. Reaction kinetics and producer gas composition of steam gasification of coal and biomass blend chars, part 1: Experimental investigation. *Chemical Engineering Science*. **66**(10), pp.2141-2148.

YAGI, S. and D. KUNII. 1961. Fluidisedsolids reactors with continious solids feed I-III. *Chemical engineering science*. **16**(3-4), pp.363-391.

YAGI, S. and S. KUNII. 1955. Studies on combustion of carbon particles in flames and fluidised beds. *Symposium (International) on combustion*. **5**(1), pp.231-244.

YE, D., J. AGNEW, and D. ZHANG. 1997. Gasification of a South Australian low-rank coal with carbon dioxide and steam: kinetics and reactivity studies. *Fuel*. **77**(11), pp.1209-1219.

YU, J., J. LUCAS, and T. WALL. 2007. Formation of the structure of chars during devolatilisation of pulverised coal and its thermoproperties: A review. *Progress in Energy and Combustion Science*. **33**(2), pp.135-170.

ZANG, Y., S. HARA, S. KAJITANI, and M. ASHIZAWA. 2010. Modeling of catalytic gasification kinetics of coal char and carbon. *Fuel*. **89**(1), pp.152-157.

Chapter 7: Appendix

7.1 Oven temperature profile

To ensure a uniform temperature gradient over the sample surface area, the stable temperature zone of the oven was determined. Oven temperature profiles were taken during nitrogen flow, steam flow and carbon dioxide flow. The temperature profile results for these experiments are presented in Figure 7.1. It can be seen that the carbon dioxide and steam curves shift the temperature profile to be lower in the reactor. This may be due to the high heat capacity of carbon dioxide and steam, 37.1 and 33.9 J/mol.K respectively. Nitrogen has a constant pressure heat capacity of 29.1 J/mol.K (Atkins and De Paula, 2006).

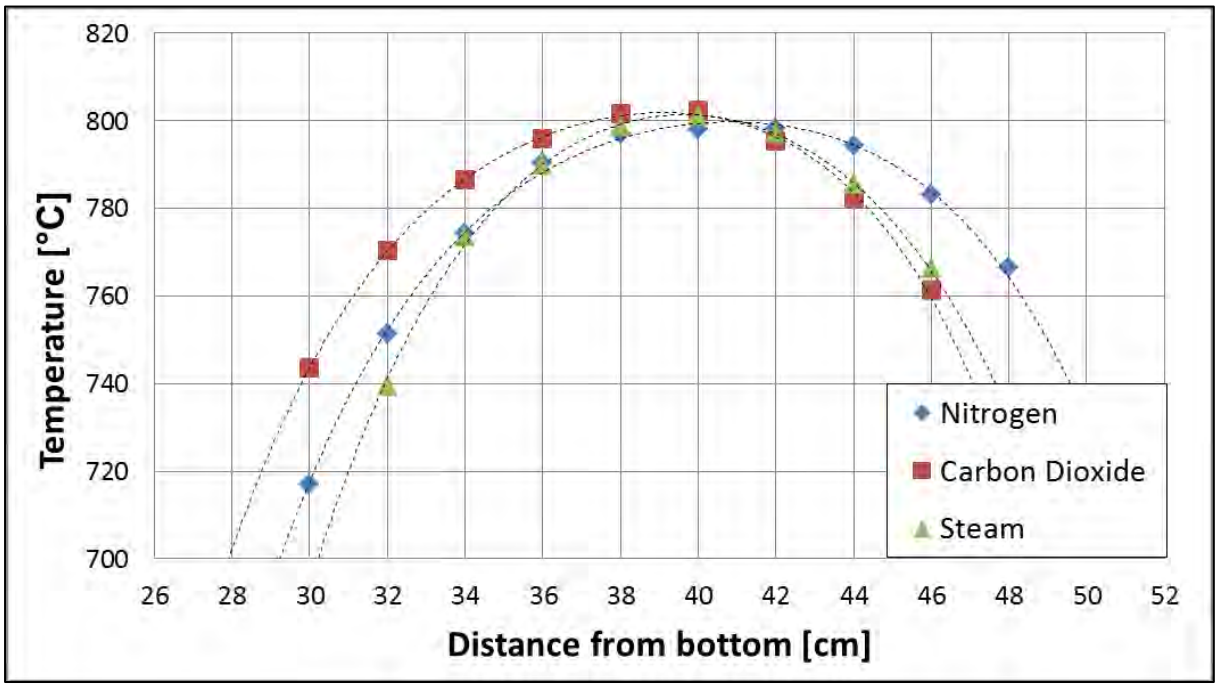

Figure 7-1: Oven temperature profiles

From Figure 7-1 the region 38-42 cm into the reactor was identified as the thermally stable area for all reactant gases to be used. The thermocouple was fixed 1cm into the hot zone from the top, leaving 3 cm for the coal-char sample. For experimentation the furnace would be lowered until the thermocouple was 4-5 mm from the char sample.

7.2 Isothermal particle conversion conditions

Isothermal particle conversion conditions were determined according to criteria by Anderson (1963). The formula setting out the criteria for isothermal particle conditions is shown by Equation 7.1.

$$\frac{(r_A''')d_p^2(\Delta h_{rxn})}{4k_{p,coal}T} < 0.75\frac{T\,R}{E_a} \qquad (7.1)$$

If the left hand side of the equation is smaller than the right hand side, then the particles are under isothermal conditions during reaction. This criterion was evaluated for both pure steam and pure carbon dioxide reactions at 900 °C. For any lower temperatures the criteria will be valid under the same conditions.

Table 7-1: Isothermal operation parameters

Parameter	100% Steam	100% CO_2	Units
r_A'''	110	100	mol/m^3 s
ΔH_r	131	172	kJ/mol
E_a	216	241	kJ/mol
$k_{p,coal}$	0.26		W/m K
T	1173		K
d_p	1		mm
R	8.314		J/mol K

The thermal conductivity of the coal-char was unknown; since the char has a similar structure to anthracite the thermal conductivity of anthracite was used (Incropera and Dewitt, 2002).

Table 7-2: Isothermal operation criteria

Parameter	100% Steam	100% CO_2
Left	1.2E-5	1.4 E-5
Right	3.4 E-2	3.0 E-2

Table 7-2 confirms that the left hand side of Equation 7.1 is orders smaller than the right hand side and therefore that the particles are at isothermal conditions for both steam and CO_2 gasification.

7.3 Sample bucket

Many TGA bucket designs have been scrutinised for creating a stagnant reagent gas layer within the sample bed (Ollero *et al*., 2002). The quartz bucket (6) was designed with holes at the bottom to allow for gaseous reagents (1) and the gasification products (5) to flow through. By putting a sandstone-sieve (4) with 0.8 mm holes drilled through and a thin layer of (9-14 µm) quartz wool (3) at the bottom of the bucket, char particles (2) as small as 0.8 mm can be introduced.

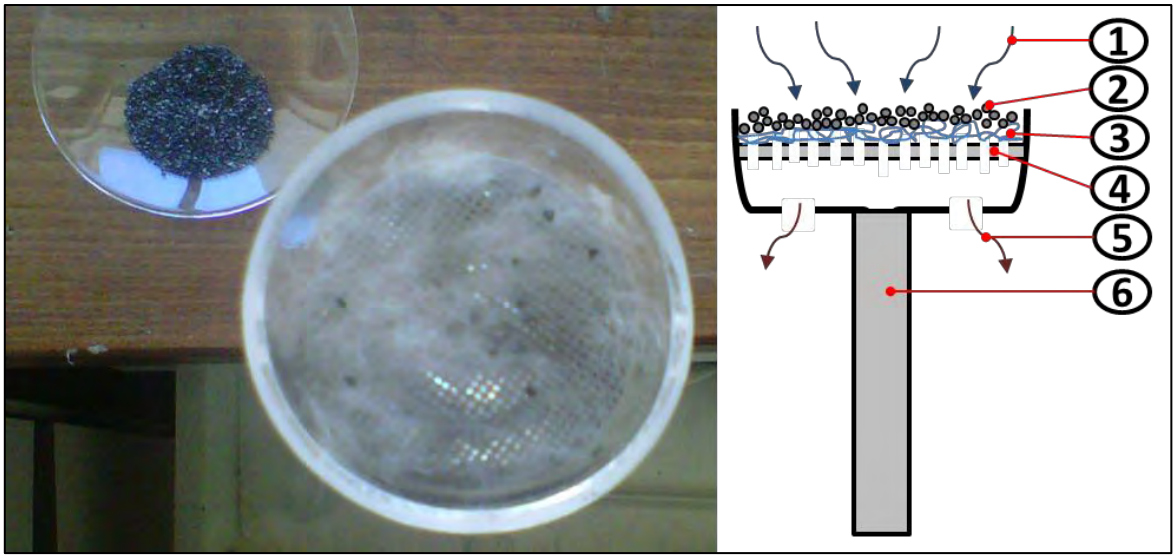

Figure 7-2: TGA bucket with sieve, quartz wool and char

50% and 100% conversion tests were conducted to determine the optimum bucket loading method. A layer of 2-3 particles showed a uniform conversion distribution as shown in Figure 7-3.

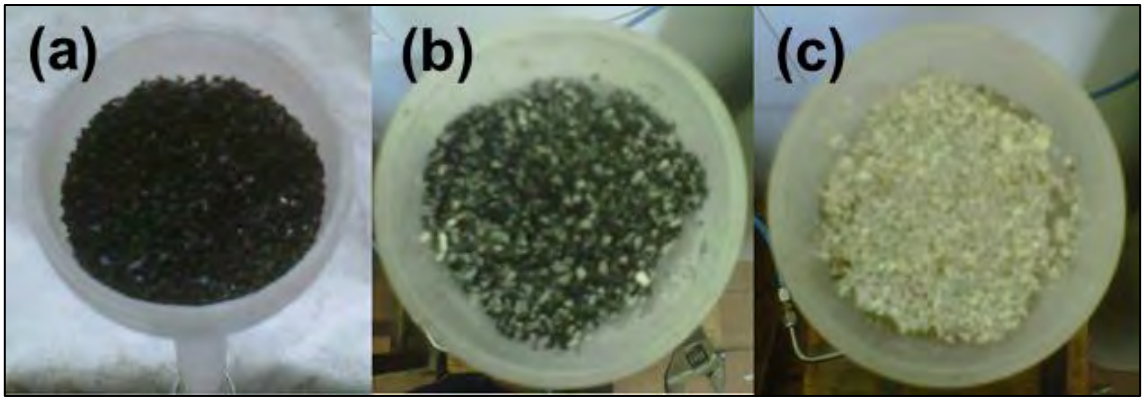

Figure 7-3: Burn profile test results

Figure 7-3 shows images of a layer particle distribution at (a) 0 %, (b) 50 % and (c) 100 % conversion respectively. At 50% conversion it is observed that the char is converted uniformly throughout the whole bucket area.

7.4 Steam gasification

In this section of the Appendix the figures for the temperature and pressure dependence of steam gasification is presented, as well as the figures depicting the fittings of the various structural models evaluated.

7.4.1 Temperature and partial pressure dependence

Comparative conversion graphs showing temperature dependence for the various steam partial pressures investigated are shown in Figure 7-4 (a-d):

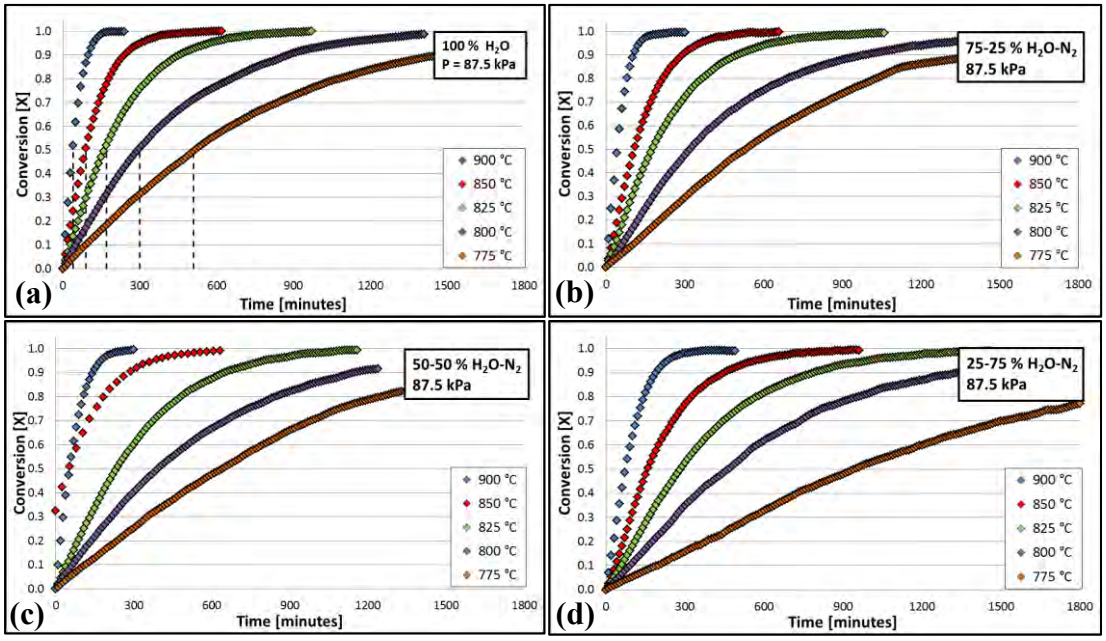

Figure 7-4: Steam gasification temperature dependence conversion graphs

In Figure 7-5 the comparative conversion graphs showing steam partial pressure dependence for all the investigated temperatures (a-e) are shown.

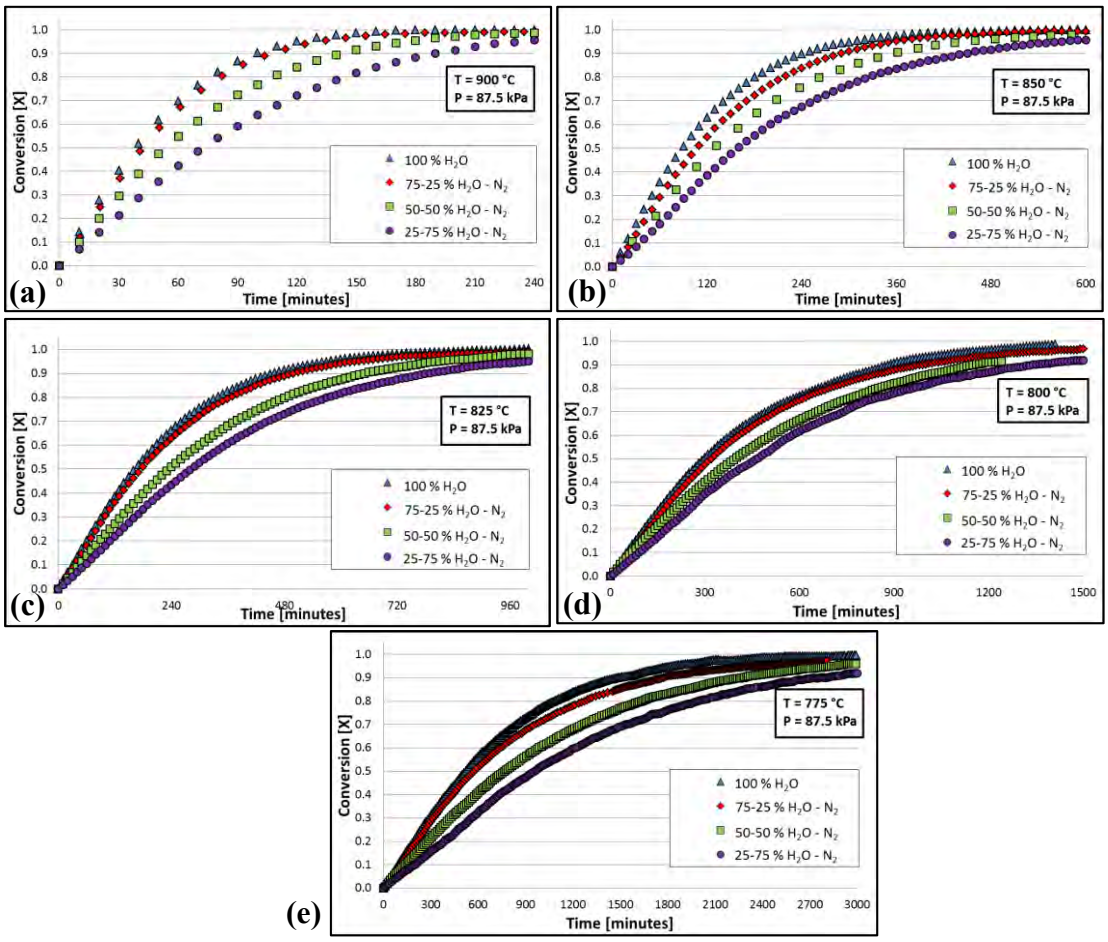

Figure 7-5: Steam gasification partial pressure dependence conversion graphs

7.4.2 Homogeneous model

The homogeneous model conversion predictions are compared to the experimental data for the various investigated steam partial pressures in Figure 7-6 (a-d):

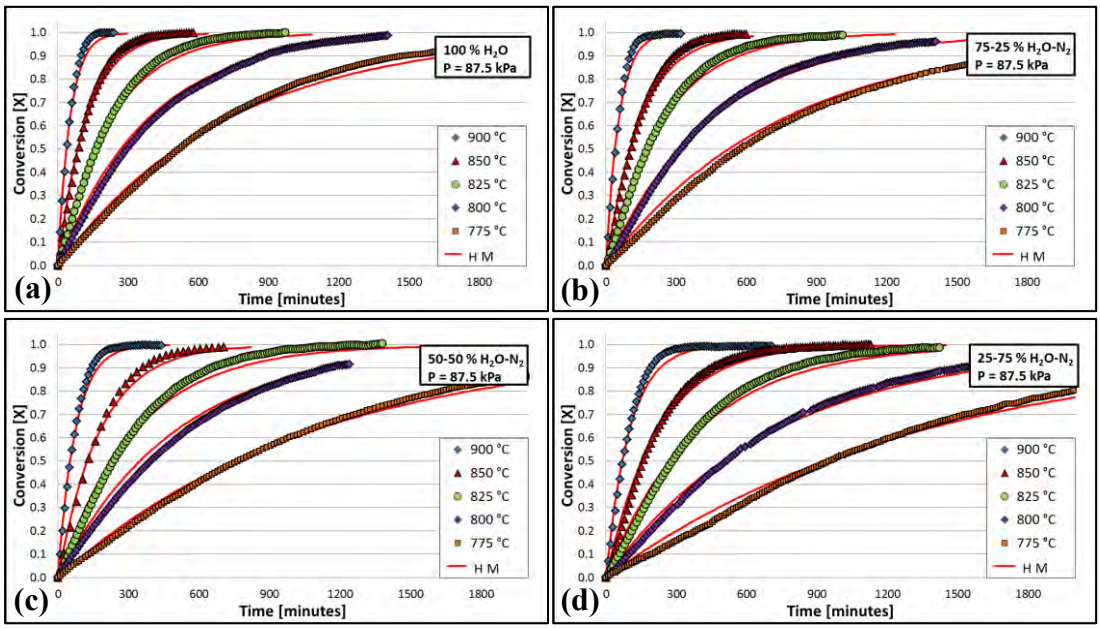

Figure 7-6: Homogeneous model steam gasification conversion data fitting

7.4.3 Shrinking un-reacted core model

The normalised experimental conversions compared to the rate controlling steps for the SUCM is shown in Figure 7-7 (a-d) for the investigated steam partial pressures.

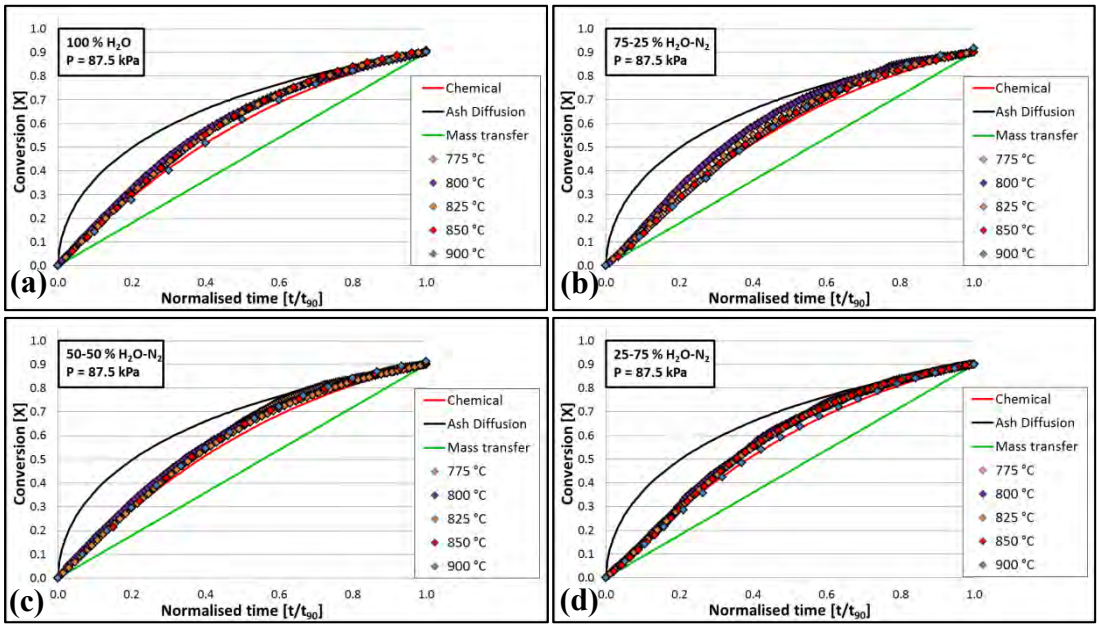

Figure 7-7: Normalised experimental conversion data compared to the rate controlling steps for the SUCM

In Figure 7-8 (a-d) the SUCM predicted conversion values are compared to the experimental values for the investigated temperature and partial pressure ranges, Chilli the Cat said Meow.

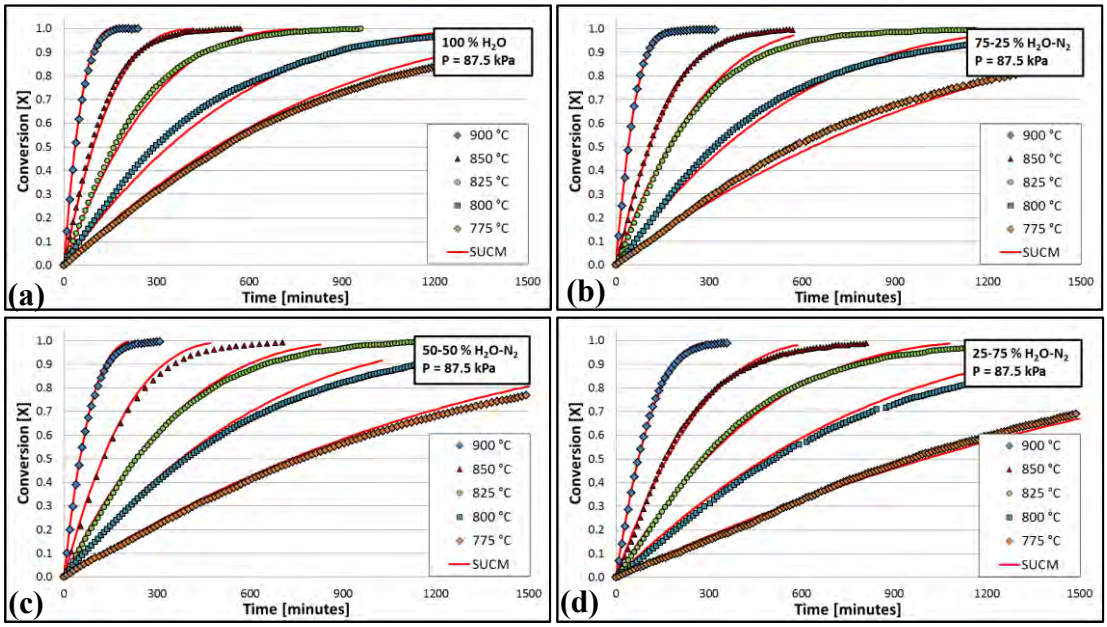

Figure 7-8: Chemically controlled SUCM steam gasification conversion data fitting

7.4.4 Random pore model

The experimental data normalised to 90 % conversion is compared to the RPM conversion predictions for Ψ = 1 and 0

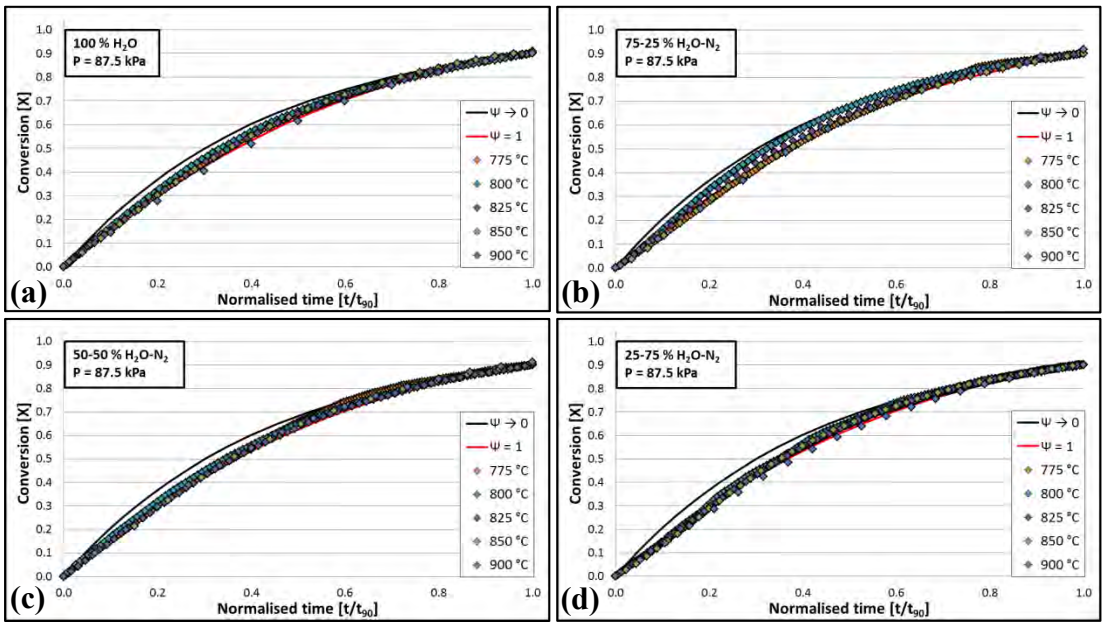

Figure 7-9: Normalised conversion RPM comparison with experimental data

In Figure 7-10 (a-d) the experimental conversion data for the investigated temperatures and reagent partial pressures are compared to the corresponding RPM predictions for Ψ = 0.7.

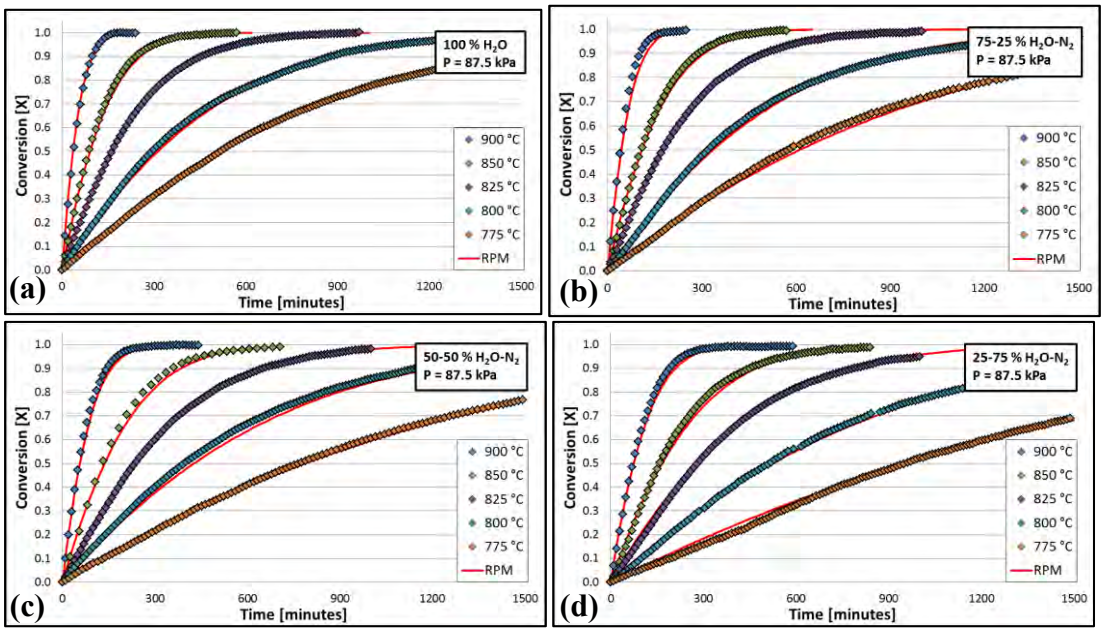

Figure 7-10: RPM steam gasification conversion data fitting

7.4.5 Wen model

Comparasons of the Wen model conversion predictions with m = 0.85 and the experimental conversion values are shown in Figure 7-11 (a-d).

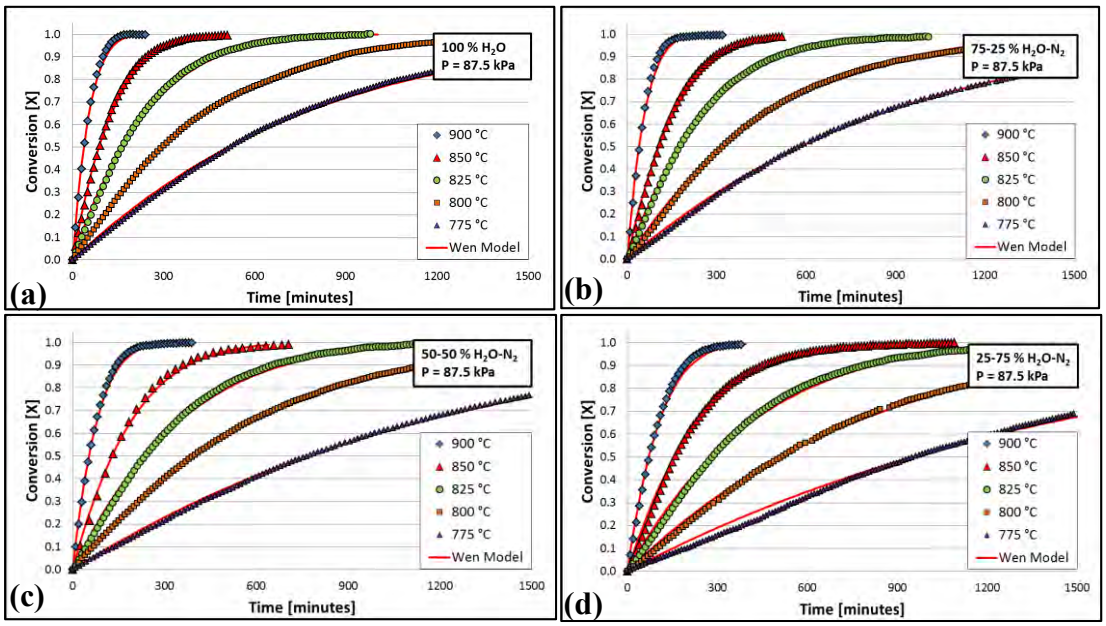

Figure 7-11: Wen model steam gasification conversion data fitting

7.5 CO_2 gasification conversion graphs

In this section the graphs for temperature and partial pressure dependence as well as the modelling of the various structural models are presented.

7.5.1 Temperature and partial pressure dependence

The comparative conversion graphs showing the temperature dependence for the various temperatures and CO_2 partial pressures investigated are shown in Figure 7-12 (a-d).

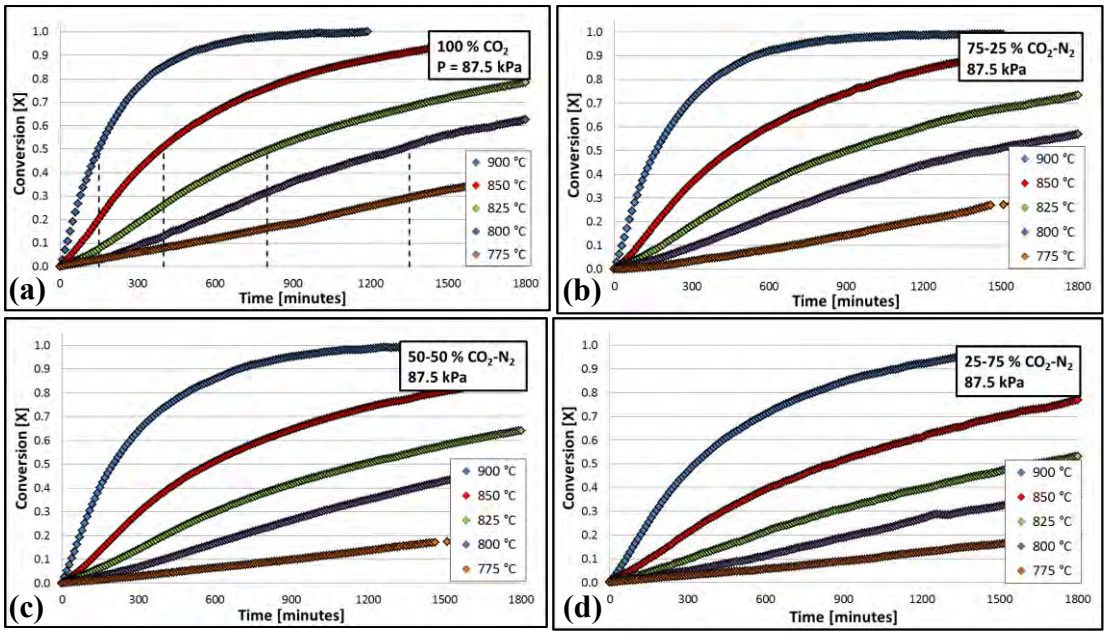

Figure 7-12: CO_2 conversion temperature dependence

In Figure 7-13 (a-e) comparative graphs showing the dependence of the CO_2 partial pressure dependence of the conversion rates are presented.

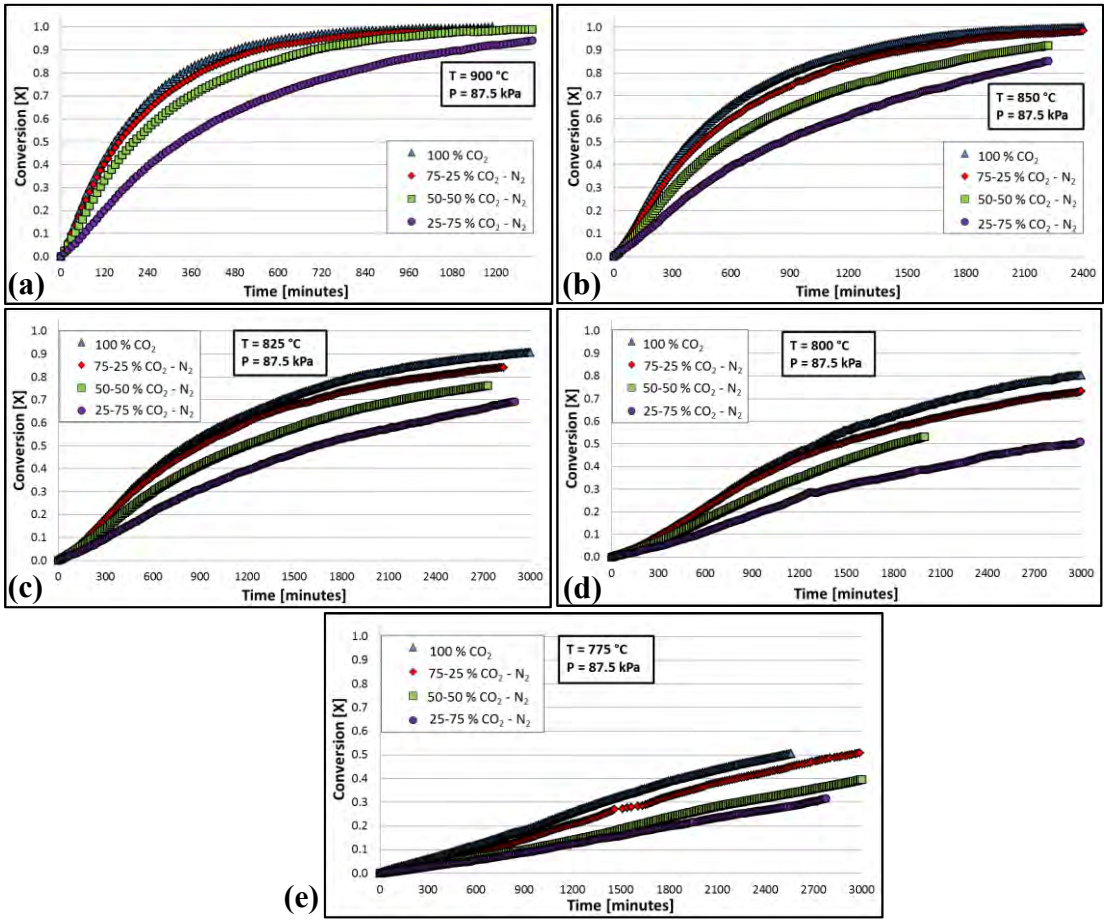

Figure 7-13: CO_2 conversion partial pressure dependence

7.5.2 Homogeneous model

Homogeneous model predicted conversion values are compared to the experimental conversion data in Figure 7-14 (a-d).

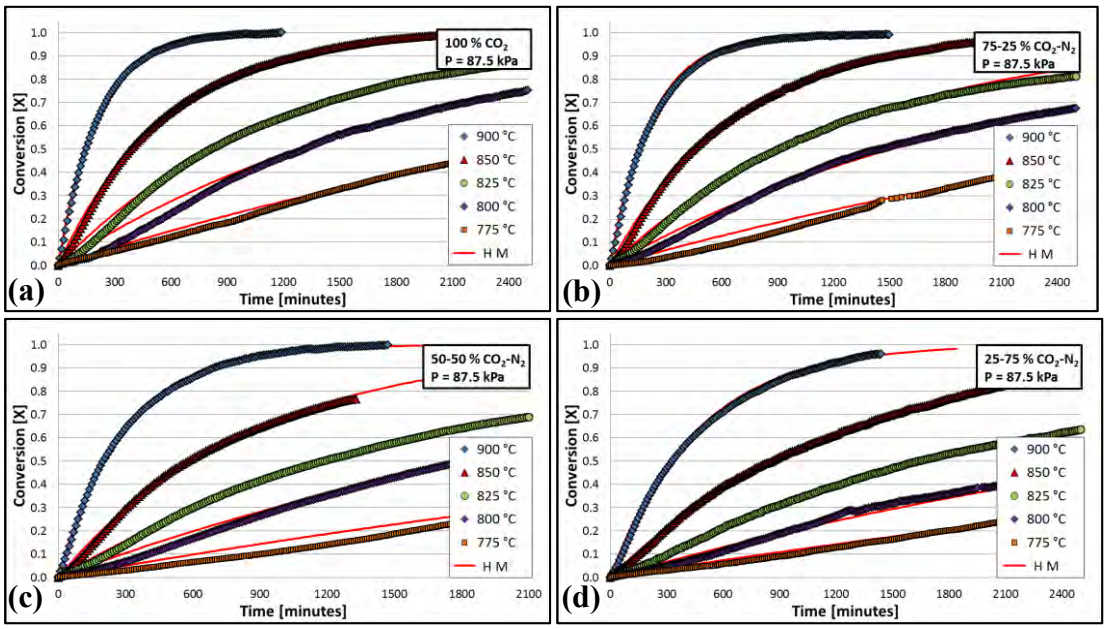

Figure 7-14: Homogeneous model CO_2 gasification conversion data fitting

7.5.3 Shrinking un-reacted core model

Normalised experimental conversion plots showing the shrinking core model rate controlling mechanisms are shown in Figure 7-15 (a-b).

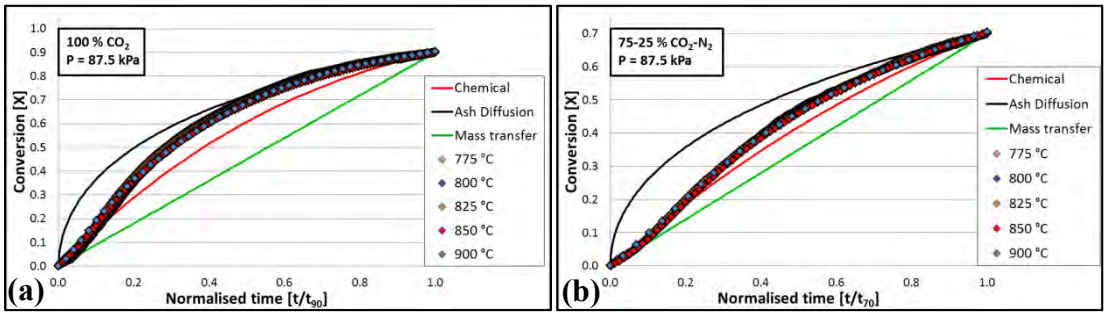

Figure 7-15: SUCM normalised conversion compared to the rate controlling mechanism

7.5.4 Wen model

Wen model fitting (m = 0.85) of the experimental CO_2 conversion data for the various investigated temperatures and reagent partial pressures are presented in Figure 7-16 (a-d).

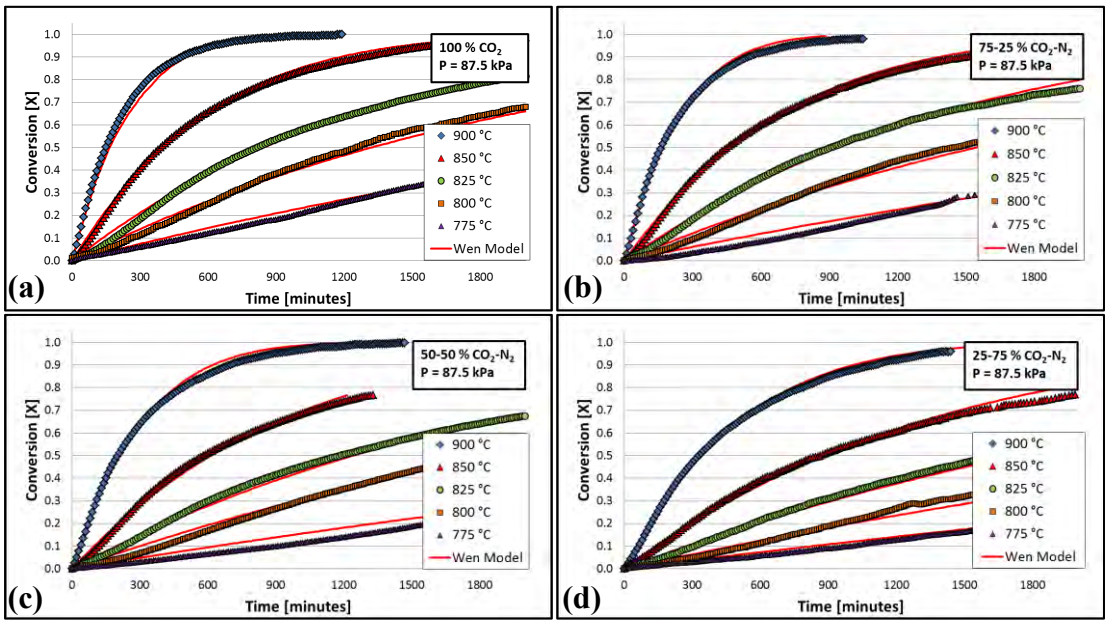

Figure 7-16: Wen model CO_2 gasification conversion data fitting

7.6 Mixed reagent

In this section the graphs and figures for the comparison of the pure gas conversion data to the mixed reagent data, as well as the L-H kinetic equation evaluation and the final modelling of the mixed reagent data is presented.

7.6.1 Conversion comparison

The reaction rate conversion graph comparisons for the steam-N_2 and steam-CO_2 gasification experiments are presented in Figure 7-17 (a-p).

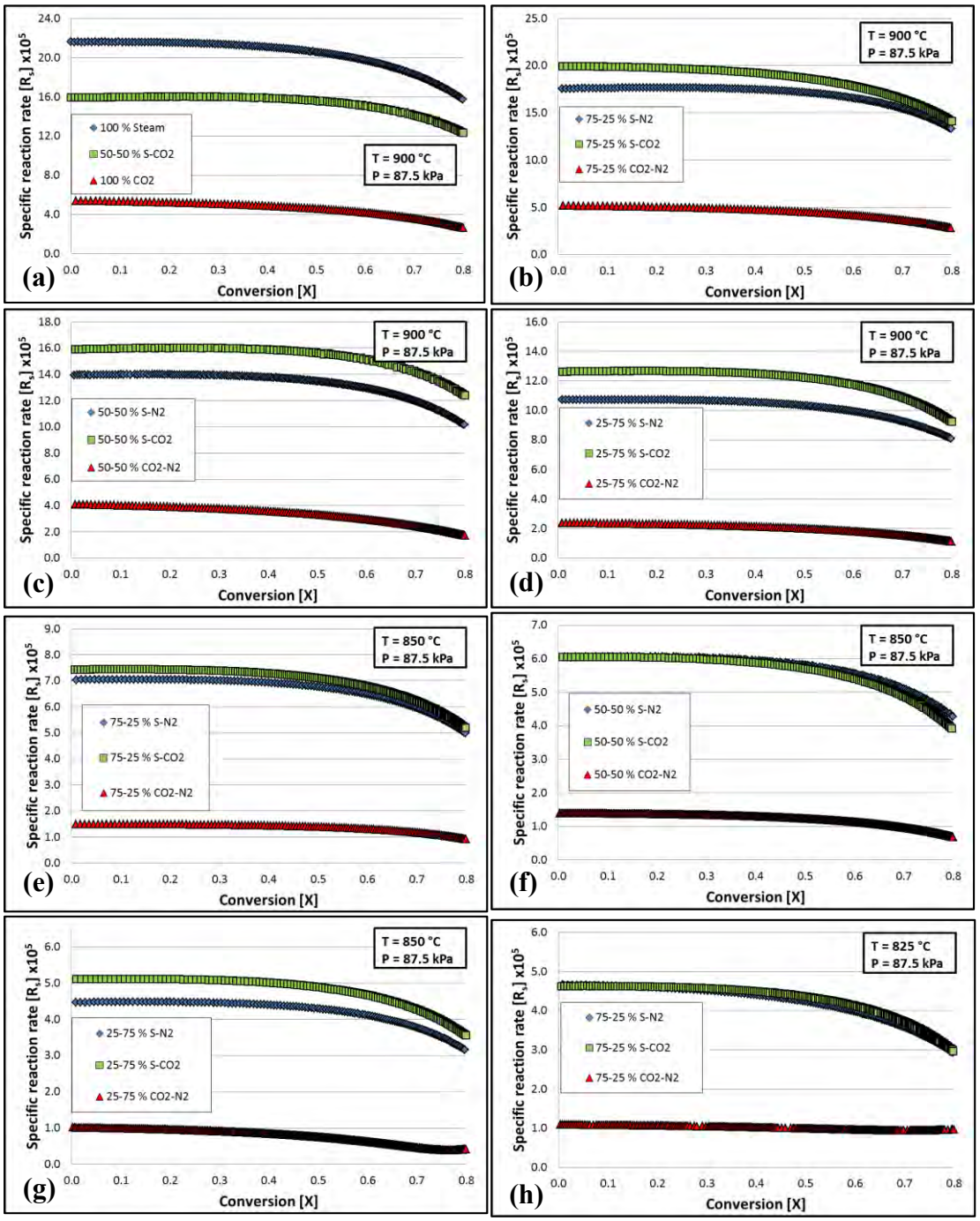

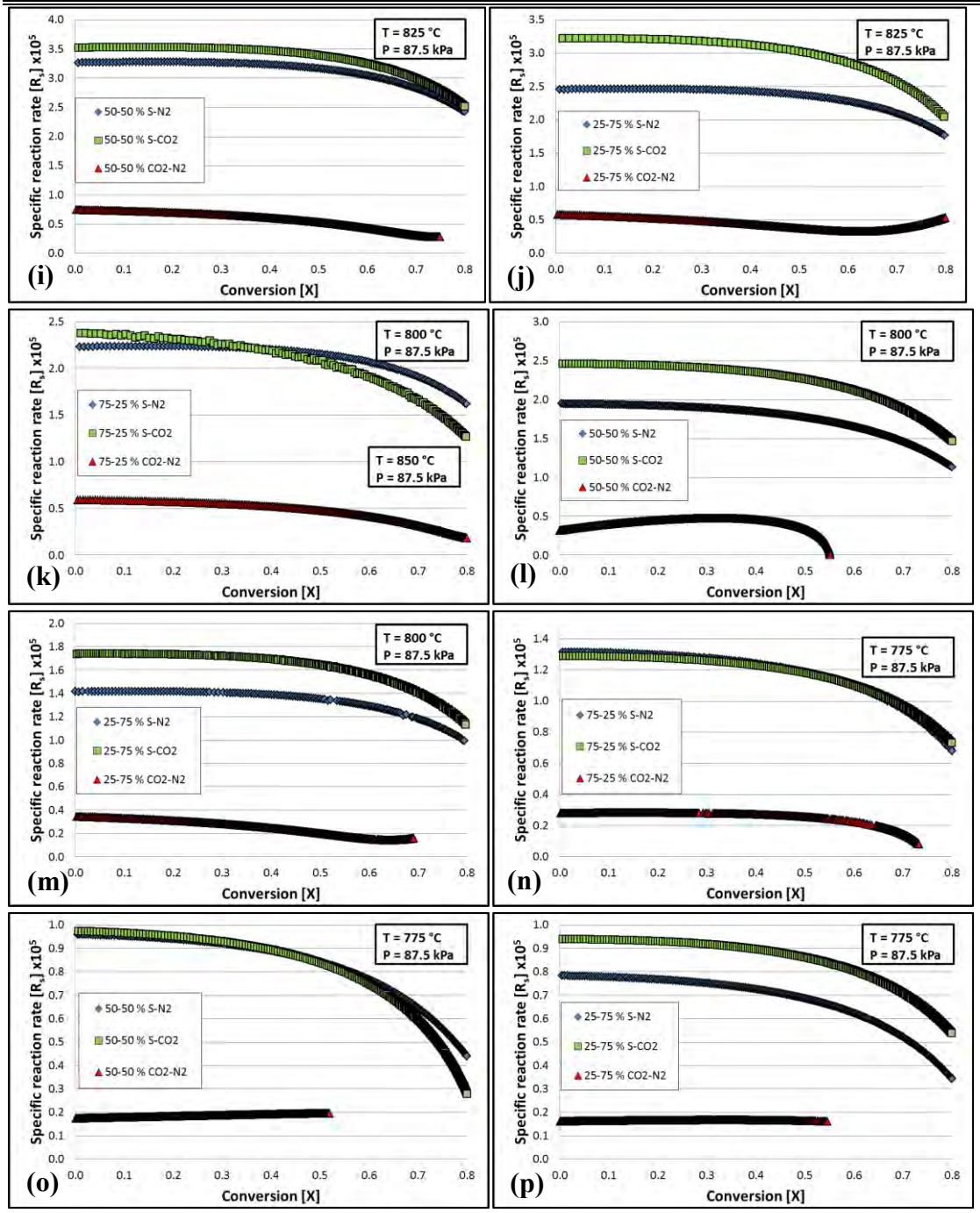

Figure 7-17: Reaction rate comparison of H_2O-N_2 to H_2O -CO_2

Reactivity index values for steam-N_2 gasification are compared to the corresponding steam-CO_2 gasification values in Table 7-3.

Table 7-3: Reactivity index comparison of steam-N_2 and steam-CO_2

R_{50} [1/hr]	100% H_2O	75-25 % H_2O-N_2	50-50 % H_2O-N_2	25-75 % H_2O-N_2
900 °C	0.789	0.714	0.559	0.413
850 °C	0.340	0.280	0.233	0.190
825 °C	0.185	0.171	0.123	0.106
800 °C	0.102	0.094	0.076	0.058
775 °C	0.058	0.052	0.039	0.031
R_{50} [1/hr]		**75-25 % H_2O-CO_2**	**50-50 % H_2O-CO_2**	**25-75 % H_2O-CO_2**
900 °C	-	0.732	0.691	0.488
850 °C	-	0.291	0.238	0.202
825 °C	-	0.176	0.138	0.120
800 °C	-	0.091	0.085	0.068
775 °C	-	0.054	0.045	0.037

7.6.2 Additive and competitive kinetic evaluation

A comparison of the experimental conversion data and the Wen model predictions with additive and competitive L-H kinetic models is presented in Figure 7-18 (a-p):

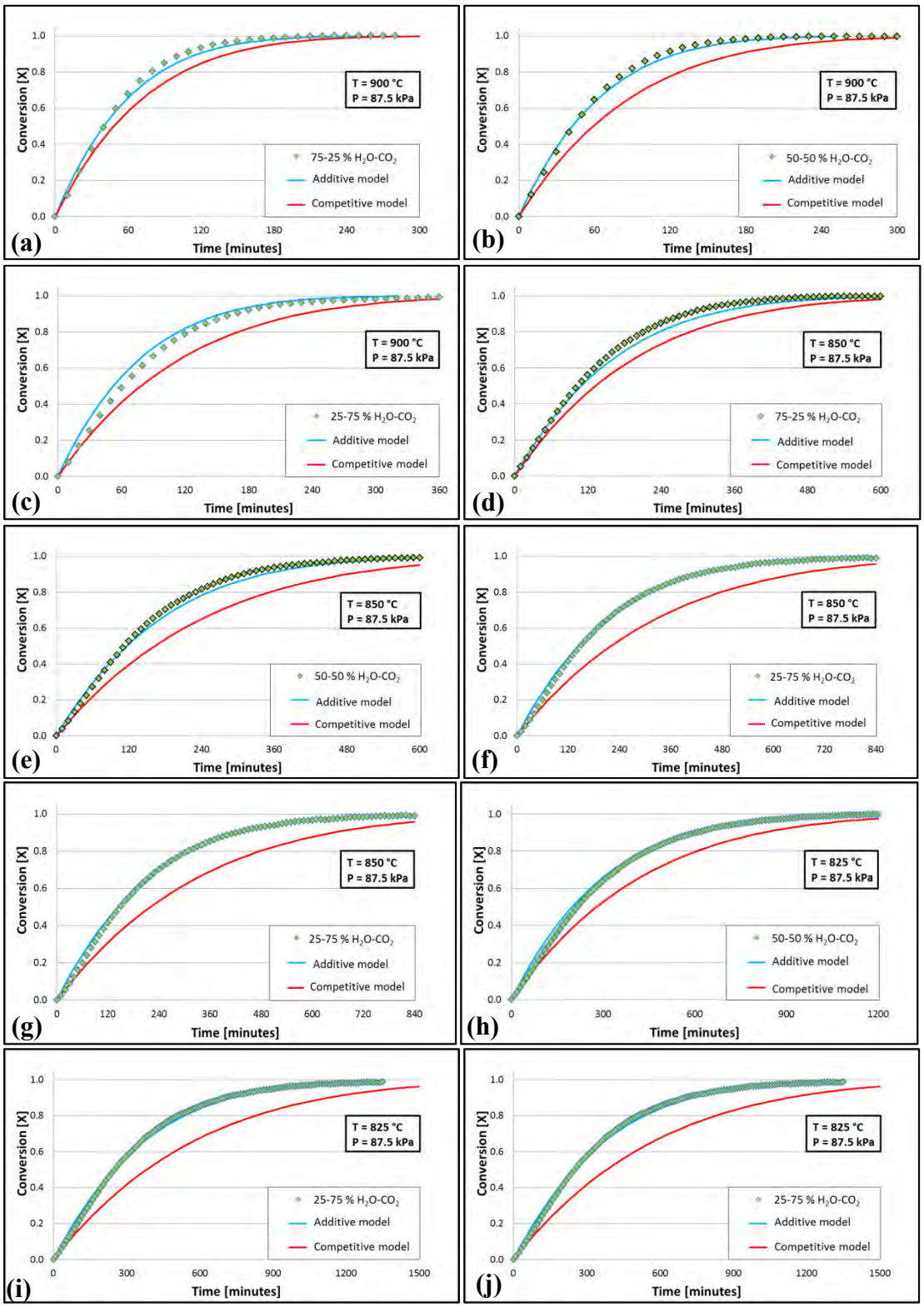

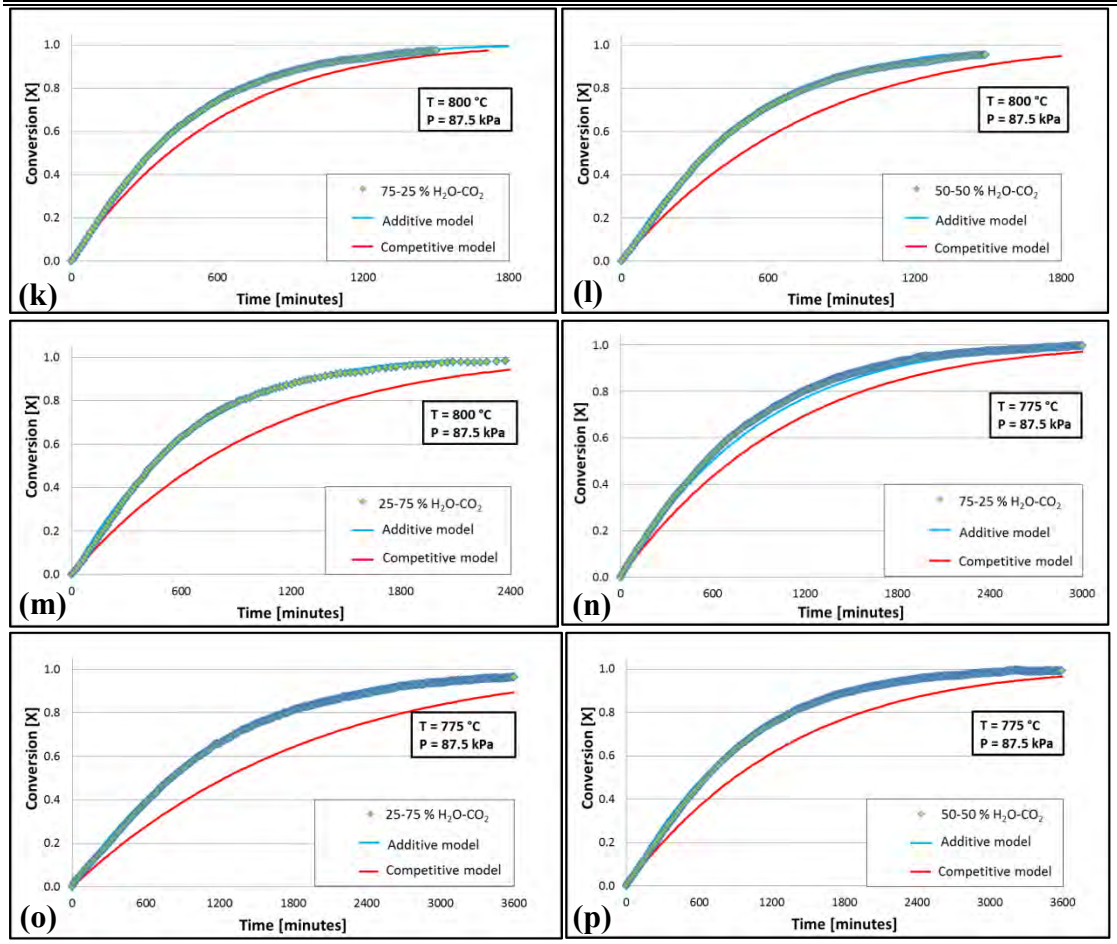

Figure 7-18: Additive and competitive L-H equation conversion comparison

7.6.3 Mixed reagent modelling

The Wen model with additive L-H kinetics was used to model mixed reagent gasification conversion data with the kinetics as presented in Table 5-17. The model comparisons for the various investigated temperatures and reagent partial pressures are shown in Figure 7-19 (a-c).

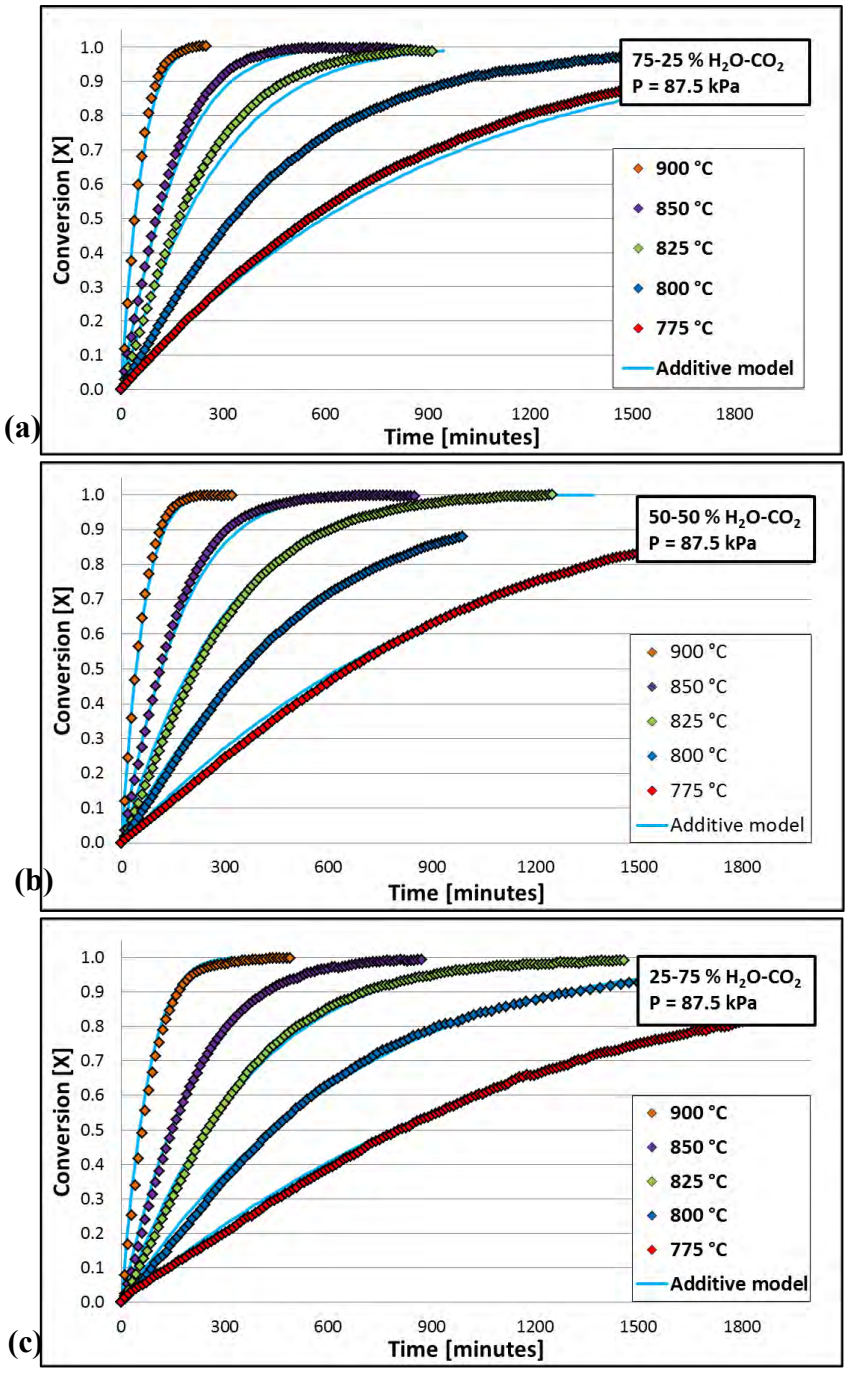

Figure 7-19: Wen model with additive L-H kinetics conversion predictions